Functional studies on the role of IκB$_{NS}$ in T helper cell differentiation

Dissertation

zur Erlangung des akademischen Grades

doctor rerum naturalium
(Dr. rer.nat.)

Genehmigt durch die Fakultät für Naturwissenschaften
der Otto-von-Guericke Universität Magdeburg

von:	Dipl.-Biol. Michaela Annemann
geb. am:	14. August 1983 in Neindorf-Beckendorf
Gutachter:	Prof. Dr. Ingo Schmitz
	Prof. Dr. Vigo Heissmeyer

eingereicht am:	18. Dezember 2013
verteidigt am:	05. Mai 2014

Summary

The NF-κB/Rel signalling pathway plays a crucial role in numerous biological processes, including innate and adaptive immunity. Although the cytoplasmic regulation of NF-κB is well characterised, its nuclear regulation mechanisms is only recently started to become elucidated. The nuclear IκBs contribute significantly to the modulation of NF-κB activity. $I\kappa B_{NS}$, an atypical IκB protein, regulates the proliferation of T and B cells. Furthermore, the expression of various cytokines is modulated via $I\kappa B_{NS}$ by its ability to specific activation or termination of NF-κB function at certain cytokine promoters. The aim of this thesis was to obtain a better understanding of the role of $I\kappa B_{NS}$ during the regulation of NF-κB activity in health and disease.

The activation of the TCR rapidly induces $I\kappa B_{NS}$ expression. However, it is unknown if $I\kappa B_{NS}$ itself affects this activation cascade or if it modulates the expression of NF-κB subunits. Analysis of $CD4^+$ T cells *ex vivo* revealed that $I\kappa B_{NS}$ does neither affect the proximal TCR signalling nor the expression of NF-κB subunits upon cell activation. The nuclear IκB protein IκBζ regulates the proliferation of T_H17 cells as well as the expression of IL17A. This thesis uncovered $I\kappa B_{NS}$ as a second IκB protein intrinsically involved in the development of T_H17 cells. In addition, *in vitro* experiments revealed that $I\kappa B_{NS}$ regulates the expression of IL10 in T_H17 cells. In *in vivo* experiments, $I\kappa B_{NS}$ seems to be almost dispensable for the course of EAE. In contrast, in the colitis models $I\kappa B_{NS}$-deficient mice suffered from more severe inflammation of the gut and were more susceptible to *Citrobacter rodentium* infections. Additionally, $I\kappa B_{NS}$ was crucial for the formation of T_H1 and T_H7 cells in gut inflammation as well as infection. Furthermore, the induction of T_H17 cell was modulated by $I\kappa B_{NS}$, while it was less important for T_H1 cell development during inflammation and infection of the gut.

In this thesis was demonstrated that $I\kappa B_{NS}$ does not only regulate the transition of immature Treg precursor into immuno-suppressive Treg cells, but is also necessary for the generation of pro-inflammatory T_H17 cells *in vitro* and *in vivo*. Thus, $I\kappa B_{NS}$ exhibits diverse regulatory functions for T cell proliferation and cytokine secretion. Consequently, $I\kappa B_{NS}$ may represent a T cell specific pharmacological target in the future.

Contents

1 Introduction....1

1.1 The key players of the immune system....1

1.2 Thymic maturation of T cells....2

1.3 T helper cell differentiation....4

1.4 The differentiation of T_H17 cells....6

1.5 T_H17 cells, a pro-inflammatory T cell subset in health and disease....8

1.6 The transcription factor nuclear factor (NF)-κB....10

1.7 The IκB protein family - regulators of NF-κB....11

1.8 The cytoplasmic regulation of NF-κB by IκBs....13

1.9 $I\kappa B_{NS}$ - the novel regulator of NF-κB....15

1.10 Aims of the thesis....17

2 Material and methods....18

2.1 Molecular biological methods....18

2.1.1 Eukaryotic RNA or DNA extraction....18

2.1.2 cDNA synthesis by reverse transcription....18

2.1.3 Polymerase chain reaction....18

2.1.4 Agarose gel electrophoresis....20

2.1.5 Quantitative real-time detection PCR....20

2.1.6 Transformation....22

2.1.7 Cell transfection and lentiviral transduction....22

2.2 Protein biological approaches....23

2.2.1 Cell lysis and determination of protein concentration....23

2.2.2 Fractionated cell lysis....24

2.2.3 SDS-polyacrylamide gel electrophoresis (SDS-PAGE)....25

2.2.4 Western blotting....26

2.2.5 Urea-PAGE....28

2.2.6 Immunoprecipitation....28

2.2.7 MicroLink™ Protein Coupling Kit 29
2.3 *In vitro* techniques 29
2.3.1 Cultivation of A20 cell line 29
2.3.2 Organ isolation and single cell suspension preparation 30
2.3.3 Flow-cytometric analysis 30
2.3.4 Cell isolation by flow cytometry 33
2.3.5 *In vitro* generation of T helper cell subsets 33
2.3.6 *In vitro* expansion of $CD4^+CD25^-$ T cells 35
2.3.7 *In vitro* activation of *ex vivo* or expanded T cells 35
2.3.8 Proliferation analysis with alamarBlue® 35
2.3.9 Proliferation analysis via CFSE or CellTrace™ Violet Proliferation Dye staining 36
2.3.10 Enrichment of T_H17 cells via mouse IL17 Secretion Assay 36
2.3.11 Analyses of cytokine expression by Proteom Profiler™ Array 37
2.3.12 Analyses of cytokine expression by FlowCytomix Kit 37
2.4 *In vivo* techniques 37
2.4.1 Mouse strains 37
2.4.2 Dextran sulphate sodium induced chronic colitis (chronic DSS colitis) 38
2.4.3 Adoptive transfer colitis 38
2.4.4 *Citrobacter rodentium* infection 40
2.4.5 Experimental autoimmune encephalomyelitis (EAE) 41
2.5 Statistics 42
3 Results 43
3.1 Characterisation of $I\kappa B_{NS}$-deficient mice 43
3.1.1 The loss of $I\kappa B_{NS}$ affects the $B220^+$ B cells frequency but not apoptosis sensitivity 43
3.1.2 $I\kappa B_{NS}$ is not crucial for the activation of $CD4^+$ T cells 47
3.1.3 Both $I\kappa B_{NS}$ forms (35 and 70 kDa) are stable to denaturation by urea 49
3.2 The role of $I\kappa B_{NS}$ in T_H17 cell development 54
3.2.1 Setup of an efficient *in vitro* polarisation of T_H17 cells 54

3.2.2 $I\kappa B_{NS}$ drives the differentiation of both T_H17 and T_H1 cells.....59

3.2.3 The loss of $I\kappa B_{NS}$ alters the *in vitro* expression of cytokines by T_H17 cells.....65

3.3 Function of $I\kappa B_{NS}$ in autoimmunity and inflammation 72

3.3.1 $I\kappa B_{NS}$ deficiency mildly delayed the onset of EAE.....72

3.3.2 $I\kappa B_{NS}$ deficiency results in impaired T_H17 development and high susceptibility to chronic gut inflammation.....73

3.4 Mice defective in $I\kappa B_{NS}$ display a high susceptibility to *Citrobacter rodentium* gut infection associated with an impaired T_H17 development.....77

4 Discussion.....80

4.1 The loss of $I\kappa B_{NS}$ alters the development of B cells.....80

4.2 Novel isoform of $I\kappa B_{NS}$ may arise from posttranslational modifications.....82

4.3 $I\kappa B_{NS}$ is essential for T_H17 development and enhances the expression of IL10.....83

4.4 T_H17 formation is supported by $I\kappa B_{NS}$ in the inflamed gut 87

4.5 $I\kappa B_{NS}$ promote the development of T_H17 cells in *Citrobacter rodentium* gut infection....88

4.6 Concluding remarks.....89

5 Abbreviations.....91

6 References.....93

7 Acknowledgments.....106

8 Declaration of originality.....107

9 Curriculum vitae.....108

1 Introduction

1.1 The key players of the immune system

From birth, the immune system is constantly exposed to a rich diversity of microorganisms. For example 100 trillion microorganisms, composed of 500 to 5,000 different species are present in the human intestine [1–3]. Nevertheless, most of the organisms within the intestinal tract are well-tolerated because of mutual benefits. The human intestine offers a relatively stable environment, well-tempered and nutrient-rich, to the commensal bacteria. In turn, human benefits from an increased digestive capacity and increased protection against pathogenic organisms [1,3,4] During the course of live, a disruption of this balance by changes of diet, antibiotic treatment or invasion of pathogens can result in immune-mediated diseases. For instance inflammatory bowel diseases (IBD), like Crohn's disease and ulcerative colitis are linked to a dysregulated intestinal micro-environment. Furthermore, experimental autoimmune encephalomyelitis (EAE) [5,6], rheumatoid arthritis [7] and diabetes [8] have also been suggested to be associated with a change of the commensal gut flora. Therefore, the immune system needs to tolerate commensal organisms as well as self-antigens, but has to defend the body from pathogenic microorganisms from outside and tumours from the inside.

During evolution, vertebrates developed the adaptive immune system in addition to innate immune responses. This was an essential step, because both, the rapidity of the innate and the diversity of the adaptive immune response are crucial for effective protection of the human organism [9]. The innate immune system of the vertebrates is able to recognise conserved pathogen-associated molecular pattern (PAMPs) of invading microorganisms. This is possible via the pattern recognition receptors (PRR) of cells of the innate immune system. Thereby, innate immune cells distinguish pathogenic components and harmless antigens [2,4,10]. Thus, antigen-presenting cells (APCs) recognise and engulf pathogenic microorganisms. Afterwards, APCs degrade and process the microbial proteins intracellularly and subsequently the foreign antigens are presented via the major histocompatibility complex (MHC) class II [10]. Additionally, the transcription factor nuclear factor-kappa B (NF-κB) becomes activated by the recognition of pathogens followed by cytokine expression and up-regulation of co-stimulatory molecules on APCs in peripheral lymphoid organs. The produced cytokines attracts T and B cells, which are parts of the adaptive immune response, thereby creating a link between innate and adaptive immunity. [4,10] Naïve T cells recognise the APC-bound non-self antigen via their T cell

receptor (TCR). The recognition of the cognate antigen together with the binding of co-stimulatory molecules of the APC activates the T cell and initiates a new gene expression program. This initiates an expansion phase of T cells. Within this phase T cells starts to proliferate and finally differentiate into effector T cells, which migrate to the infected areas of the body. When all pathogens/ antigens have been cleared, the immune system enters the contraction phase. Within this phase most of the effector cells die by apoptosis to return to homeostasis. The surviving cells differentiate into long-lasting memory cells, which are available for a faster and stronger response the next time the immune system is challenged with this specific pathogen. [11,12]

1.2 Thymic maturation of T cells

The T cell life begins as a hematopoietic stem cell (HSC) in the bone marrow. The HSCs leave the bone marrow, circulate in the blood and enter the thymus as thymus-settling progenitors (TSPs) [13–15]. The development of $CD4^+$ or $CD8^+$ T cells depends on the microenvironment of the thymus, at which each of the four major thymic compartments (subcapsular zone, cortex, medulla, corticomedullary junction) is involved in a specific stage of the thymocyte development [16–21]. The T cell development in the thymus is a tightly controlled cascade of separate developmental steps [14,20]. The most important cell-surface markers, which allow the identification of different developmental stages of thymocytes, are CD4, CD8, CD25, CD44 and CD117. The expression of these markers retains within the rearrangement steps of the T cell receptor (TCR) chains. [14,19] After tiny numbers of TSPs enters the thymus, they go through four CD4/CD8 double-negative (DN) stages (DN1-DN4) [14,19,20,22]. The earliest DN cells, DN1 express high levels of CD117 as well as CD44 but are negative for CD25 [14]. The DN1 cells are first detectable in the corticomedullary junction (CMJ) of the thymus, where they undergo proliferation [14,16–19]. Furthermore, via Notch1 signalling the DN1 cells become a more T cell-restricted progenitor and less multipotent, a process called T cell lineage commitment [14,19]. The DN1 thymocytes migrate to the subcapsular zone (SCZ), deeper in the cortex [14,16,17]. Stimulatory signals from cortical thymic epithelial cells (cTECs) and fibroblasts induce the differentiation into DN2 cells ($CD25^+CD44^+CD117^{int}$) [14,20]. The DN2 thymocytes further proceed in T cell lineage commitment [14,20]. Furthermore, this step is characterised by the TCR β-chain rearrangement [14,20]. This process is also called β-selection and is finished in the DN3 stage [14,20]. The DN3 ($CD25^+CD44^{lo}CD117^{lo}$) thymocytes are still present within

the SCZ and mature to DN4 cell ($CD25^-CD44^-CD117^-$) [14,16,17,20]. During the migration back to the thymic medulla, DN4 thymocytes up-regulate CD4 and CD8 after successful pre-TCR signalling within the outer cortex [14,16,17,20]. In these double-positive (DP) thymocytes the rearrangement of the TCR α-chain occurs [14,23]. Furthermore, in the DP stage the developing T cells undergo a process called positive selection [14,20,23]. During this process, DP thymocytes recognising self-peptides presented by MHC-complexes of cTECs, DCs and fibroblasts [14,20,23]. Those DP cells which recognise self-peptides with low affinity survive and further differentiate into single-positive (SP) thymocytes, either expressing CD4 or CD8 [14,20,23–25]. Additionally, those thymocytes with a low affinity to self-peptides are protected from neglect and switch off further TCR α-chain gene rearrangement [23]. The newly formed SP thymocytes migrate into the thymic medulla [14,20]. The medulla is the place for negative selection, eliminating SP cells with a high affinity to self-peptides presented by medullary TECs (mTECs) [14,20,22–25]. Consequently, negative selection is an process to eliminate autoreactive T cells [14,20,22–25].

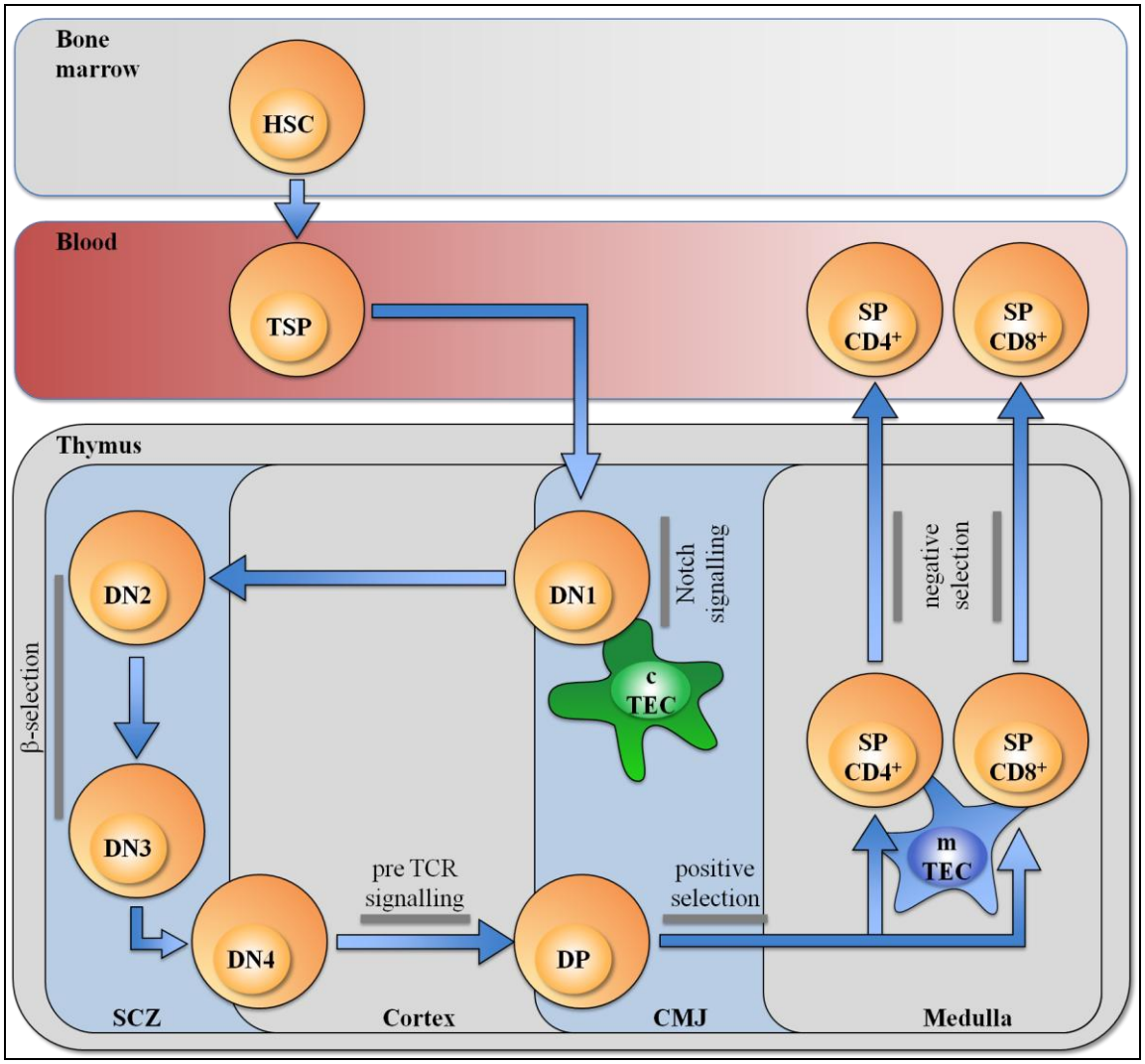

Figure 1: Thymic migration of maturating T cells: Hematopoietic stem cells (HSC) leave the bone marrow, circulate in blood and enter the thymus as thymus-settling progenitors (TSPs) at the corticomedullary junction (CMJ). TSPs run through four CD4/CD8 double-negative (DN) maturation stages. Via Notch-signalling DN1 cells ($CD25^-CD44^+CD117^{hi}$) start to become more committed to the T cell linage. DN1 cells migrate to the subcapsular zone (SCZ) and mature to DN2 cells upon stimulation by thymic epithelial cells (cTECs). In DN2 cells ($CD25^+CD44^+CD117^{int}$) the β-selection starts and is completed in DN3 cells ($CD25^+CD44^{lo}CD117^{lo}$). The DN3 cells mature to DN4 cells ($CD25^-CD44^-CD117^-$), which start to migrate back to thymic medulla. Within the outer cortex DN4 cells become double-positive (DP) for CD4 and CD8. Within DP cells the rearrangement of the TCR α-chain occurs. Self-antigens presented by cTECs induce the positive selection of DN cells, which afterwards mature to single-positive (SP) cells. The negative selection of SP cells takes place within the medulla and eliminates highly autoreactive cells. The newly formed $CD4^+$ and $CD8^+$ T cells exit the thymus.

1.3 T helper cell differentiation

The presence of two distinct $CD4^+$ T cell subsets was first described by Mosmann *et al.* showing a unique cytokine expression by these T cells [26]. Hence, Mosmann *et al.* named them T helper 1 and T helper 2 (T_H1 and T_H2) cells according to their cytokine production [26]. A further peripheral T_H cell subset was discovered recently and named T_H17

cells [27–33]. These three major T_H cell types are distinguishable by their unique cytokine production and their function [28,30,31,34,35]. The T_H1 cells, which predominantly express interferon-γ (IFN γ) are essential in protecting the host against intracellular viruses and bacteria [28,30,31,34]. T_H2 cells on the other hand, are important for the defence against extracellular pathogens (e.g. helminths) and produce interleukin 4 (IL4), IL5, IL9, IL13 and IL25 [28,30,31,34]. T_H17 cells are characterised by the production of IL17A, IL17F as well as IL22 and control extracellular bacteria and fungi [27–31,34]. Next to their immune-protective function, both T_H1 and T_H17 cells are implicated in autoimmune diseases and T_H2 cells are involved in allergic responses [35,36]. The fourth T cell subset, known as regulatory T (Treg) cells can either differentiate from peripheral naïve $CD4^+$ T cells (induced Treg; iTreg), as the other T_H cells or develop in the thymus (thymic derived Treg; tTreg) [28,30,31,37–39]. In contrast to other T_H cells, which promote immune responses, Treg cells are immune suppressive [28,30,31,37–39].

After triggering of the TCR, the differentiation of T_H cells is directed by several T_H cell subset specific requirements. Firstly, the surrounding cytokine milieu at the time of TCR stimulation plays a critical role in determining the T_H cell commitment [28–31]. A unique combination of cytokines is required for the differentiation of a specific T_H cell lineage (Figure 2) [28–31]. Secondly, members of the signal transducer and activator of transcription (STAT) family and master transcription factors collaborate in T cell differentiation and expansion (Figure 2) [29,31]. Thirdly, the T_H cell commitment is additionally supported by one of the effector cytokines of the particular T_H cell subset, thereby providing a powerful positive feedback loop (Figure 2) [29,31]. Finally, cytokines of the IL1 family are suggested to induce the effector cytokine production together with STAT activators in a TCR-independent manner (IL18 for Th1, IL33 for Th2 and IL1 for Th17 cells) [31]. Consequently, the commitment of T cell subsets takes place, they selectively maturate and the master regulator of the committed T cell actively suppress an alternative lineage fate [29,31]. For instance, IFNγ and IL27 activate STAT1, which initiates the development of T_H1 cells [29,31]. The master transcription factor of T_H1 cells, Tbet is induced by STAT1 together with TCR-activated transcription factors and Tbet in turn initiates the production of IFNγ [29,31]. Furthermore, IL12 secreted by APCs activates STAT4, which induce together with Tbet induces the expression of IFNγ within T_H1 cells. Hence, via a positive-feedback loop IFNγ intensifies the T_H1 cell commitment by further activation of STAT1 (Figure 2) [29,31].

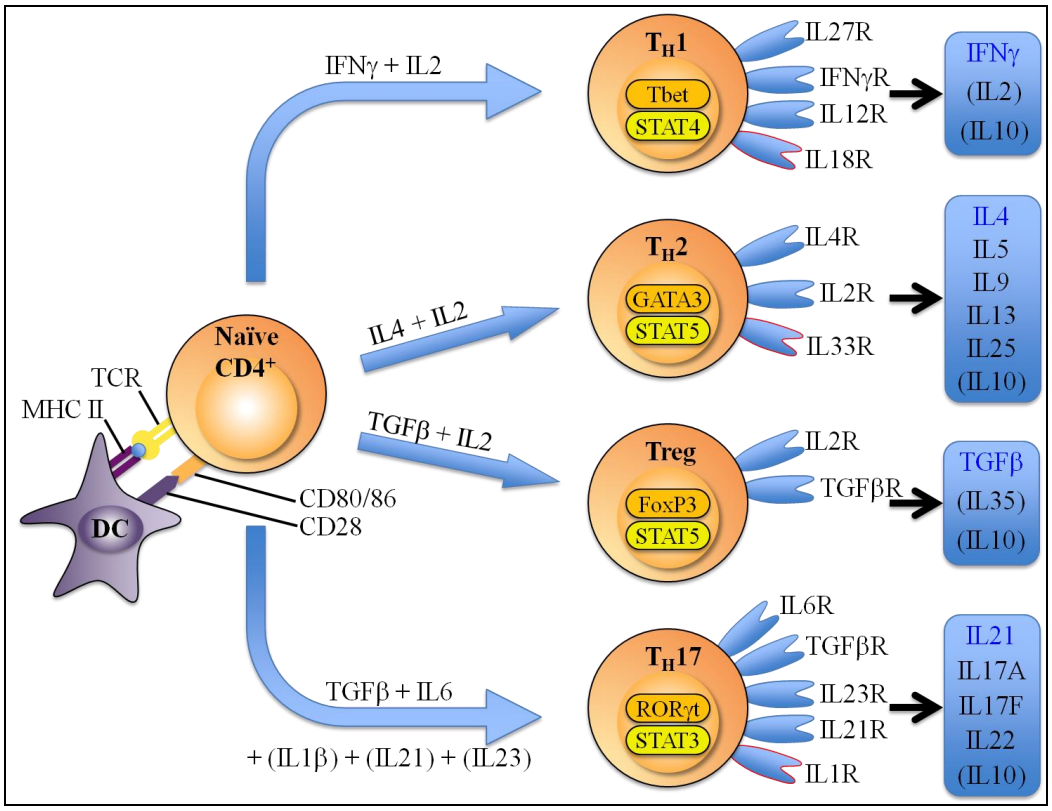

Figure 2: T helper cell differentiation. Upon the TCR activation triggered by antigen-presenting cells (e.g. DCs) a naïve $CD4^+$ T cell can differentiate into four subsets, namely, T_H1, T_H2, T_H17 or Treg cell. Each T cell differentiation depends on a critical combination of cytokines: IL12 and IFNγ for T_H1, IL4 and IL2 for T_H2, TGFβ and IL6 (IL21/IL23) for T_H17, and TGFβ and IL2 for iTreg cells. The lineage commitment involves the up-regulation of lineage characteristic master transcription factors (highlighted in orange) and the activation of STAT proteins (highlighted in yellow). Each committed T_H cell expresses a unique combination of effector cytokines (highlighted in blue), and one of these cytokines promotes further lineage commitment (written in blue). In addition, committed T cells express receptors directed to IL1 cytokine family members (red-rimmed), which induce an effector cytokine expression in a TCR-independent way.

1.4 The differentiation of T_H17 cells

The differentiation of T_H17 cells (Figure 2) is a subject of ongoing research and further investigations are necessary to decrypt the exact mechanism [29–31,34]. T_H17 cell differentiation is independent of cytokines and transcription factors, which are important in T_H1 and T_H2 development [33,40–42]. IFNγ and IL4 are essential cytokines in T_H1 or T_H2 differentiation, but inhibit the development to IL17 producing T cells [33,40,42]. Furthermore, the cytokine IL2, which is required for T_H2 and Treg cell development and clonal expansion, blocks T_H17 cells by the activation of STAT5 [41,43,44]. During T_H17 cell differentiation the secretion of IL2 is suppressed by binding of Aiolos, a member of the Ikaros transcription factor family, to the *Il2* locus [41].

The member of the STAT family STAT3 and the retinoic-acid-receptor-related orphan receptor-γt (RORγt) are essential proteins in T_H17 cell differentiation (Figure 2) [45–47]. RORγt is the master transcription factor of T_H17 cells [48–51]. The necessity of RORγt in T_H17 cell formation was detected by analysing mice deficient for RORγt, which showed a reduced development of IL17 expressing cells [46,49,52]. Furthermore, the disruption of STAT3 in mice resulted in the absence of T_H17 cells [46,52,53]. Fork-head box P3 (Foxp3), the master transcription factor of Treg cells, inhibits the master transcription factor of T_H17 cells, RORγt, by direct binding and, thus, blocks the T_H17 cell differentiation [29]. Both the transforming growth factor β (TGFβ) and IL6 are essential to promote the T_H17 cell differentiation at the time of TCR activation [40,54–56]. While TGFβ inhibits the differentiation of T_H1 and T_H2 cells, it promotes Treg and T_H17 cell development by the induction of the transcription factors Foxp3 and RORγt [29,40,42,54,55,57,58]. The level of TGFβ is one pivotal factor of the T_H17 or Treg fate decision [59]. The induction of Foxp3 for Treg development requires high concentrations of TGFβ [59], while a low level of TGFβ promote T_H17 cell differentiation [59]. In contrast to TGFβ, IL6 induces the development of T_H17 cells, while inhibiting Treg cell development [46,52,55,59,60]. Thus, the presence of TGFβ together with IL6 induces T_H17 cell development by the activation of STAT3 [46,52,61]. STAT3 itself leads to the induction of RORγt expression [45,46]. Subsequently, additionally to its ability to support RORγt expression [45,46] STAT3 inhibits the expression of Foxp3 and its interaction with RORγt [45,55,62]. The increased availability of RORγt enhances the commitment of the T_H17 lineage fate [46,48,50,59]. Furthermore, upon the initiation of T_H17 differentiation STAT3 together with IL6 induce the expression of IL21 and the IL23 receptor (IL23R) [46,53,61,63]. The three cytokines IL6, IL21 and IL23 are activators of STAT3 [45,46,60,63]. Thus, a positive-feedback loop leads to exacerbated STAT3 expression via endogenous IL21 as well as APC-derived IL6 and IL23 [45,46,60,63]. Due to the lack of IL23R on naïve $CD4^+$ T cells, IL23 is not essential for T_H17 cell differentiation but for their survival and expansion [30,45,56]. Furthermore, IL21 and IL23 promote the expansion of T_H17 cells and finalize T_H17 cell development [55,56]. The expression of the effector cytokine of T_H17 cells, IL17A is induced by RORγt and STAT3 [46,48,49,51]. Furthermore, RORγt synergistically regulates the IL17A expression together with runt-related transcription factor 1 (Runx1) [48]. The optimal expression of RORγt is induced by Runx1, both bind to the *Il17* locus and induce the expression of IL17A and IL17F [48].

Recently the participation of IL1β to the T_H17 differentiation was identified [44,56,64–67]. Mice deficient for IL1β or its receptor failed to generate a robust T_H17 cell response in infections (e.g. *Candida albicans*) [64,66]. Furthermore, IL1R-deficient mice are less susceptible to experimental autoimmune encephalomyelitis (EAE) induction, since T_H17 cells in contrast to T_H1 and T_H2 cells were defective to become autoreactive in these mice [68]. Moreover, IL1β acts together with TNFα and synergizes with IL6 and IL23 to promote the induction as well as the amplification of the T_H17 cell commitment [44,56,64–67]. IL1β may support T_H17 cell differentiation due to its ability to antagonise the effects of IL2 [44] and IL12 [66]. In addition, IL1β contributes to T_H17 cell differentiation by induction of the transcription factor IFN regulatory factor 4 (IRF4) [67], which is involved in IL21-mediated T_H17 cell development [63,69].

1.5 T_H17 cells, a pro-inflammatory T cell subset in health and disease

T_H17 cells can be found throughout the body and most of them are present in the lung and intestinal tract [44]. An incomplete matured immune response as well as the absence of T_H17 cells were found in adult mice that grow up in a germ-free environment as well as in neonates [4,5,70]. It was shown, that gut dendritic cells from germ-free mice were reduced in their ability to induce proinflammatory T cells [5]. Within days, a robust T_H17 cell compartment is induced by the administration of commensal microorganisms to germ-free mice [70]. Especially the gut colonising segmented filamentous bacteria (SFB) were able to promote the T_H17 cell differentiation [5,7,71,72]. The intestinal microorganisms induced the expression of IL1 by intestinal macrophages, which in turn initiated T_H17 cell development [65]. Hence, the composition of the gut microflora regulates the T_H17 cell differentiation [5,7,65,70–72]. On the other hand, T_H17-derived cytokines such as IL17 and IL22 contribute to the regulation of the commensal gut microflora [2]. Furthermore, host protection to extracellular pathogens could be linked to T_H17 cells and their effector cytokines [73]. For instance, IL17 activates epithelial cells to produce anti-microbial peptides and monocyte-recruiting chemokines [73,74]. Parenchymal cells are initiated by IL17 to release inflammation mediators like cytokines and chemokines [73,74]. In addition, IL17R-signaling promotes the generation, attraction and activation of neutrophils and monocytes to clear infection by phagocytosis [73,74]. Secreted IL22 induces the proliferation of epithelial cells for repairing invasion-induced damage and promotes the expression of anti-microbial peptides [73]. T_H17 cells are necessary to promote the defence against a immense diversity of

pathogens e.g. *Candida albicans*, *Citrobacter rodentium*, *Klebsiella pneumoniae*, *Salmonella typhimurium* and *Staphylococcus aureus* [66,73,75–78].

First T_H1 cells were thought to be the inducers of autoimmunity, but since the discovery of IL17 secreting cells, numerous autoimmune diseases were shown to depend partially or mainly on a T_H17 cell immune responses [7,36,73,75,79–84]. A crucial role of IL23 rather than the T_H1 cytokine IL12 was suggested in EAE, arthritis, inflammatory bowel disease and psoriasis [73–75,85,86]. Furthermore, *in vivo* studies indicate that the protective immune response of T_H17 cells as well as their autoimmunity depend on IL23 rather than IL6 and TGFβ [40,85]. For instance, in *Citrobacter rodentium* infection the T_H17 differentiation depend on TGFβ and IL6 but not IL23 [40]. However, IL23 is essential in host protection, since IL23-deficient mice are more susceptible to *Citrobacter rodentium* infection compared to wildtype mice [40]. The disruption of the myelin in the central nervous system during multiple sclerosis and the corresponding mouse model, EAE depends on autoreactive T_H1 and T_H17 cells [82–84]. Similar to Citrobacter rodentium infection, studies of EAE suggest that the pathogenic function of T_H17 cells depends on IL23 rather on IL6 and TGFβ [85]. Myelin-autoreactive T cells, stimulated with IL6 and TGFβ, were present in the central nervous system of immunised mice, but were not able to induce demyelinisation [85]. On the contrary, myelin-specific T cells stimulated with IL23 established inflammation of the central nervous system [85]. IL6 and TGFβ stimulated T cell produced anti-inflammatory IL10 in contrast to IL23 stimulated cells, which was suggested to reduce the anti-inflammatory function of the myelin-specific T_H17 cells [85]. Additionally, mice deficient for IL23 are protected from EAE, supporting the essential role of IL23 in autoimmunity [86]. A similar pattern of resistance to autoimmunity was identified in mice deficient for granulocyte-macrophage colony-stimulating factor (GM-CSF) [87,88]. The studies on GM-CSF showed that IL23 together with RORγt direct the expression of GM-CSF in T_H17 cells and by a positive feedback loop GM-CSF of T_H17 cells activates APCs to produce IL23 [87,88]. T_H17-secreated GM-CSF itself sustained the neuroinflammations in EAE, because it activate myeloid cells to infiltrate the central nervous system [87,88]. Thus, the manipulation of the T_H17 lineage commitment may provide new opportunities for the enhancement of mucosal immunity and the treatment of autoimmune diseases.

1.6 The transcription factor nuclear factor (NF)-κB

In 1986 the nuclear factor-κB (NF-κB) was first described by Sen and Baltimore as a transcription factor interacting with the immunoglobulin κ light chain enhancer in B cells [89]. Since then it has been shown that NF-κB is a key mediator of inducible gene expression in a wide range of cellular processes [90–94]. The NF-κB network is a global mechanism regulating cell survival and differentiation as well as the interaction between cells [90–94]. NF-κB is crucial in the immune system for both innate and adaptive immune responses [93,95]. For instance, NF-κB regulates lymphocyte survival, development and activation [93,95–97]. Moreover, it is essential in the formation of tissues important for lymphocyte development and activation [93,95–97].

The mammalian NF-κB (also named Rel) protein family (Figure 3) includes the five members p50/p105 (NF-κB1), p52/p100 (NF-κB2), p65 (RelA), cRel and RelB [92,96,98]. Both p105 and p100 are precursors and the two Rel proteins p50 and p52 are generated by post-translational cleavage for later dimerisation [94,95,98]. All members exhibit an N-terminal Rel-homology domain (RHD) including a nuclear localisation signal (NLS), a DNA-binding motif and a dimerisation domain [92,96,98]. Via the latter domain, two NF-κB proteins form a dimer and the DNA-binding motif allows the binding of the dimer to κB sites on the DNA [92,96,98]. Moreover, the Rel family members p65, cRel and RelB have a transcription activation domain (TAD), which is essential for the binding of co-activators [96,98]. NF-κB dimers containing at least one TAD can induce the transcription of the target gene [96,98]. The TAD is missing in p50 and p52, so that these two Rel proteins are only transcriptionally active when forming heterodimers with p65, cRel or RelB [96,98]. When bound to κB sites on the DNA, homodimers of p50 or p52 repress the transcription of the corresponding gene [96,99].

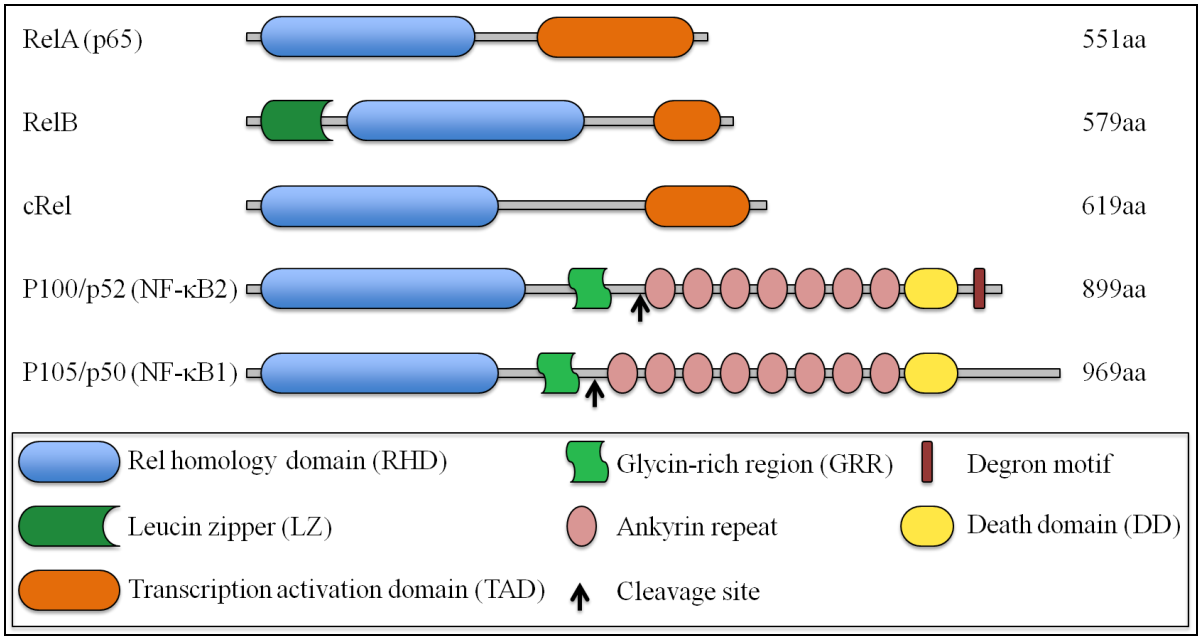

Figure 3: The members of the NF-κB family: The five members of the NF-κB/ Rel protein family p50/p105 (NF-κB1), p52/p100 (NF-κB2), p65 (RelA), cRel and RelB are illustrated. The post-translational cleavage of the precursor proteins p105 and p100 leads to the generation of the two proteins p50 and p52 (cleavage sites are marked with an arrow). The N-terminal Rel-homology domain (RHD) includes a nuclear localisation signal (NLS), a DNA-binding motif and a dimerisation domain. The Rel family members p65, cRel and RelB have a transcription activation domain (TAD).

1.7 The IκB protein family - regulators of NF-κB

The activity of NF-κB is regulated by the inhibitors of NF-κB (IκBs) protein family. The classical function of the IκB family members (Figure 4) is to retain NF-κB dimers in the cytoplasm by masking their NLS and thereby inhibiting its transcriptional function [95,99–102]. Over the years of extensive research, it became apparent that the IκB family is a functionally heterogeneous group of NF-κB regulators, which can either inhibit or enhance its activity [99,100,102].

The common structural motif of all IκBs is the ankyrin repeat domain (ARD) containing six to eight single ankyrin repeats [92,93,96,100,102–104]. Each ankyrin repeat comprises 33 amino acids folded into a helix-loop-helix conformation [100,103]. The ARD is essential for the protein stability and the interaction with the RHDs of NF-κB dimers [100,101]. Furthermore, classical IκBs exhibit an unfolded structure N-terminal of the ARD with a signal response domain (also called degron motif), containing serine residues for stimulation-dependent phosphorylation by IKK [100]. In addition, the polyubiquitination of typical IκB proteins occurs at lysine residues, located upstream of the phosphorylation sites [100]. Two of the typical IκBs have a region called PEST (rich in proline, glutamic acid, serine and

threonine), which is suggested to mediate fast protein turnover [100]. The NF-κB family members p100 and p105 contain C-terminal NF-κB-inhibiting ankyrin repeats as well as an N-terminal Rel homology domain. Hence, they belong to both the Rel and the IκB protein family [91,100].

The IκB protein family is divided into two groups the classical IκBs (IκBα, IκBβ, IκBε) and the atypical IκBs (Bcl3, IκBζ, $IκB_{NS}$, IκBη, IκBL) (Figure 4) [91,100–102]. In contrast to the mainly cytoplasmic classical IκBs, the atypical IκBs are predominantly located in the nucleus [91,100–102]. The cytoplasmic IκBs primarily inhibit basal NF-κB activity in unstimulated cells and are degraded upon stimulation to release NF-κB dimers for rapid transcriptional activity [91,100]. Atypical IκBs on the other hand have a low expression level in resting cells, which drastically increase upon cell stimulation [91,100,102]. Furthermore, nuclear IκBs can act as inhibitors or enhancers of NF-κB and thereby provide a fine-tuning mechanism for transcriptional responses [91,100,102]. The atypical IκB protein Bcl3 was first identified as a protooncogene in chronic lymphatic leukaemia [105]. Later it was reported that Bcl3 is important to promote B cell proliferation and development, germinal centre formation, humoral immune responses as well as formation of antigen-specific antibodies [106,107]. In stimulated macrophages, Bcl3 is detectable in the nucleus and inhibits lipopolysaccharide-induced (LPS-induced) TNFα production, but not IL6 [108]. It is known that Bcl3 preferentially associates with p50 and p52 homodimers [109–112] and thereby either activates or inhibits their function [111–114]. The activation of p50 homodimers is mediated by the transcription activation domain (TAD) of Bcl3 [113]. Next to Bcl3, the only IκB protein with a TAD is the nuclear IκBζ (also called MAIL), which mediates a gene-specific recruitment of NF-κB to its target promoter [115,116]. Furthermore, IκBζ negatively regulates the activity of p65/p50 heterodimers and p50/p50 homodimers [117,118]. IκBζ is induced by cell stimulation with LPS and IL1β, but not TNFα [118,119] and seems to be important for the regulation of apoptosis [118,120]. Furthermore, IL6 and IL12p40 are regulated by IκBζ [119]. The development of T_H17 cells depends on IκBζ, shown in IκBζ-deficient mice exhibiting a defect in T_H17 proliferation and resistance to EAE induction [121]. Additionally, IκBζ cooperates with RORγt and RORα to bind to the IL17A gene and induces its expression [121]. IκBη [122] and IκBL [123,124] are two recently identified atypical IκB proteins. The expression of IκBη is stimulation-dependent (e.g. LPS), as it was shown for atypical IκBs [122]. IκBη associates with p50 NF-κB subunits and regulates the expression of

proinflammatory cytokines such as IL6 and IL1β [122]. IκBL prevents the development of experimental autoimmune arthritis and is suggested to suppress the LPS-induced NF-κB activation and transcription of TNFα and IL6, but not IL1β [123,124].

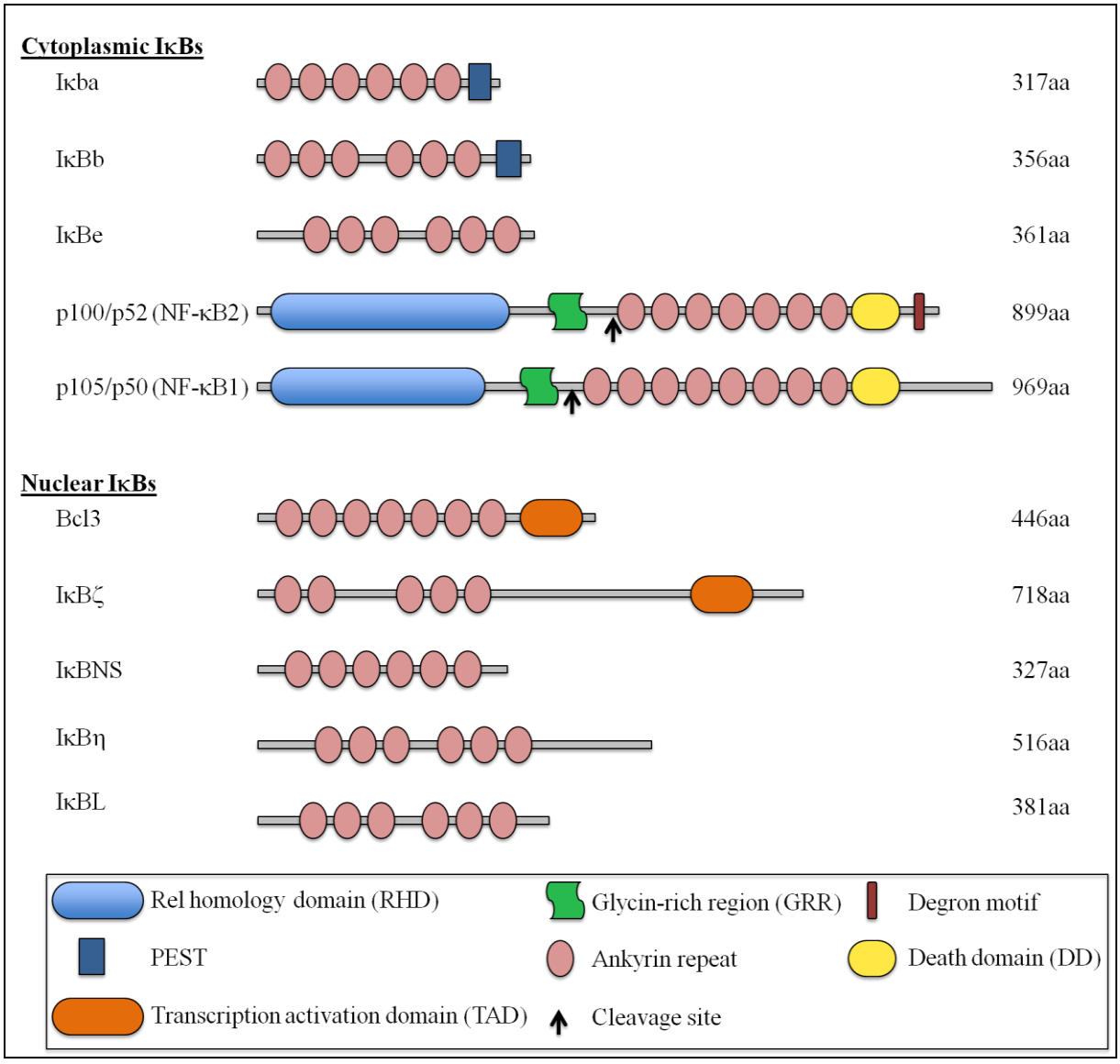

Figure 4: The pleiotropic IκB protein family: The IκB family is divided into the cytoplasmic (IκBα, IκBβ, IκBε, p100, p105) and the atypical nuclear IκBs (Bcl3, IκBζ, $IκB_{NS}$, IκBη, IκBL). All members contain ankyrin repeats (ANK). Bcl3 and IκBζ exhibit a transcription activation domain (TAD). The proteins p100 and p105 have both ankyrin repeats as well as Rel-homology domain (RHD). Consequently, they are grouped into both Rel and IκB protein families.

1.8 The cytoplasmic regulation of NF-κB by IκBs

In unstimulated cells, NF-κB dimers are inactivated via binding to cytoplasmic IκBs, which mask the NLS of the Rel protein (Figure 5) [93,99,125]. Several cell-activating signals can initiate the NF-κB pathway. These signals range from pro-inflammatory cytokines (e.g. TNF, IL1, IL17), cell stress (e.g. reactive oxygen species, DNA double-strand breaks)

and PAMPs (e.g. nucleic acids, peptides, lipoprotein) to TCR or BCR engagement [96]. Upon cell activation, the NF-κB-bound IκBα becomes phosphorylated at the two serine residues 32 and 36 [98,103,126]. This phosphorylation is conducted by the IκB kinase (IKK) complex, which consists of the regulatory subunits IKKγ (NEMO) and two catalytic units IKKα and IKKβ [95,99,101,126]. The phosphorylation of IκBα induces polyubiquitination and its proteasomal degradation [95,99,101,126]. This allows the translocation of the functionally active NF-κB into the nucleus where it binds to its cognate κB-binding motif on the DNA and induces gene expression [93,99,103,104]. One target of NF-κB is its own inhibitor IκBα, the prototypical member of the IκB family, and the intracellular level of IκBα is refilled upon gene induction by NF-κB [100,103]. Subsequently, IκBα mediates, via its nucleocytoplasmic-shuttling properties, the translocation of NF-κB back to the cytoplasm and thereby contributes to the termination of the NF-κB-induced gene transcription in a negative feedback loop [99,100,103]. Beside the IκB proteins, several mechanisms essential for the termination of transcription and the displacement of NF-κB from the DNA have been described [99]. This includes the altered binding of co-factors, the degradation of NF-κB after ubiquitination, and the displacement of NF-κB dimers from the DNA by small ubiquitin-like modifiers (SUMOylation) [99].

In addition to the canonical or classical pathway, which is outlined above, there exists a second NF-κB pathway [12,91,101,103,104,126]. This non-canonical or alternative Rel pathway is induced by the tumour necrosis factor (TNF) cytokine family including CD40 ligands, BAFF and lymphotoxin B [91]. In contrast to the canonical pathway, the non-canonical NF-κB pathway is independent of IKKγ, but depends on IKKα [91,103,104]. In canonical NF-κB signalling, TRAF/RIP complexes process and transfer the activation signals to IKK [91,103,104]. On the contrary, the non-canonical pathway depends on the NF-κB inducing kinase (NIK), which phosphorylates and activates IKKα [91,101,103,104]. The activation of IKKα causes the phosphorylation of p100 followed by a proteasomal processing of p100 to p52 [91,101,103,104]. The p100 is processed until a glycine rich region (GRR), which serves as proteasomal termination signal [101]. Subsequently, the generated p52/RelB heterodimers translocate into the nucleus, bind to κB sites and initiate the expression of the corresponding gene [91,101,103,104].

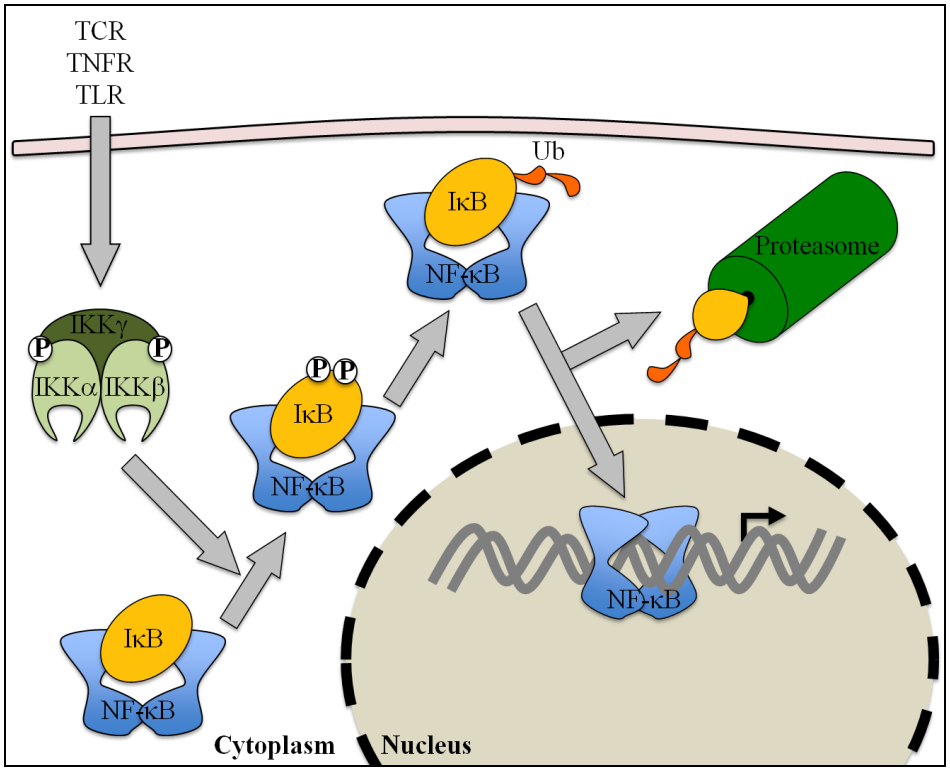

Figure 5: The canonical NF-κB pathway: Two NF-κB subunit proteins form a dimer, which is sequestered into the cytoplasm by binding to inhibitors of NF-κB proteins (IκBs). The IκB kinase complex (IKK), consisting of IKKα, IKKβ and IKKγ becomes activated upon cell stimulation. The IKK phosphorylates the IκB protein at the serine residues 32/36 and is followed by polyubiquitination and proteasomal degradation of IκB. Then the released NF-κB dimer translocate into the nucleus, binds to specific κB-sites and induces gene expression.

1.9 $I\kappa B_{NS}$ - the novel regulator of NF-κB

The product of the NFkB gene $I\kappa B_{NS}$ is also known as T cell activation NF-κB-like protein (TA-NFKBH). It is the smallest member of the nuclear IκB protein family and consists of 327 amino acids [127]. Fiorini *et al.* showed the TCR-induced expression of $I\kappa B_{NS}$ in thymocytes for the first time in 2002 [127]. Beside the TCR-triggered induction of $I\kappa B_{NS}$ [127,128], it is now known that the expression of $I\kappa B_{NS}$ as well as Bcl3 is also inducible by IL10 [108,129]. Furthermore, upon IL10 production an elevated expression of $I\kappa B_{NS}$ and Bcl3 was observed in LPS triggered regulatory DCs, which express less proinflammatory cytokines and instead preferentially IL10 compared to usual DCs [130]. Fiorini and colleagues identified that $I\kappa B_{NS}$ transcription was activated by peptides triggering negative but not positive selection [127]. Thus, it was first suggested that $I\kappa B_{NS}$ might play an important role in central tolerance. Interestingly, the transcription of NF-κB reporter proteins was blocked by $I\kappa B_{NS}$. In addition, the interaction of $I\kappa B_{NS}$ with NF-κB was observed within the nucleus [127].

In contrast to the suggested central role of IκB$_{NS}$ in negative selection in the thymus, IκB$_{NS}$-deficient mice did not develop autoimmune diseases and no changes in thymocytes or T cell subsets were detectable [128,131]. However, B cells from IκB$_{NS}$-deficient animals were defective in their proliferation upon LPS stimulation [132,133]. In addition to the proliferation defect of IκB$_{NS}$-deficient B cells, the serum IgM and IgG3 were drastically reduced upon the loss of IκB$_{NS}$ [132,133]. Furthermore, the defect of IκB$_{NS}$ induced a reduction of antibody-producing cells and diminished levels of influenza-specific antibodies were detected upon infection [132]. Additionally, IκB$_{NS}$-deficient T cells revealed a proliferation defect upon LPS stimulation [128,132] and are highly susceptible to LPS induced endotoxin shock as well as intestinal inflammation [131]. Furthermore, the LPS-triggered expression of IL6 and IL12p40, but not TNFα is increased in macrophages lacking IκB$_{NS}$ [129,131]. The IL6 expression is regulated by IκB$_{NS}$ by its association with p50. Both proteins are recruited to the IL6 promoter and inhibit as well as terminate the binding of p65 [129,131]. In contrast to the inhibitory effect of IκB$_{NS}$ on the IL6 production, it is dispensable for the expression of TNFα [129,131]. It has been reported that cRel and IκBζ regulate the activity of NF-κB in an opposite manner compared to IκB$_{NS}$. For instance, in contrast to IκB$_{NS}$, Bcl3 inhibits the expression of TNFα by its cooperative binding with p50 to the TNFα promoter [108]. Furthermore, while IκB$_{NS}$ inhibits the expression of IL6, Bcl3 is dispensable for the its expression [108] and IκBζ enhance the IL6 production [119]. IκBζ regulates this induction by its association with p50 (presumably p50 of p50/RelA heterodimers). Both are recruited to the IL6 promoter and support the IL6 expression [119]. In addition, IκB$_{NS}$ is important for the expression of IL2 and IFNγ in thymocytes and T cells [128]. IκB$_{NS}$ enhances the expression of IL2 via the association to its promoter, presumably by the interaction to cRel or p50, but also other still unknown DNA-binding proteins are suggested [128]. Since IκB$_{NS}$ itself has no DNA binding domain, it needs to cooperate with DNA-binding proteins to bind to promoters [128].

Interestingly, a recent report on IκB$_{NS}$ revealed its function for Treg cell development [134]. IκB$_{NS}$-deficient mice showed a significant reduction of mature Treg cells, although Treg precursor cells (GITR$^+$CD25$^+$Foxp3$^-$) accumulated in the thymus. Furthermore, a transient expression of IκB$_{NS}$ during thymic Treg development was observed. It was shown that IκB$_{NS}$ is essential for the transition of immature thymic Treg precursor cells into mature Foxp3$^+$ Treg cells, but does not modulate the suppressive capacity of Treg cells. IκB$_{NS}$ associates with p50 and cRel on the Foxp3 promoter and the conserved non-coding

sequence 3 (CNS3) of the Foxp3 gene and, thereby, IκB$_{NS}$ induces Foxp3 expression. It was further suggested that IκB$_{NS}$ coordinates chromatin remodelling at the Foxp3 locus via recruitment of histone modifying enzymes. [134] Taken together, IκB$_{NS}$ specifically regulates cytokine expression by modulating the NF-κB activity at certain promoters. Furthermore, it is important for the transition of Treg cell precursors to mature Treg cells via the induction of Foxp3.

1.10 Aims of the thesis

The transcription factor NF-κB is essential in cell survival and development. Furthermore, NF-κB induces host defence during pathogenic invasion by activating the transcription of a broad range of proteins. [93,95–97] Diverse cancers, inflammatory and autoimmune diseases are initiated by a dysfunction of lymphocytes induced by a hampered NF-κB signalling [95,135]. For this reason NF-κB became an important target for pharmaceutical treatment [95]. Most promising are the members of the IκB protein family, due to their ability to modulate the function of a specific NF-κB subunit or specific NF-κB pathways [100,102,126,136]. The aim of this thesis was to obtain a better understanding of the role of IκB$_{NS}$ in the regulation of NF-κB activity in health and disease.

Since IκB proteins regulate the development and functionality of B and T cells, as well as the expression of cytokines, in this thesis it was analysed if IκB$_{NS}$ has an effect on the composition of the B cell subsets *in vivo*. Furthermore, it was investigated if IκB$_{NS}$ is involved in the TCR-triggered cell activation or the expression of NF-κB subunits. It is known that the nuclear IκBζ is important in T$_H$17 cell development and the expression of IL17A, therefore the involvement of IκB$_{NS}$ in T$_H$17 cell differentiation was analysed *in vitro*. Furthermore, the effect of the IκB$_{NS}$ deficiency on the cytokine expression of T$_H$17 cells was examined. The function of IκB$_{NS}$ within the progression of disease as well as T$_H$17 cell formation was analysed/ examined by induction of EAE, DSS and transfer colitis in mice defective for IκB$_{NS}$ or by infecting these mice with *Citrobacter rodentium*.

2 Material and methods

2.1 Molecular biological methods

2.1.1 Eukaryotic RNA or DNA extraction

Eukaryotic primary cells were isolated and purified. RNA was isolated via the Qiagen RNeasy® Mini Kit and QIA shredder™ according to the supplier´s manual. Afterward the RNA concentration was determined by absorption measurement at 260 nm with the spectrophotometer Nanodrop 1000 (peqlab).

Tail biopsies from mice were used for the isolation of PCR-ready DNA. The mouse tissue was lysed using the KAPA mouse genotyping hot start kit from peqlab as described in instruction manual. 1µl of the DNA-containing supernatant was used directly in polymerase chain reaction to determine the genotype of the particular mice.

2.1.2 cDNA synthesis by reverse transcription

For PCR analysis 100ng of the previously purified RNA (2.1.1) was transcribed into complementary DNA (cDNA) according to the protocol of the RevertAid^{TM} Premium First Strand cDNA Synthesis Kit (Thermo Scientific). For RNA transcription oligo-dT primers were used. The cDNA-synthesis mix was incubated in the peqSTAR 96 Universal thermocycler (peqlab).

2.1.3 Polymerase chain reaction

After the reverse transcription step of mRNA into cDNA (2.1.2) or the isolation of DNA (2.1.1), the cDNA was amplified using the ready-to-use 2x KAPA2G Fast ReadyMix (peqlab). Like a normal wild-type Taq polymerase the KAPA2G Fast DNA polymerase has no proofreading activity and the specificity with 1 error per 1.7 x 10^5 incorporated nucleotides is similar too. For one polymerase chain reaction (PCR) the components shown in Table 1 were mixed in the indicated order.

The PCR was performed in the peqSTAR 96 Universal thermocycler (peqlab) and various salt free primer (Eurofins MWG Operon, Table 2) were used to identify the expression of different genes. The chosen annealing temperature was 3 °C below the melting temperature (T_M) of the particular primer pair. Below in Table 3 a usual PCR program is shown.

Table 1: Components for polymerase chain reaction.

Component	Amount	Final concentration
cDNA template	1-2 µl	50-100 ng
2x Kapa2G Fast ReadyMix	12.5 µl	1x
Forward primer 100 µM	1 µl	0.4 µM
Reverse primer 100 µM	1 µl	0.4 µM
Dest. water	Add to 25 µl	

Table 2: Oligonucleotides used in PCR.

Primer name	Sequence (5´→3´)	T_M	Application
β-actin fwd	TGT TAC CAA CTG GGA CGA CA	60.4	RT PCR
β-actin rev	TCT CAG CTG TGG TGG TGA AG	62.4	RT PCR
IκB$_{NS}$ fwd	GCT GTA TCC TGA GCC TTC CCT GTC	66.1	RT PCR
IκB$_{NS}$ rev	GCT CAG CAG GTC TTC CAC AAT CAG	64.4	RT PCR
IκB$_{NS}$ fwd	CTC CTC CCA GGC TGT GTT TA	59.4	genotyping
IκB$_{NS}$ rev	CAT TTA GTG CCC CTG GAC AT	57.3	genotyping
IκB$_{NS}$ Neo	AAG CGC ATG CTC CAG ACT GCC TT	64.2	genotyping
IFNγ fwd	TT GAG GTC AAC AAC CCA CA	58.3	RT PCR
IFNγ rev	CGC AAT CAC CGT CTT GGC TA	60.4	RT PCR
GATA3 fwd	CTT ATC AAG CCC AAG CGA AG	60.4	RT PCR
GATA3 rev	AGA GAT GTG GCT CAG GGA TG	62.4	RT PCR
Tbet fwd	GGT GTC TGG GAA GCT GAG AG	64.5	RT PCR
Tbet rev	TCT GGG TCA CAT TGT TGG AA	58.3	RT PCR
RORγ fwd	TTT TGA GGA AAC CAG GCA TC	58.3	RT PCR
RORγ rev	TTG GCA AAC TCC ACC ACA TA	58.3	RT PCR
IL17 fwd	GCC CTC CAC AAT GAA AAG AA	58.3	RT PCR
IL17 rev	TTT CAC CCC ATT CAG AGG AG	60.4	RT PCR

Table 3: Program flow of PCR.

Cycle step	Temperature	Time	Number of cycles
Inital denaturation	94 °C	5 min	
Denaturation	94 °C	30 sec	
Annealing	x °C	30 sec	25-32
Elongation	72 °C	30 sec	
Terminal elongation	72 °C	10 min	

2.1.4 Agarose gel electrophoresis

PCR products were separated by size by gel electrophoreses. Therefore a 1- 2 % agarose gel containing 0.5 µg/ml ethidium bromide in 1x TAE buffer (40 mM Tris Base, 20 mM acetic acid, 1 mM EDTA, pH 8.5) was prepared. For separation the gel electrophoresis system perfectBlue^{TM} (peqlab) and the power supply EPS 301 (Amersham Bioscience) was used at 12V for 45- 60 min. The gel was documented in a gel documentation system from Intas via ultraviolet light (λ=254 nM). The GeneRuler^{TM} Low-Rage DNA ladder from Thermo Scientific was used to determine the DNA fragment size.

2.1.5 Quantitative real-time detection PCR

For quantitative real-time detection PCR (qPCR) 1x10^6 *in vitro* differentiated T cells (see 2.3.5) were harvested and washed. The RNA was isolated as described in 2.1.1 and used for cDNA syntheses (see 2.1.2). The cDNA was used as template in qPCR using the cyanine- dye SYBER Green (Roche). During the qPCR progression the SYBER Green intercalates into double-stranded DNA. The resulting DNA- fluorescent dye- complex is absorbing blue light (494 nm) and the emitted light was measured after each qPCR cycle. Ubiquitin C (UBC) was used as housekeeping gene for later normalisation. Measurements were run in duplicates using the LightCycler® 480 (Roche) system and the primers shown in Table 4. The qPCR was performed together with PhD student Carlos Plaza-Sirvent from the department Systems-oriented Immunology and Inflammation Research at the HZI (Braunschweig).

Table 4: Quantitative real-time detection PCR primer.

Primer name	Sequence (5´→3´)
GM-CSF fwd and rev	QuantiTect primer assay Mm_Csf2_1_SG, Cat.Nr. QT00251286, (NM_009969), Qiagen
IFNγ fwd	ATC TGG AGG AAC TGG CAA AA
IFNγ rev	TTC AAG ACT TCA AAG AGT CTG AGG TA
IL10 fwd	TGC CAA GCC TTA TCG GAA ATG
IL10 rev	CCC AGG GAA TTC AAA TGC TCC
IL17A fwd	CAG GGA GAG CTT CAT CTG TGT
IL17A rev	GCT GAG CTT TGA GGG ATG AT
IL17F fwd	CTG TTG ATG TTG GGA CTT GCC
IL17F rev	TCA CAG TGT TAT CCT CCA GG
IL2 fwd	CCT GAG CAG GAT GGA GAA TTA CA
IL2 rev	TCC AGA ACA TGC CGC AGA G
IL6 fwd	GGT ACA TCC TCG ACG GCA TCT
IL6 rev	GTG CCT CTT TGC TGC TTT CAC
IκB$_{NS}$ fwd	GGG CTC TTTT CCC ATT CTC T
IκB$_{NS}$ rev	GGA CAC AAT CCA GCC TGT CT
MIP1α fwd	ATG AAG GTC TCC ACC ACT G
MIP1α rev	GCA TTC AGT TCC AGG TCA
RORγt fwd	TGC AAG ACT CAT CGA CAA GG
RORγt rev	AGG GGA TTC AAC ATC AGT GC
Tbet fwd	CAA CCA GCA CCA GAC AGA GA
Tbet rev	ACA AAC ATC CTG TAA TGG CTT G
UBC fwd	AAG AGA ATC CAC AAG GAA TTG AAT G
UBC rev	CAA CAG GAC CTG CTG AAC ACT G

2.1.6 Transformation

For the transformation of plasmids into competent *E. coli* Top10 bacteria (Life technologies) the bacteria were thawed on ice. 100 to 200 ng plasmid DNA was added to the E. coli. The bacteria were incubated with the plasmid DNA at 42 °C for 30 sec followed by incubation on ice for 20 min. For heat shock the bacteria were incubated in a water bath at 42 °C for 30 sec followed by relaxing an ice for 2 min. After the addition of 500µl LB-medium (1% w/v tryptone, 0.5% w/v yeast extract, 85.6 mM NaCl, 1 mM NaOH) the bacteria were incubated at 37 °C, 800rpm in the Thermomixer comfort (Eppendorf) for 45 min. The bacteria were plated to LB-agar plates containing the suitable antibiotics (100 µg/ml ampicillin or 50 µg/ml kanamycin). The plates were incubated at 37 °C over night. The next day, colonies were picked into 5 ml LB medium and incubated at 37 °C, 280 rpm over night. 500 µl of the previous culture was inoculated into 200 µl LB-medium containing flasks and incubated at 37 °C, 180 rpm over night. The plasmid DNA was isolated using the QIAfilter™ Plasmid Maxi kit (Qiagen) following the suppliers manual. After isolation the DNA concentration was determined by absorption measurement at 260 and 280 nm using the Nanodrop 1000 spectrophotometer from peqlab.

2.1.7 Cell transfection and lentiviral transduction

A20 cells were stably transduced by lentiviral infection of shRNA (Table 5) which targets $I\kappa B_{NS}$. The $I\kappa B_{NS}$ shRNA was generated and purchased by Addgene using the pLKO.1 (puro) cloning vector. The shRNA was cloned into the lentiviral vector pLKO.1 which were transfected together with the lentiviral envelop vector pMD2.G (Addgene) and the lentiviral gag-pol expression plasmide pCMV-dR8.2dvpr (Addgene) into HEK293T cells using JetPEI (polyplus transfection) according to the manufacturer´s manual. After 24 h the medium (DMEM containing 10% fetal calf serum and 50 µg/ml penicillin/ streptomycin) was exchanged. 48 h after transfection, the lentiviral particle were collected, filtered (0.45µm PVDF-Filter, Merck Millipore) and frozen. A20 cells were infected by adding 1ml lentiviral particle plus 8 µg/ml polybrene (Sigma Aldrich) to $2*10^6$ cells followed by centrifugation at 2,000 rpm at 25 °C for 2 h. After the incubation over night at 37 °C, stably transfected cells were selected by adding RPMI1640 (10% fetal calf serum, 50 µg/ml penicillin/ streptomycin, 0.05 mM β-mercaptoethanol) containing 5 µg/ml puromycin (Sigma Aldrich) for 2 weeks. The specific knockdown of $I\kappa B_{NS}$ was verified by Western blotting.

$I\kappa B_{NS}$ shDNA was also introduced to A20 cells by electroporation. Therefore cells were washed in the serum free medium Opti-MEM® (Invitrogen) and resuspended in 400 µl of Opti-MEM®. After the transfer into a cuvette (gap size 4 mm, BTX® Harvard Apparatus), 10 µg DNA was added and pulsed in a BioRad Gene Pulser® II with 300 V/ 700 µF, high capacitance. Cells were transferred to cell culture flask with RPMI1640 (10% fetal calf serum, 50 µg/ml penicillin/ streptomycin, and 0.05 mM β-mercaptoethanol) and led rest for one day, followed by a 2 weeks selection phase with 5 µg/ml puromycin (Sigma Aldrich).

Table 5: Small-hairpin (sh) RNA for $I\kappa B_{NS}$ knock down.

Primer name	Sequence (5´→3´)	Restriction enzyme
shRNA1 (fwd)	GTG CAG ATG TTA CTG CAA ATG CTC GAG CAT TTG CAG TAA CAT CTG CAC	Age I (ACCGGT)
shRNA1 (rev)	CAA AAAGTG CAG ATG TTA CTG CAA ATG CTC GAG CAT TTG CAG TAA CAT CTG CAC	EcoR I (GAATTC)
shRNA2 (fwd)	GGG GCT TTC TAG GTG STC TCG AGA TCA CCT AGA AAG CCC CTT TTT G	Age I (ACCGGT)
shRNA2 (rev)	CAA AAA GGG GCT TTC TAG GTG ATC TCG AGA TCA CCT AGA AAG CCC C	EcoR I (GAATTC)
shRNA3 (fwd)	TCG AGC CCA CTT GAT TGC TCG AGC AAT CAA GTG GGC TCG ATT TT G	Age I (ACCGGT)
shRNA3 (rev)	CAA AAA TCG AGC CCA CTT GAT TGC TCG AGC AAT CAA GTG GGC TCG A	EcoR I (GAATTC)
shRNA4 (fwd)	CCC AGA ACC TGG ACT GAC TCG AGT CAG TCC AGG TTC TGG GTT TTT G	Age I (ACCGGT)
shRNA4 (rev)	CAA AAA CCC AGA ACC TGG ACT GAC TCG AGT CAG TCC AGG TTC TGG G	EcoR I (GAATTC)

2.2 Protein biological approaches

2.2.1 Cell lysis and determination of protein concentration

To get the total-cell-lysate 5-10x10^6 cells were washed twice in 1x PBS ($CaCl_2$ and $MgCl_2$ free, invitrogen) and lysed in 50 µl TPNE lysis buffer (Table 6) with 1 mM phenylmethylsulfonyl fluoride (PMSF), 1x protease inhibitor mix (Table 6) and 0.4 mM

sodium orthovanadate (Sigma-Aldrich). The cell buffer mix was incubated for 20 min on ice followed by centrifugation at 14,000 rpm, 4 °C for 15 min in an Eppendorf table centrifuge 5417R. The supernatant was transferred into a new reaction tube for following experiments.

Table 6: Cell lysis buffers and additives.

Buffer or additive	Contents
TPNE lysis buffer	1x PBS (invitrogen) 300 mM NaCl 2 mM EDTA 1 % v/v Titron X-100
100x protease inhibitor mix	100 µg/ml aprotinin 100 µg/ml leupeptin 100 µg/ml pepstatin A 100 µg/ml chymostatin

The protein concentration of the lysate was determined by bicinchoninic acid (BCA) assay as described in the supplier´s manual (Thermo Scientific). The protein concentration was detected in the Infinite M200 microplate- reader (TECAN) by absorbance measurement at 562 nm.

2.2.2 Fractionated cell lysis

To get cytoplasmic and nuclear proteins separated from each other a two step lysis was performed. For the cytoplasmic extracts the washed cells were lysed for 10min on ice in buffer A (10 mM HEPES, pH 7.9, 1.5 mM $MgCl_2$, 10 mM KCl, 300 mM sucrose, 0.5 % NP-40) supplemented with 1 mM phenylmethylsulfonyl fluoride (PMSF), 1x protease inhibitor mix (Table 6) and 0.4 mM sodium orthovanadate (Sigma-Aldrich). After centrifugation (15 min, 2500 g) the supernatant representing the cytoplasmic fraction was transferred into a new reaction tube for following experiments. The pellet was washed two times in 500µl buffer A and resuspended in buffer B (10 mM HEPES, pH 7.9, 5 mM $MgCl_2$, 100 mM KCl, 1 mM DTT, 10 % glycerol, 0.1 % NP-40) again supplemented with 1 mM phenylmethylsulfonyl fluoride (PMSF), 1x protease inhibitor mix (Table 6) and 0.4 mM sodium orthovanadate (Sigma-Aldrich). The nuclear pellets were sonicated in three cycles of 15 sec sonication at the highest power setting plus 15 sec chilling using a Bioruptor™ NextGen (Diagenode). Residues of the nuclear wall were removed by

centrifugation for 5 min, 10,500 g at 4 °C. The nuclear fraction was transferred into a new reaction tube for following experiments.

2.2.3 SDS-polyacrylamide gel electrophoresis (SDS-PAGE)

For protein separation via SDS-polyacrylamid gel electrophoresis (SDS-PAGE) 20-40 µg of the protein lysate was mixed with 5x reducing sample buffer (RSB, Table 7) to a final concentration of 1x RSB. The RSB-lysate mix was boiled for 5 min at 95 °C.

Table 7: SDS-Page buffers.

Buffer or additive	Contents
5x reducing sample buffer (RSB)	50 mM Tris, pH 6.8 50 % v/v glycerol 10 % w/v SDS 25 % v/v β-mercaptoethanol 0.25 mg/ml bromphenol blue
1x Running buffer	25 mM Tris, pH 8.0 192 mM glycerol 1 % v/v SDS

Proteins were separated in a 12 % polyacrylamide gel (Table 8) in 1x running buffer (Table 7) at 80-120 V using BioRad "Tetra Cell". To determine different protein sizes the standard PageRuler^{TM} protein ladder (Thermo Scientific) was used.

Table 8: Composition of a 12 % polyacrylamide gel.

Solution	Concentration
Water	0.33 %
30 % acrylamide mix (Rotiphorese® Gel 30)	12 %
1.5 M Tris (pH 8.8)	3.75 mM
10 % SDS	0.1 %
10 % APS	0.1 %
TEMED (99% p.a.)	0.04 %

For further analysis the proteins were blotted onto a PVDF membrane (see 2.2.4) or the gel was stained with Coomassie Brilliant Blue (BioRad). To prepare the SDS-PAGE gel for Coomassie® Brilliant Blue staining the gel was washed 3 times for 10 min in MilliQ

water. The Coomassie® Brilliant Blue solution was added to the gel for 1 to 2 hours followed by five washing steps or washing over night to remove background staining.

2.2.4 Western blotting

Proteins separated by SDS-PAGE were transferred to PVDF membrane (GE Healthcare) using a BioRad "Criterion Blotter" in 1x transfer buffer (Table 9) at 80 V for 1- 1.5 h. Afterwards the membrane was incubated in blocking buffer (Table 9) for 1h at room temperature (RT) followed by the incubation in primary antibody (Table 10, with reactivity against hu- human, ms- mice, rt- rat) diluted in blocking buffer over night at 4 °C.

Table 9: Buffers for Western blotting.

Buffer or additive	Contents
1x Transfer buffer	25 mM Tris, pH 8.0 192 mM glycerol 20 % v/v methanol
10x TBS	137 mM NaCl 2.68 mM KCl 24.76 mM Tris
Blocking buffer	1x TBS 5 % w/v non-fat dry milk 0.05 % v/v Tween-20
Wash buffer	1x TBS 0.05 % v/v Tween-20

The next day the membrane was washed three times 10 min in wash buffer to remove unbound antibodies. After the incubation in horseradish peroxidase-conjugated secondary antibodies (1 h, RT, Table 11) the membrane was washed as described above. Finally, the membrane was incubated with chemiluminescent substrates of Thermo Scientific, SuperSignal® West Dura Extended Duration Substrate or SuperSignal® West Femto Maximum Sensitivity and developed in the Fusion FX-7 camera (Vilber Lourmat). If required, the volume of bands were quantified with the program BIO-1D (Peqlab). For further re-use of the blotted membrane the bound antibodies were removed by using the ReBlot plus mild antibody stripping solution from Merck Millipore according to the company´s protocol. For the re-use of blotted membrane with anti- phosphorylated protein antibodies the background of the first anti-phosphorylated protein antibody was reduced by

the incubation with 1 % azide solution in washing buffer for 35 min. After re-blotting the membrane was blocked again in blocking buffer.

Table 10: Primary antibodies for Western blotting.

Antibody	Clone/ notation	Isotype	Species	Reactivity	Company
β-actin	AC-74	IgG2a	mouse	hu, ms	Sigma Aldrich
α-tubulin	DM-1A	IgG1	mouse	hu, ms	Sigma Aldrich
cRel	290512	IgG2a	rat	ms	R&D
Erk	9102	IgG	rabbit	hu, ms, rt	Cell Signaling
IκB$_{NS}$		IgG	rabbit	ms	Self-made
IκB$_{NS}$	138	IgG2b	mouse	hu, ms	Self-made
IκBα	C-21	IgG	rabbit	hu, ms, rt	Santa Cruz
p38	9212	IgG	rabbit	hu, ms	Cell Signaling
p50/105	E381	IgG	rabbit	hu, ms, rt	Epitomics
p52/100	4882	IgG	rabbit	hu, ms, rt, mk	Cell Signaling
p65	C-20	IgG	rabbit	hu, ms, rt	Santa Cruz
P-Akt	4060	IgG	rabbit	hu, ms, rt	Cell Signaling
P-Erk	4370	IgG	rabbit	hu, ms, rt	Cell Signaling
P-IκBα	2859	IgG	rabbit	hu, ms, rt	Cell Signaling
P-p38	9211	IgG	rabbit	hu, ms	Cell Signaling
P-SAPK-JNK	9251	IgG	rabbit	hu, ms, rt	Cell Signaling
P-Tyrosine		IgG	mouse	ms	Self-made
RelB	C-19	IgG	rabbit	ms	Santa Cruz

Table 11: Horseradish peroxidase-conjugated secondary antibodies for Western blotting.

Antibody	Species	Dilution	Company
mouse IgG	goat	1:20,000	Southern Biotchnology
mouse IgG, Fab-Fragment	goat	1:20,000	Dianova
mouse IgG1	goat	1:20,000	Southern Biotchnology
mouse IgG2a	goat	1:20,000	Southern Biotchnology
mouse IgG2b	goat	1:20,000	Southern Biotchnology
rabbit IgG, Fab-Fragment	goat	1:10,000	Dianova
rabbit IgG	goat	1:20,000	Southern Biotchnology
rat IgG	goat	1:20,000	Southern Biotchnology

2.2.5 Urea-PAGE

To test proteins for their dimer stability the samples were prepared as described in 2.2.3. SDS- PAGE and Urea- PAGE have the same composition except that the Urea- PAGE gel additionally contains 6M urea in both the stacking and the separating gel. For further analysis the proteins were blotted onto a PVDF membrane (see 2.2.4).

2.2.6 Immunoprecipitation

To get a enrichment of a particular protein out of a cell lysat a immunoprecipitation was performed. Protein A sepharose beads (30µl of 1x PBS containing 50% protein A sepharose, Sigma Aldrich) were washed three times with 500µl 1x PBS (invitrogen). Zentrifugation steps were performed at 4 °C, 6000rpm for 1min. 200µl lysis puffer with 2µg $I\kappa B_{NS}$ antibody (selfmade, mouse IgG2b or rabbit IgG $I\kappa B_{NS}$ antibody) were added to the beads. After the incubation (4 h, rotation at 4 °C) the protein A sepharose beads were washed three times with 500µl lysis buffer. A20 cells (B cell line) were lysed as described in 2.2.1 or 2.2.2 and the lysate was added to the antibody labelled beads. The labelled protein A sepharose beads and the cell lysate were incubated over night while rotating at 4 °C. The beads were washed three times with 500µl 1x PBS (invitrogen) to get rid of

unbound protein. The beads were re-suspended in 20µl 1x RSB (Table 7), incubated for 5 min at 95 °C and analysed by SDS-PAGE and Western blotting (2.2.3 and 2.2.4).

2.2.7 MicroLink™ Protein Coupling Kit

To get an enrichment of a particular protein free from antibody contamination the MicroLink™ Protein Coupling Kit from Thermo Scientific was used. According to the manual rabbit $I\kappa B_{NS}$ antibodies or rabbit IgG antibodies were bound to the column. For the coupling of rabbit $I\kappa B_{NS}$ antibody 300µl of a 1mg/ml solution (in binding buffer) and for the rabbit IgG antibody 600µl of a 0.5mg/ml solution (in binding buffer) was used. $1.5*10^8$ cells were lysed (2.2.1) in 2ml TPNE lysis buffer (Table 6) with 1 mM phenylmethylsulfonyl fluoride (PMSF), 1x protease inhibitor mix (Table 6) and 0.4 mM sodium orthovanadate (Sigma-Aldrich), the lysate was added to the affinity column. After incubation and elution steps as described in the instruction manual the eluate was analysed in SDS-PAGE and western blotting assay (2.2.3 and 2.2.4) or the SDS-PAGE gel was stained with Coomassie Brilliant Blue (BioRad, 2.2.3).

2.3 *In vitro* techniques

2.3.1 Cultivation of A20 cell line

The B cell line named A20 was cultured in culture flasks, 6-well, 12-well or 96-well (NUNC- Thermo Scientific) in the incubator HERAcell 240i (Thermo Scientific) at 37 °C, 5% CO_2, and 95% air humidity. The A20 cells were cultured in RPMI 1640 (Gibco) supplemented with 10% fetal calf serum (FCS, PAA), 50 µg/ml penicillin/ streptomycin (Gibco), and 0.05 mM β-mercaptoethanol (Gibco). For the handling of the cell line the following materials were used: 1.5 ml and 2 ml reaction tubes (Sarstedt), sterile 10 µl, 200 µl and 1000 µl pipette tips (Starlab), 5 ml, 10 ml and 25 ml pipettes (Sterilin - Thermo Scientific), 15 ml and 50 ml reaction tubes (Greiner-bio-one), 45 µm and 22 µm sterile syringe filters (Merck Millipore), centrifuges 5810R (Eppendorf). Cells were handled in sterile hoods SterilGARD® III Advance (The Baker Company). Cell numbers were determined by Neubauer improved cell counting chambers (BRAND scientific) or Cellometer™ Auto T4 (Nexcelom).

2.3.2 Organ isolation and single cell suspension preparation

For the removal of murine lymphoid organs like the peripheral lymph nodes (pLN), mesenteric lymph nodes (mLN) and the spleen mice were euthanised by carbon dioxide inhalation. The organs were collected in 1xPBS (invitrogen) containing 0.2 % BSA. A 70 µm nylon mesh was used for the homogenisation of the organs. After a washing step with 1x PBS containing 0.2 % BSA the erythrocytes were removed by the incubation with ACK lysis buffer (0.15 M NH_4Cl, 1 mM $KHCO_3$, 0.1 mM EDTA, pH 7.3) for 2 min at room temperature. After another washing step the primary cells were used for the isolation of naïve T cells by flow cytometry (2.3.4) or directly in cell culture. The primary cells were cultured in primary T cell medium (Table 12) till further use.

Table 12: Composition of primary T cell medium.

Additive	Concentration	Company
IMDM		Gibco
Fetal calf serum	10 %	Biochrom
Penicillin/streptomycin	50 µg/ml	Gibco
HEPES	25 mM	Biochrom
β-Mercapthoethanol	0.05 mM	Gibco
Non-essential amino acids	1 %	Gibco
Sodium pyruvate	1 mM	Gibco

2.3.3 Flow-cytometric analysis

For the cell analysis via flow cytometry cells were harvested and $1x10^6$ cells were washed twice in 1 ml 1x PBS (invitrogen). All centrifugation steps were performed at 4 °C, 1500 rpm for 5 min. A live/dead staining was performed in 100 µl 1x PBS (invitrogen) containing one of the LIVE/DEAD® dyes from Life technologies (Table 13, 30 min, 4 °C, in the dark).

Previously to surface staining the cells were washed again. Surface markers were stained with fluorochrome-conjugated antibody (Table 14) in flow cytometry buffer (1x PBS, 2% w/v BSA, 0.01% v/v NaN_3) at 4 °C, for 15 to 20 min in the dark. By a following wash step with flow cytometry buffer unbound antibodies were washed away.

Table 13: Fluorescent dyes for flow cytometric analysis.

Dye	Excitation	Emission	Company
LIVE/DEAD® near IR fluorescent reactive dye	750 nm	775 nm	Life technologies
LIVE/DEAD® Blue fluorescent reactive dye	350 nm	450 nm	Life technologies
LIVE/DEAD® aqua fluorescent reactive dye	367nm	526	Life technologies

If intracellular cytokine staining is requested the cells were stimulated for 4 hours with phorbol myristate acetate (PMA, 10 ng/ml, Sigma Aldrich) and ionomycin (1 µM, Sigma Aldrich). For the last 2 hours Brefeldin A (10 µg/ml, Sigma Aldrich) was added as well. Afterwards the cells were fixed and permeabilised using the Foxp3 Staining Buffer Set (Miltenyi Biotech). To prepare a fixation/ permeabilisation working solution one part Fixation/ Permeabilisation Concentrate was diluted with three parts Fixation/ Permeabilisation Diluent. Cells were incubated with 100 µl fixation/ permeabilisation working solution for 30 min (4 °C, in the dark) and washed with 1 ml 1x permeabilisation buffer prepared from 10x permeabilisation buffer with deionised/ distilled water. The intracellular cytokine staining was performed in 100 µl 1x permeabilisation buffer with the according amount of RORγ, IFNγ and/or IL17A antibody (4 °C, for 30 min in the dark, Table 14). Finally cells were washed in 1x permeabilisation buffer and used in flow cytometry analysis. The labelled cells were analysed via the BD™ LSR II Flow Cytometer System or the BD LSRFortessa™ (BD Bioscience).

To assay apoptosis in flow cytometry analysis cells were washed in 1x PBS and incubated in 250µl Nicoletti buffer (2% v/v Triton X-100, 0.1% $C_6H_5Na_3O_7$, 50 µg/ml PI) for at least 1 h at 4 °C in the dark. After flow cytometric measurement cells with sub-G1 DNA were quantified.

Table 14: Fluorochrome- conjugated antibody for flow cytometry.

Reactivity	Fluorochrome	Clone/ notation	Isotype	Company
CD3	APC-eFluor780	17A2	Rat IgG2b.k	eBioscience
CD3	FITC	145-2C11	hamster IgG1, κ	BD
CD3	PECy7	145-2C11	hamster IgG	eBioscience
CD4	AlexaFluor488	RM4-5	rat IgG2a, κ	BD
CD4	APC	RM4-5	rat IgG2a, κ	eBioscience
CD4	FITC	RM4-5	rat IgG2a, κ	eBioscience
CD4	Horizon V500	RM4-5	rat IgG2a, κ	BD
CD4	PacificBlue	RM4-5	rat IgG2a, κ	BioLegend
CD4	PE	RM4-5	rat IgG2a, κ	BD
CD4	PerCP-Cy5.5	RM4-5	Rat IgG2a,k	eBioscience
CD8	APC	53-6.7	mouse IgG2a, κ	BD
CD8	FITC	53-6.7	mouse IgG2a, κ	BD
CD8	PerCP-eFluor 710	53-6.7	rat IgG2a, κ	eBioscience
CD11b	PECy7	M1/70	mouse IgG2b, κ	eBioscience
CD11c	APCeFluor780	N418	hamster IgG	eBioscience
CD19	FITC	1D3	mouse IgG2a, κ	BD
CD24	FITC	M1/69	mouse IgG2b, κ	BD
CD25	APC	PC61	rat IgG1, λ	BD
CD44	PE	IM7	mouse IgG2b, κ	eBioscience
CD62L	Pacific blue	MEL-14	rat IgG2a, κ	eBioscience
CD62L	PerCPCy5.5	MEL-14	rat IgG2a, κ	eBioscience
F4/80	PE	BM8	rat IgG2a, κ	eBioscience
Foxp3	eFluor450	FJK-16s	Rat IgG2a,k	eBioscience
Gr1	Pacific blue	RB6-8C5	rat IgG2b, κ	eBioscience
IFNγ	FITC	XMG1.2	rat IgG1, κ	eBioscience
IFNγ	PE	XMG1.2	rat IgG1, κ	eBioscience
IFNγ	PE-Cyan7	XMG1.2	Rat IgG1,k	eBioscience
IL17A	APC	eBio17B7	rat IgG2a, κ	eBioscience
RORγt	PE	Q31-378	mouse IgG2a, κ	BD
RORγt	PE	B2D	rat IgG1,k	eBioscience

2.3.4 Cell isolation by flow cytometry

As described before lymph nodes and spleens were isolated (2.3.1) and stained with surface markers (2.3.3). In cooperation with Dr. Lothar Groebe (flow cytometry facility of the Helmholtz Center for Infection Research, Braunschweig, Germany) the cells were isolated in the FACS Aria II (BD Bioscience) or the MoFlo (Beckman and Coulter). Cells were collected in tubes containing 1ml 1xPBS with 0.2 % BSA.

2.3.5 In vitro generation of T helper cell subsets

$CD4^{+}CD62L^{high}CD25^{-}$ naïve T cells were isolated as described in 2.3.4 and re-suspended in primary T cell medium (Table 12). Per 96- well $2*10^5$ cells were activated with plate bound anti-CD3 and anti-CD28 (Table 15) or Dynabeads® Mouse T-Activator CD3/CD28 (invitrogen) in a ratio of 1 to 1.25 were used. The cells were cultured in the presence of priming cytokines and inhibitory antibodies according to the respective T helper subset (Table 15). At day 4 or 5 the cells were analysed.

Table 15: Additives for T helper cell polarisation.

T_H subset	Additive	Concentration	Clone	Company
Non-priming (T_H0)	αCD3	2 µg/ml	145-2C11	BioLegend
	αCD28	2 µg/ml	37.51	BioLegend
	αIL4	10 µg/ml	11B11	Self made
	αIFNγ	10 µg/ml	XMG1.2	Self made
T_H1	αCD3	2 µg/ml	145-2C11	BioLegend
	αCD28	2 µg/ml	37.51	BioLegend
	αIL4	10 µg/ml	11B11	Self made
	IL12	10 ng/ml	recombinant	R&D
T_H17	αCD3	3 µg/ml	145-2C11	BioLegend
	αCD28	5 µg/ml	37.51	BioLegend
	αIL2	10 µg/ml	JES6-1A12	BioLegend
	αIFNγ	10 µg/ml	XMG1.2	Self made
	pTGFβ	2 ng/ml	recombinant	R&D
	IL6	30 ng/ml	recombinant	R&D
	IL1β	10 ng/ml	recombinant	R&D
	TNFα	20 ng/ml	recombinant	Preprotech

T_H subset	Additive	Concentration	Clone	Company
T_H17-basic	αCD3	2 µg/ml	145-2C11	BioLegend
	αCD28	2 µg/ml	37.51	BioLegend
	αIL4	10 µg/ml	11B11	Self made
	αIFNγ	10 µg/ml	XMG1.2	Self made
	pTGFβ	0,5 ng/ml	recombinant	R&D
	IL6	20 ng/ml	recombinant	R&D
T_H17-IL21	αCD3	2 µg/ml	145-2C11	BioLegend
	αCD28	2 µg/ml	37.51	BioLegend
	αIL4	10 µg/ml	11B11	Self made
	αIFNγ	10 µg/ml	XMG1.2	Self made
	pTGFβ	0,5 ng/ml	recombinant	R&D
	IL6	20 ng/ml	recombinant	R&D
	IL21	80 ng/ml	recombinant	R&D
T_H17-IL23	αCD3	2 µg/ml	145-2C11	BioLegend
	αCD28	2 µg/ml	37.51	BioLegend
	αIL4	10 µg/ml	11B11	Self made
	αIFNγ	10 µg/ml	XMG1.2	Self made
	pTGFβ	0,5 ng/ml	recombinant	R&D
	IL6	80 ng/ml	recombinant	R&D
	IL23	50ng/ml	recombinant	R&D
T_H17-IL21/23	αCD3	2 µg/ml	145-2C11	BioLegend
	αCD28	2 µg/ml	37.51	BioLegend
	αIL4	10 µg/ml	11B11	Self made
	αIFNγ	10 µg/ml	XMG1.2	Self made
	pTGFβ	0,5 ng/ml	recombinant	R&D
	IL6	20 ng/ml	recombinant	R&D
	IL21	80 ng/ml	recombinant	R&D
	IL23	50ng/ml	recombinant	R&D
T_H17-IL1β	αCD3	2 µg/ml	145-2C11	BioLegend
	αCD28	2 µg/ml	37.51	BioLegend
	αIL4	10 µg/ml	11B11	Self made
	αIFNγ	10 µg/ml	XMG1.2	Self made
	pTGFβ	0,5 ng/ml	recombinant	R&D
	IL6	20 ng/ml	recombinant	R&D
	IL1β	20 ng/ml	recombinant	R&D

2.3.6 In vitro expansion of $CD4^+CD25^-$ T cells

After isolation of $CD4^+CD25^-$ T cells (2.3.4) $4*10^6$ of these cells were expanded. First cells were re-suspended in 4 ml RPMI supplemented with 10 % FCS (PAA), 1mM sodium pyruvate (Gibco), 1x non-essential amino acids (Gibco), 50 ng/ml penicilline/ streptomycin (Gibco) and 50 µM β-mercaptoethanol (Gibco). The $CD4^+CD25^-$ T cells were stimulated in a 6-well plate with 1 µg/ml plate bound anti-CD3 and 2 µg/ml soluble anti-CD28 in the present of 10 ng/ml murine IL2. At day 3, cells were transferred to a 10-cm dish into a total volume of 15ml fresh RPMI with supplements (10 % FCS, 1mM sodium pyruvate, 1x non-essential amino acids, 50 ng/ml penicilline/ streptomycin and 50 µM β-mercaptoethanol). Cells were used on day 6 for activation analysis (2.3.7).

2.3.7 *In vitro* activation of *ex vivo* or expanded T cells

$CD4^+$ or $CD8^+$ T cells were isolated by cell isolation (2.3.4) and used directly in activation assay or isolated $CD4^+$ were expanded (2.3.6) before. $5*10^6$ to $10*10^6$ cells were seeded into a 12-well plate and centrifuged down for 2 min, 800rpm at room temperature. Cells were either stimulated with coated anti-CD3 (10µg/ml) plus anti-CD28 (5µg/ml) or PMA (10 ng/ml) plus ionomycin (1 µM) or left untreated. Anti-CD3/CD28 stimulation was performed for 15 min, 30 min, 1 h, 2 h and 4 h or the cells were stimulated for 2 hours with PMA/ ionomycin. After harvesting the cells were washed two times with 1x PBS and lysed for Western Blot (2.2.1, 2.2.3 and 2.2.4).

2.3.8 Proliferation analysis with alamarBlue®

To quantitatively measure the proliferation of $I\kappa B_{NS}$ knockdown A20 cells alamarBlue® was used. AlamarBlue® is an indicator dye containing an oxidation- reduction indicator that changes the fluorescence as well as the colour upon chemical reduction of the culture medium. $1*10^4$ A20 cells were plated to a 96-well. One-tenth of the volume of the well AlamaBlue® was added. The A20 cells were cultured for 8 h to 7 days. Absorbance was measured at 570nm and 600nm using Infinite M200 microplate- reader (TECAN). The percentage of reduction of alamarBlue® was calculated as described in the supplier manual.

2.3.9 Proliferation analysis via CFSE or CellTrace™ Violet Proliferation Dye staining

To analyse the proliferation of T cells naïve T cells were isolated (2.3.4). Prior to the cultivation the cells were stained with carboxyfluorescein succinimidyl ester (CFSE, eBioscience) or CellTrace™ Violet Proliferation dye (invitrogen). Therefore, T cells were washed two times with 1x PBS (invitrogen) and re-suspended in 1xPBS to a concentration of $2*10^6$/ml. CFSE or CellTrace™ Violet Proliferation Dye were added to a final concentration of 5µM/ml. Cells were incubated for 10 min (CFSE) or 20 min (Violet Proliferation Dye) at 37 °C in the dark. After two washing steps with pre-warmed medium cells were cultured (2.3.5). At day 4 cells were stained for surface markers and intracellular proteins as in 2.3.3 and analysed in flow cytometry.

2.3.10 Enrichment of T_H17 cells via mouse IL17 Secretion Assay

As described in 2.3.4 and 2.3.5 naïve T cells were isolated and cultured under T_H17 polarising conditions. At day 4 the cells were stimulated with PMA (10ng/ml, Sigma Aldrich) and ionomycin (1µM, Sigma Aldrich) for 3 hours at 37 °C. For the following enrichment of IL17 positive cells the mouse IL17 secretion assay from Miltenyi was used. Two washing steps with MACS buffer (1x PBS, pH 7.2, 0,5% bovine serum albumin, 2mM EDTA) were performed before the cells were coated with a mouse IL17 catch reagent (directed to CD45). For the IL17 secretion period of 45 min the cells were diluted with warm medium and $1*10^7$ cells in 15 ml medium were incubated in a 15 ml Falcon tube under slow continuous rotation using a MACSmix Tube Rotator. The cells were further incubated with IL17 detection antibodies (biotin labelled), Biotin-PE antibodies and anti-PE MicroBeads followed by a magnetic separation according to the supplier instructions manual. Isolated cells were used to analyse cytokine secretion as described in 2.3.11 or 2.3.12.

2.3.11 Analyses of cytokine expression by Proteom Profiler™ Array

To analyse the cytokine secretion IL17 secreting cells were enriched like in 2.3.10 and $0.8*10^6$ cells were stimulated with PMA (10ng/ml, Sigma Aldrich) and ionomycin (1µM, Sigma Aldrich). After 4 hours the supernatant was taken and used for cytokine analysis using the Proteom Profiler™ Array (R&D Systems). The array membrane was activated and afterwards incubated with the T_H17 supernatant as described in the user manual. Finally, the chemiluminescence of the membrane was measured in the Fusion FX-7 camera (Vilber Lourmat) and the volume of bands were quantified with the program BIO-1D (Peqlab).

2.3.12 Analyses of cytokine expression by FlowCytomix Kit

To analyse the cytokine secretion of T_H17 cells by flow cytometry IL17 secreting cells were enriched (2.3.10) and $0.8*10^6$ cells were stimulated with PMA (10ng/ml, Sigma Aldrich) and ionomycin (1µM, Sigma Aldrich). After 4 hours the supernatant was taken and used for cytokine analysis via FlowCytomix kit from eBioscience. The supernatant was used directly or after 1:10 or 1:50 dilution. The mouse $T_H1/T_H2/T_H17/T_H22$ 13plex Kit FlowCytomix (eBioscience) was combined with five Simplex FlowCytomix kits (eBioscience) required to measure the cytokine secretion of GM-CSF, IL1β, IL17F, IL23 and MIP1α simultaneously with the secretion of the 13plex kit cytokines (IFNγ, IL1α, IL2, IL4, IL5, IL6, IL10, IL13, IL17A, IL21, IL22, IL27 and TNFα). According to the product information the standard curves and samples were prepared and measured by flow cytometry in the BD™ LSR II Flow Cytometer System or the BD LSRFortessa™ (BD Bioscience).

2.4 *In vivo* techniques

2.4.1 Mouse strains

The mice line B6.129/SV-NFKBID(tm1Clay), later named as $I\kappa B_{NS}$-mice were a kind gift of Prof. Dr. Linda Clayton from the Harvard Medical School (Boston, USA)[128]. The B6.PL-Thy1^a/CyJ-mice provided by René Teich from the Helmholtz-Centre for Infections Research (Braunschweig, Germany) was later designated as Thy1.1-mice[137]. Both mice lines were bred under specific pathogen free (SPF) conditions in the animal facility of the Helmholtz-Center for Infection Research (Braunschweig, Germany).

B6.129S7-Rag1^{tm1Mom}-mice, later referred to as RAG1-mice were bred at the animal facility of the Charité (Berlin, Germany)[138].

2.4.2 Dextran sulphate sodium induced chronic colitis (chronic DSS colitis)

To induce murine colitis mice were fed in three cycles with drinking water containing 2% (w/v) dextran sodium sulfate (DSS) for 7 days followed by 14 days feeding with DSS- free water. The inflammation of the colon was assessed at the end of the last cycle. During the progression of colitis the body weight was measured. The consistency of the stool and the rectal bleeding were scored as shown in Table 16. After the three cycles of DSS treatment the length of the colon was measured from the caecum to the anus. Colon samples were fixed in 4% paraformaldehyde. The fixed colon samples were embedded in paraffin and were cut in 2 µm sections. The colon sections were deparaffinised, stained with hematoxylin and eosin (H&E- staining) and scored in a blinded manner. The histological score of the DSS colitis is the sum of the individual scores for inflammatory cell infiltrations and tissue damage as depicted in Table 16. The DSS colitis was performed in cooperation with Dr. Rainer Glauben and Dr. Anja A. Kühl from the Charité, Berlin (Germany).

2.4.3 Adoptive transfer colitis

For adoptive transfer colitis $CD4^+CD25^-$ T cells were isolated from the spleen and lymph nodes of $I\kappa B_{NS}$ wildtype or knockout mice using MACS separation kits (CD4 T cell isolation kit, CD25-PE Kit, Miltenyi) as described in suppliers manual. $5*10^5$ cells in 200µl 1x PBS were injected intraperitoneally into RAG1 mice.

Table 16: Scoring in DSS and transfer colitis.

Score	Symptoms		
	Stool consistency	**Rectal bleeding**	**Colon**
0	Well formed pellets	No hemoccult	No changes
1			• Minimal scattered mucosal inflammatory cell infiltrates • With or without minimal epithelial hyperplasia
2	Pasty and semi-formed, did not adhere to the anus	Positive hemoccult	• Mild scattered to diffuse mucosal cell infiltrates, sometimes extending into submucosa and accociated with erosins • With minimal to mild epithelial hyperplasia, with minimal to mild mucin depletion from goblet cells
3			• Mild to moderate cell infiltrates that were sometimes transmural, often associated with ulceration • With moderate epithelial hyperplasia and mucin depletion
4	Liquid, did adhere to the anus	Gross bleeding	• Marked inflammatory cell infiltrates that were often transmural and accociated with ulceration • With marked epithelial hyperplasia and mucin depletion
5			• Marked transmural inflammation with severe ulceration • With loss of intestinal glands

The body weight was monitored during colitis progression. The consistency of the stool and the rectal bleeding were scored as shown in Table 16. The length of the colon was measured from the caecum to the anus and colon samples were fixed in 4 % paraformaldehyde, embedded in paraffin, cut in 2 µm sections, deparaffinised, stained with hematoxylin and eosin (H&E- staining) and scored in a blinded manner. The transfer colitis histological score is the sum of the individual scores for inflammatory cell infiltrations and tissue damage as depicted in Table 16. The transfer colitis was performed in cooperation with Dr. Rainer Glauben and Dr. Anja A. Kühl from the Charité, Berlin (Germany).

2.4.4 *Citrobacter rodentium* infection

Mice were infected with the *Citrobacter rodentium* strain ICC180 (courtesy from S. Wiles). *C. rodentium* were cultured in Lennox broth (LB) medium (ROTH) at 37 °C overnight. The next day the 9 fold volume of medium was added. After 1.5 h the optical density (OD) was measured. The bacteria were adjusted to $1*10^{11}$ colony forming units (CFU) in 1ml 1x PBS. Mice were administered orally with $1*10^{10}$ *C. rodentium* and were analysed at day 10 post infection. The body weight was monitored during progression of infection. At day 10 the length of the colon was measured from the caecum to the anus. The stool was collected in 1 ml LB, weighted, smashed and diluted serially to detect the bacterial load in faeces. Serial dilutions were added onto MacConkey Agar (ROTH) and cultured at 37 °C for 24 h. CFU were counted and bacterial burden was normalised to stool weight. To determine the bacterial load in organs liver and spleen were homogenised, serial dilutions were plated onto MacConkey Agar plats and incubated at 37 °C for 24 h before counting. To isolate cells from lamina propria colons were placed into 15 ml ice-chilled 0.5 mM EDTA for 30min (on ice) followed by sufficient rinsing with 1x PBS to remove residual epithelium. Afterward tissue was cut into fine pieces and digested in DMEM medium (Gibco) supplemented with 1 mg/ml collagenase D (Roch) and 0.1 mg/ml DNase I (Roch) three times for 30min at 37 °C. After each round of incubation cells were suspended by passing through a 100 µm mesh. After centrifugation cell pellet was re-suspended in a 40% isotonic Percoll solution (GE Healthcare) and underlaid with an 80% isotonic Percoll solution. After centrifugation at 900xg at room temperature for 20 min lamina propria lymphocytes (LPLs) were yielded from the interface cell ring of the 40-80% Percoll gradient. Cells were then washed with PBS containing 2% FCS and used for further studies. For flow cytometric analysis cells from spleen and mLN as well as LPLs were re-stimulated in medium containing IL23 (20ng/ml) with PMA (10 ng/ml, Sigma Aldrich) and ionomycin (1 µg/ml, Sigma Aldrich) for 6 hours. For the last 3 hours Brefeldin A (10 µg/ml, Sigma Aldrich) was added as well. Cells were processed for flow cytometry as previously described (2.3.3) with a Fc-block step (10min, on ice), which was included after cell surface staining. For the intracellular flow cytometry staining the fixation/ permeabilisation buffers from eBioscience were used. For histology, whole colon samples were placed in a shape of ´swiss rool` and fixed in 4 % Rosto-HistoFix (Roth), embedded in paraffin, cut in 8 µm sections, deparaffinised, stained with hematoxylin and eosin (H&E- staining) and scored in a blinded manner. The histological sections were analysed for epithelial hyperplasia, epithelial integrity and mononuclear cell infiltration

(Table 17). The maximal score that could result from scoring was 9. Samples were imaged with a microscope from Carl Zeiss and progressed with the software Nuance2.10.0 (Carl Zeiss, Inc.). The *Citrobacter rodentium* infection was performed in cooperation with Zuobai Wang (Institute for infection immunology, TWINCORE, Hannover, Germany).

Table 17: Histological scoring in *Citrobacter rodentium* infection

Score	Symptoms		
	Epithelial hyperplasia	**Epithelial integrity**	**Mononuclear cell infiltration**
0	No change	No change	No change
1	1- 50%	Mild epithelial ulceration and cryptic destruction	Mild
2	51- 100%	Moderate epithelial ulceration and cryptic destruction	Moderate
3	100%	Severe epithelial ulceration and cryptic destruction	Severe

2.4.5 Experimental autoimmune encephalomyelitis (EAE)

Experimental autoimmune encephalomyelitis (EAE) the mouse model of multiples sclerosis was induced in 10-12 weeks old mice. Mice were injected subcutaneously at four sites with a 200µl of a 1:1 emulsion of 200µg/200µl MOG(35-55)- peptide (resolved in 1x PBS, MEVGWYRSPFSRVVHLYRNGK) and complete Freund´s Adjuvant (CFA) with 4mg/ml *Mycobacterium tuberculosis*. Additionally, the mice were injected intraperitonally (i.p.) with 200ng pertussis toxin in 200µl (in 1x PBS) to open the blood- brain- barrier. At day 2 the i.p. injection of pertussis toxin was repeated. From day 3 to 40 the mice were monitored daily for clinical EAE sings according to the Table 18. Mice with a score higher 3 were sacrificed.

Table 18: Scoring of the clinical symptoms of EAE.

Score	Symptom
0	None
0.5	Partial limp tail
1	Limp tail
2	Delayed rotation from dorsal position
2.5	Hindlimp weakness
3	Complete hindlimp paralysis
3.5	Starting foreleg weakness
4	Paralysis of one foreleg
5	Moribund, death

2.5 Statistics

The Graph Pad Prism Software (GraphPad Software) was used for all statistical analyses. To determine statistical significance two-tailed Mann-Whitney U test was used and error bars represent the standard error of the mean (SEM).

3 Results

3.1 Characterisation of IκB$_{NS}$-deficient mice

3.1.1 The loss of IκB$_{NS}$ affects the B220$^+$ B cells frequency but not apoptosis sensitivity

The transcription factor NF-κB was first identified in B cells as a protein regulating the expression of the κB light chain [139]. The deletion of members of the NF-κB protein family affects proliferation and function of B cells [140,141]. Further, a dysregulation of NF-κB subunits leads to a variety of B cell cancers like Hodgkin´s disease [142] and large B cell lymphoma [143].

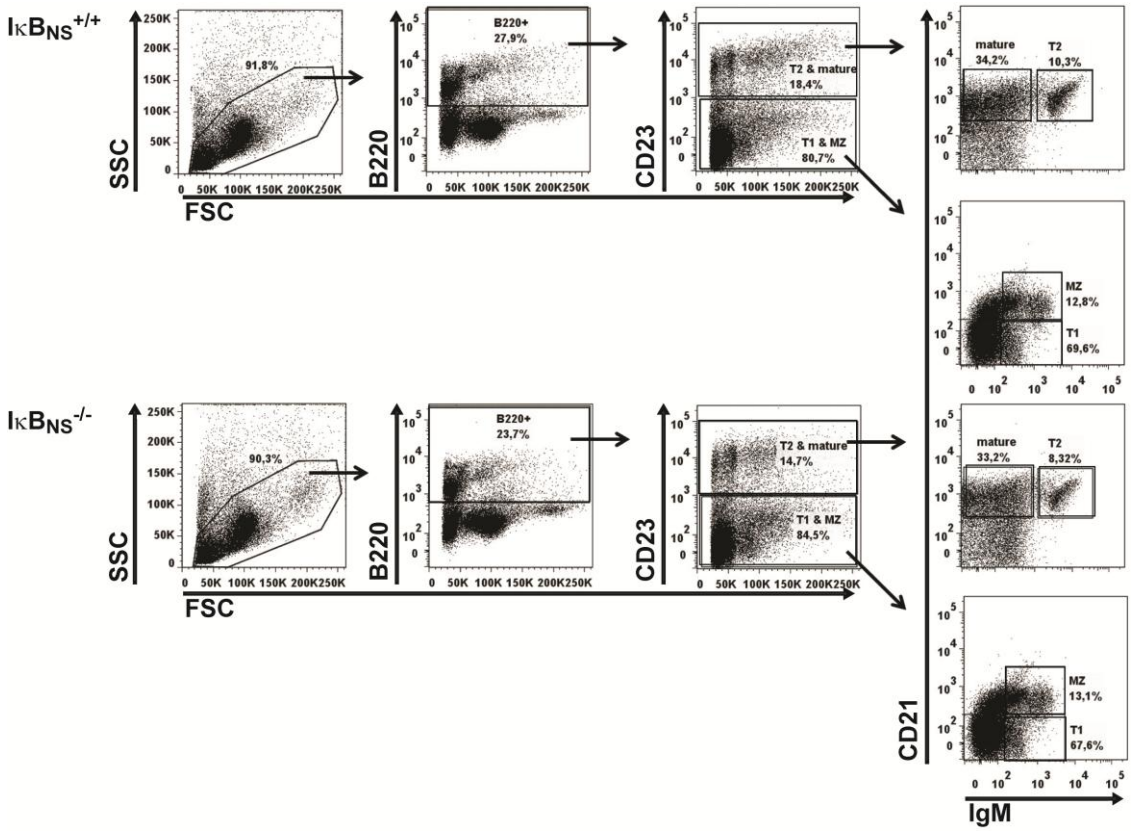

Figure 6: Flow cytometric analysis of bone marrow derived B cell subsets of IκB$_{NS}^{+/+}$ and IκB$_{NS}^{-/-}$ mice. Bone marrow cells of wildtype (upper panel) and IκB$_{NS}$-deficient (lower panel) animals were stained with antibodies directed against B220, CD21, CD23 and IgM. Dot blots show mature (B220$^+$CD23$^+$CD21$^+$IgM$^-$), T1 (B220$^+$CD23$^-$CD21$^-$IgM$^+$), T2 (B220$^+$CD23$^+$CD21$^+$IgM$^+$) and MZ (B220$^+$CD23$^-$CD21$^+$IgM$^+$) B cells. Representative dot plots from one of two independent experiments are shown.

To determine the function of the NF-κB regulator IκB$_{NS}$ in B cells, the frequencies of B220$^+$, B220$^+$CD23^{low} (including marginal zone and T1 B cells), marginal zone (MZ,

$B220^+CD23^-CD21^+IgM^+$), T1 ($B220^+CD23^-CD21^-IgM^+$), $B220^+CD23^+$ (including mature and T2 B cells), mature ($B220^+CD23^+CD21^+IgM^-$) and T2 ($B220^+CD23^+CD21^+IgM^+$) B cells as well as the cell viability were analysed *ex vivo* (Figure 6 and Figure 7). To characterise the B cell compartment of $I\kappa B_{NS}$-defective and wildtype mice, bone marrow (Figure 6 and Figure 7A) and blood (Figure 7B) were stained and analysed by flow cytometry. The dot blots of the flow cytometric measurement of $I\kappa B_{NS}$-deficient mice indicated a reduced frequency in each analysed bone marrow-derived B cell subset as well as total B cells ($B220^+$ cells) compared to wildtype mice (Figure 6). Statistical analyses of these flow cytometric data revealed a significantly reduced frequency of $B220^+$ cells in bone marrow (Figure 7A) of $I\kappa B_{NS}$-deficient compared to wildtype mice. Furthermore, $I\kappa B_{NS}$ deficiency induced a reduction of the $B220^+$ B cell frequency in the blood (Figure 7B). In contrast, an equal frequency of viable cells was observed in bone marrow (Figure 7A) and blood (Figure 7B) as well as a similar frequency of $B220^+$ $CD23^{low}$, MZ, T1, $B220^+$ $CD23^+$, mature and T2 B cells in bone marrow (Figure 7A). Thus, $I\kappa B_{NS}$ contributes to the development and/or survival of $B220^+$ B cells, but the defect induced by $I\kappa B_{NS}$ deficiency is not reflected in one specific subset.

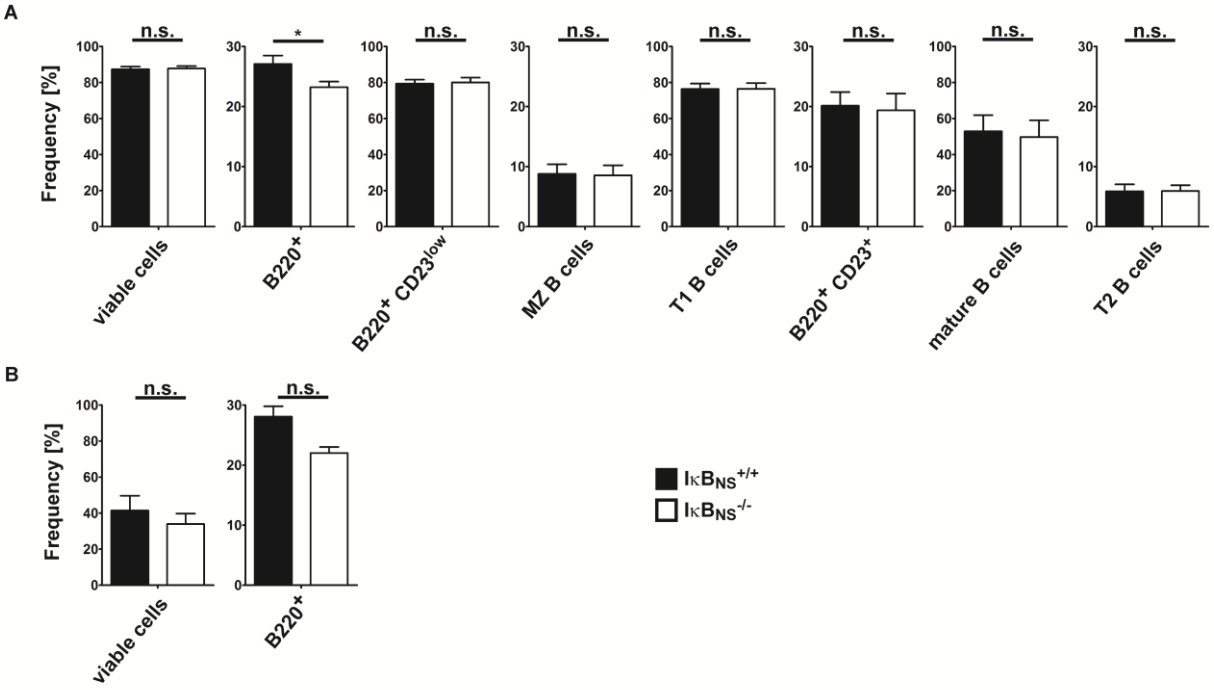

Figure 7: $B220^+$ B cell levels are reduced in $I\kappa B_{NS}$-deficient mice. Bone marrow **(A)** or blood **(B)** cells of wildtype and $I\kappa B_{NS}$-deficient animals were stained with antibodies directed against B220 **(A-B)**, CD21, CD23 and IgM **(A)** followed by flow cytometry analysis. Error bars display the standard error of the mean (s.e.m.) of four **(B)** or six **(A)** animals per genotype of two independent experiments. Statistical analyses were performed by two-tailed Mann-Whitney U test; (*) $p<0.05$.

Grumont *et al.* reported that the deficiency of NF-κB1 cause a proliferation defect in B cells by cell cycle arrest in the G1-phase and enhanced mitogen-induced apoptosis [141]. Furthermore, the deletion of cRel impairs B and T cell division and leads to an activation-associated proliferation defect [140]. In T cells, this proliferation defect is due to inadequate amounts of IL2, which in turn is crucial for *in vivo* induction of Treg but not T_H17 cells [140,144]. The proliferation defect in B cells is caused by a cell-cycle arrest within the G1 phase, as described for NF-κB1-deficient B cells [140,141]. Furthermore, cRel-deficient B cells display an impaired antibody production [140]. To investigate if the reduced frequencies of $B220^+$ B cells in $I\kappa B_{NS}$-deficient mice arise from an impaired apoptosis, the knock down of $I\kappa B_{NS}$ was conducted in the B cell line A20 by lentiviral transduction. For this, lentiviral particles with $I\kappa B_{NS}$-targeting shRNA were introduced into A20 cells by using cell spinning. The A20 cells were analysed by Western blot to assess the efficiency of the knock down. To knock down $I\kappa B_{NS}$ four sh-RNA were used (sh1-, sh2-, sh3- or sh4-RNA). Compared to wildtype A20 cells only the usage of the sh1-RNA induced a knock down of $I\kappa B_{NS}$ (data not shown). Therefore, these cells were used for the generation of single cell cultures, which resulted in seven clones (sh1-1 to sh1-7). As a control, three clones transduced with scramble (sc) shRNA (sc-1 to sc-3) were generated. Western blot analysis of these cell clones confirmed a reduced expression of $I\kappa B_{NS}$ within the four clones sh1-4 to sh1-7 (Figure 8).

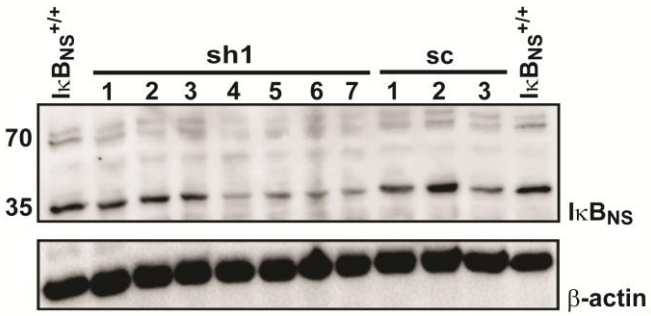

Figure 8: A20 clone cultures transduction with sh1-RNA exhibit a knock down of $I\kappa B_{NS}$. A20 cells were transfected with scramble control (sc) shRNA or sh1-RNA targeting $I\kappa B_{NS}$. Transduced A20 cells were used to generate single cell cultures (sh1-1 to sh1-7, sc-1 to sc-3). The knock down efficiency of $I\kappa B_{NS}$ cultures was analysed by Western blotting using $I\kappa B_{NS}$ antibody. The expression of β-actin was analysed to ensure equal loading.

As described above, the deficiency of NF-κB1 cause a enhanced mitogen-induced apoptosis [141]. To assay the sensitivity of the B cell line A20 to CD95-mediated apoptosis, A20 wildtype cells were stimulated using Flag-tagged CD95 ligand (CD95L) in presence or absence of Flag antibodies for 8 and 24 hours (Figure 9). Crosslinking of Flag-tagged

CD95L by addition of Flag antibodies increased the sensitivity to CD95L-induced apoptosis. DNA-fragmentation measurement showed a CD95L-induced apoptosis sensitivity in A20 cells even at low CD95L concentrations with increasing apoptosis sensitivity with higher concentrations of CD95L. The lowest CD95L concentration in addition with Flag antibodies induced considerable apoptosis. This high apoptosis sensitivity stayed constant over time and with increasing CD95L concentrations (Figure 9).

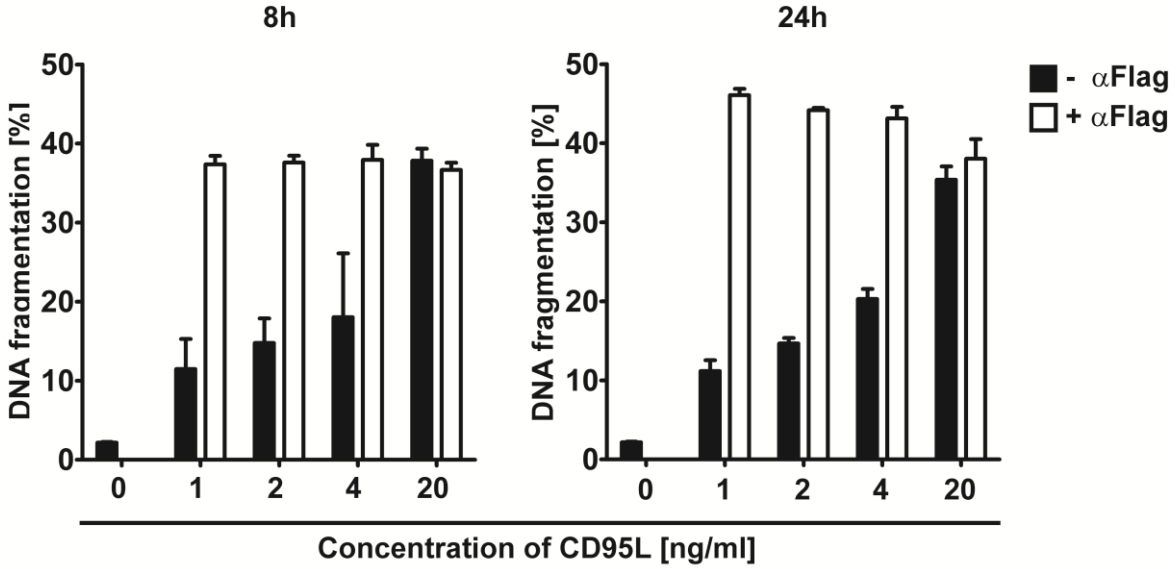

Figure 9: IκB$_{NS}$ wildtype A20 cells are sensitive to CD95-mediated apoptosis. IκB$_{NS}$ wildtype A20 cells were left untreated or stimulated for 8 h or 24 h with CD95L in the presence or absence of 1 µg/ml Flag-antibody. The amount of apoptotic cells was quantified by sub-G1 DNA level content. Error bars display the s.e.m. of two measurements.

Moreover, the CD95L-mediated apoptosis sensitivity was quantified in the A20 clone cultures containing the IκB$_{NS}$ knock down (Figure 10). The A20 clones sh1-6 and sh1-7 were not sensitive to CD95L-mediated apoptosis in as high extent as the wildtype cells (Figure 10). However, the reduced sensitivity of the clone sh1-6 was overcome by high concentrations of CD95L and the addition of anti-Flag (Figure 10). The transduced scramble cells were also less sensitive to CD95L in comparison to A20 wildtype cells. Furthermore, the two clones sh1-4 and sh1-5 were as sensitive to apoptosis induction as the A20 wildtype cells (Figure 10). Taken together, although the knock down of IκB$_{NS}$ induced a reduced sensitivity to death receptor-induced apoptosis in some A20 clones, this is not a general effect and in total there is only a mild reduction. Hence, an increased apoptosis sensitivity upon the knock down of IκB$_{NS}$ in B cells is no explanation of the reduction of B220^{+} B cells. Consequently, further analysis are necessary to identify the function of IκB$_{NS}$ in B cells as well as potential B cell specific target genes of IκB$_{NS}$.

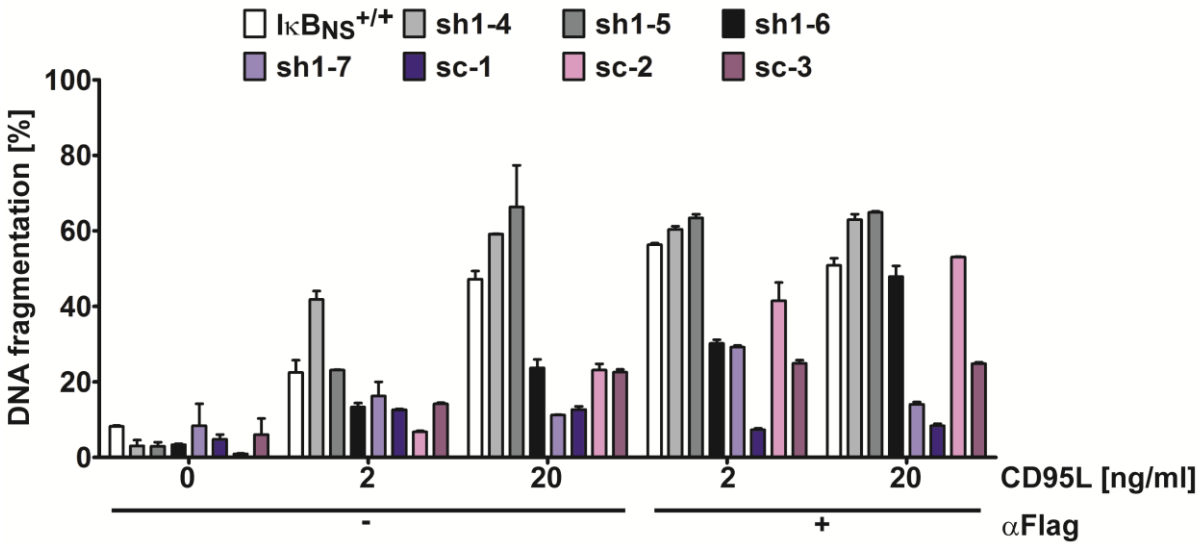

Figure 10: Apoptosis sensitivity of wildtype A20 cells or A20 cells stably transduced with $I\kappa B_{NS}$ targeting sh1-RNA. A20 cells (sh1-4 to sh1-7 sh1-RNA transduced, sc-1 to sc-3 scramble controls) were left untreated or stimulated for 13 h with CD95L in the presence or absence of 1 µg/ml Flag antibodies. The amount of apoptotic cells was determined by flow cytometry by the quantification of the sub-G1 DNA content. Error bars display the s.e.m. of two measurements.

3.1.2 $I\kappa B_{NS}$ is not crucial for the activation of $CD4^+$ T cells

Previous studies demonstrated that $I\kappa B_{NS}$ expression is induced upon TCR-triggering [127,128,134]. It is not known, whether the deficiency of $I\kappa B_{NS}$ affects the TCR-triggered activation of $CD4^+$ T cells. To clarify this questions, expanded $CD4^+$ T cells were activated and the phosphorylation of proteins at tyrosine residues, Akt and the MAP-kinases Erk and p38 as well as the expression of the IκB proteins $I\kappa B_{NS}$ and IκBα and the NF-κB family members cRel, NF-κB1, NF-κB2, p65 and RelB was monitored (Figure 11 and Figure 12).

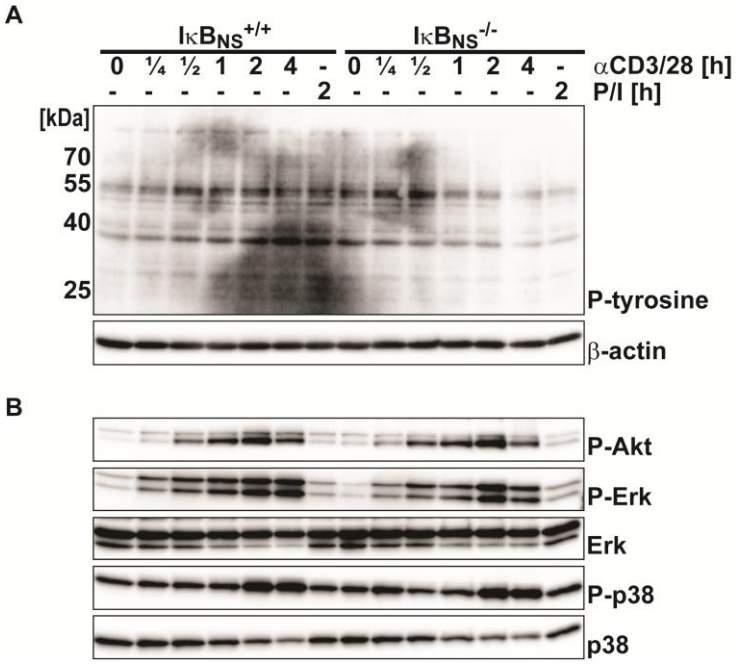

Figure 11: IκB$_{NS}$ deficiency did not affect the activation of expanded CD4$^+$ T cells. Isolated CD4$^+$CD25$^-$ T cells from IκB$_{NS}^{+/+}$ and IκB$_{NS}^{-/-}$ mice were expanded. On day 7, cells were left untreated or stimulated with anti-CD3 plus anti-CD28 for the indicated time points. As controls, cells were stimulated with PMA/ ionomycin for 2 hours. The activation was analysed by Western blotting using the indicated phospho-antibodies to tyrosine **(A)**, AKT as well as the MAP-kinases Erk and p38 **(B)**. The expression of the MAP-kinases (Erk and p38) **(B)** were analysed by Western blotting. Analysis of β-actin expression ensured equal loading. The Western blots shown are representative for three independent experiments.

Upon activation of the TCR via αCD3/αCD28, wildtype and IκB$_{NS}$-deficient cells displayed an equal activation pattern. The phosphorylation of tyrosine residues was similar between IκB$_{NS}$-deficient and wildtype cells (Figure 11A). In both genotypes, the phosphorylation of Erk and Akt started already after 15 minutes and decreased after 4 hours of stimulation (Figure 11B). The expression of the p44 isoform of Erk remained constant in the course of stimulation whereas the p42 isoform decreased after 1 hour of activation in both, wildtype and IκB$_{NS}$-deficient cells (Figure 11B). A constitutive phosphorylation of p38 was detected in both genotypes, which increased at 2 and 4 hours of αCD3/αCD28 stimulation (Figure 11B). The expression of p38 was consistent in both, wildtype and IκB$_{NS}$-deficient cells with a mild decrease to 4 hours. The activation of NF-κB was analysed by IκBα phosphorylation and degradation. IκBα was equally phosphorylated and the αCD3/αCD28 stimulation induced an comparable degradation of IκBα in both genotypes (Figure 12A). After 30 minutes, the IκB$_{NS}$ expression was induced upon αCD3/αCD28 activation of wildtype cells, as described in the literature (Figure 12A) [127,128]. The αCD3/αCD28 kinetic showed an equal expression profile of the NF-κB subunits cRel, p65, RelB, NF-κB1 and NF-κB2 in both

genotypes (Figure 12B-C). Taken together, the proximal TCR signalling as well as the T cell activation is not affected by the deficiency of IκB$_{NS}$.

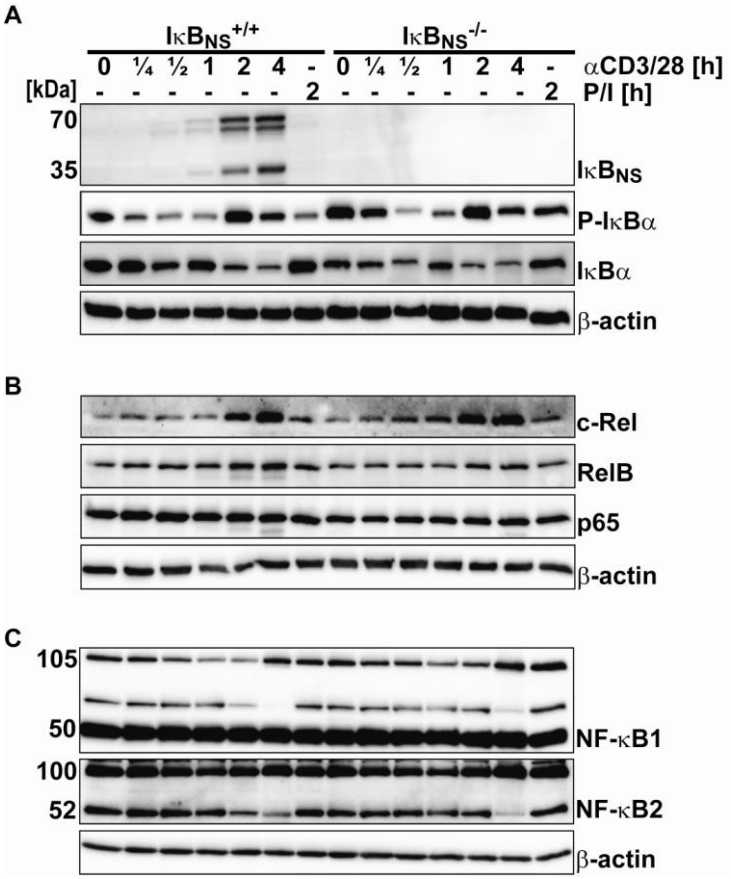

Figure 12: Similar expression of IκBα and NF-κB subunits in expanded CD4$^+$ IκB$_{NS}$-deficient and wildtype T cells. CD4$^+$CD25$^-$ T cells from IκB$_{NS}^{+/+}$ and IκB$_{NS}^{-/-}$ mice were isolated and expanded for 7 days. Cells were left untreated or stimulated with anti-CD3 plus anti-CD28 for up to 4 hours. As control, cells were stimulated with PMA/ ionomycin for 2 hours. The activation of IκBα was analysed by Western blotting by using IκBα phospho-antibodies **(A)**. The expression of the IκB-proteins IκB$_{NS}$ and IκBα **(A)** and the NF-κB family members cRel, p65, RelB **(B)** as well as NF-κB1and NF-κB2 **(C)** is shown. Equal loading was ensured by the analysis of β-actin expression. The shown Western blots are representative for three independent experiments.

3.1.3 Both IκB$_{NS}$ forms (35 and 70 kDa) are stable to denaturation by urea

IκB$_{NS}$ is described as a 35 kDa protein [127]. In addition to the 35 kDa isoform Schuster *et al.* showed two, so far undescribed 70 kDa isoforms, which appear upon activation of cells, almost simultaneously to the 35 kDa isoform. Furthermore, the 70 kDa isoforms were detected in the nucleus but not in the cytoplasm of stimulated conventional T cells (Tcon) [134].

Consistent with the report by Schuster *et al.* [134], the two 70 kDa isoforms of IκB$_{NS}$ were detected by Western blot (Figure 8and Figure 12). The 70 kDa isoforms were observed in

the B cell line A20 (Figure 8) as well as in primary T cells (Figure 12) in a stimulation-dependent manner, but was not detectable in IκB$_{NS}$-deficient (Figure 12) cells. Additionally, diverse antibodies including polyclonal sera of four different immunised rabbits and a mouse IgG2b monoclonal antibody were used to detect the expression of IκB$_{NS}$. All antibodies were able to recognise the 70 kDa isoforms (shown for instance in Figure 15). The double molecular weight of the new isoform of IκB$_{NS}$ might be a sign of formation of SDS-stable homodimers of IκB$_{NS}$, which stays stable in SDS-PAGE. To identify the nature of the 70 kDa isoforms, different concentrations of an A20 whole cell lysate were analysed by SDS-PAGE with or without 6 M urea, which destroys hydrogen bonds. SDS- and Urea-PAGE were followed by Western blot analysis. The 70 kDa isoform of IκB$_{NS}$ was detected in both SDS-PAGE as well as Urea-PAGE, suggesting posttranslational modification as the origin of the 70 kDa IκB$_{NS}$ form (Figure 13).

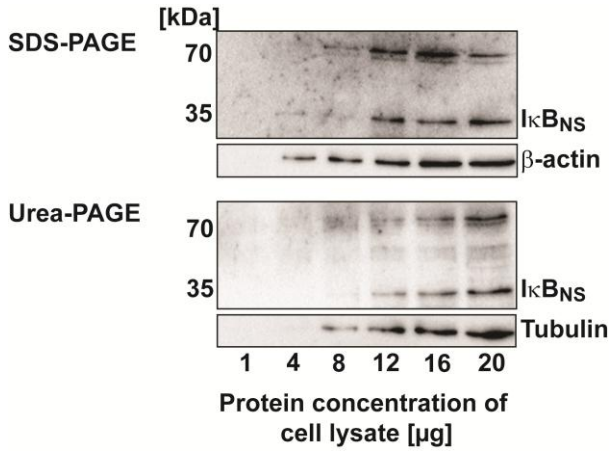

Figure 13: The 70 kDa IκB$_{NS}$ protein is a urea-stable form. A20 cell lysates were loaded to a SDS-polyacrylamide gel or a SDS- polyacrylamide gel containing 6 M urea. Lysates were analysed by Western blotting. β-actin and tubulin served as loading controls.

For further characterisation of the 70 kDa isoform of IκB$_{NS}$ additional experiments were done to enrich and purify the 70 kDa protein for later mass spectrometry analysis. This is important to reduce problems due to highly abundant proteins. First, the amount of IκB$_{NS}$ from $1*10^6$ A20 cells was analysed by Western blotting. Therefore, the lysate of $1*10^6$ A20 cells as well as 5 ng of recombinant GST-tagged IκB$_{NS}$ protein were loaded onto SDS-PAGE, IκB$_{NS}$ was detected by Western blot (Figure 14, upper panel) and quantified by the program BIO-1D from Peqlab (Figure 14, lower panel). The calculation resulted in a quantity of 1.4 ng per $1*10^6$ cells for the 35 kDa protein. For the 70 kDa protein an amount of 0.4 ng was calculated. Hence, for further experiments at least $1*10^6$ A20 cells were used.

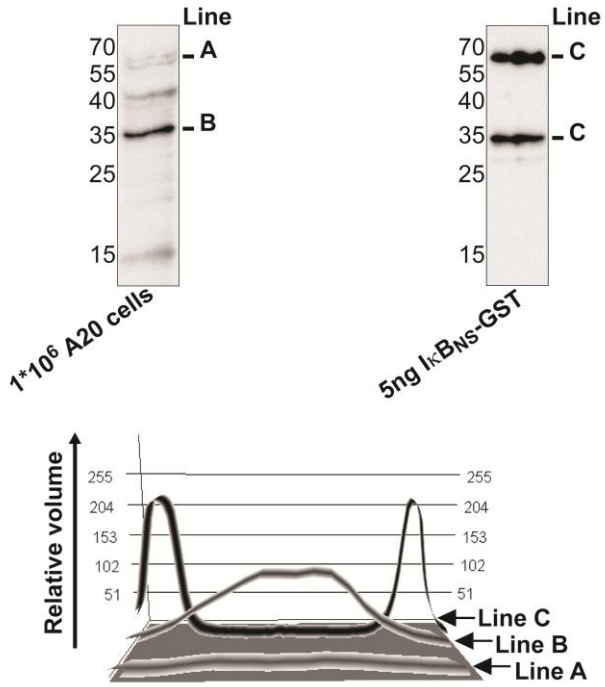

Figure 14: Calculation of the IκB$_{NS}$ protein amount from A20 cells. The cell lysate of 1*10^6 A20 cells and 5 ng recombinant GST-tagged IκB$_{NS}$ protein were loaded on an SDS-PAGE gel and analysed by Western blotting (upper panel). The amount of IκB$_{NS}$ from 1*10^6 A20 cells was calculated using the program BIO-1D (Peqlab, lower panel).

On the one hand, IκB$_{NS}$ was immunoprecipitated via protein A sepharose beads (Figure 15) and on the other hand by an affinity column (Figure 16) to enrich and purify the two IκB$_{NS}$ proteins from A20 cell lysate. For the immunoprecipitation of IκB$_{NS}$ from the lysate of 1*10^6 A20 cells using protein A sepharose beads, two monoclonal murine antibodies (Figure 15A) as well as a polyclonal rabbit IκB$_{NS}$ antibody (Figure 15B+C) were tested. The immunoprecipitations using the murine IκB$_{NS}$ antibodies were efficient enough to enrich the 35 kDa protein, but gave no evidence in terms of the 70 kDa IκB$_{NS}$, because of unspecific protein bands at the same molecular weight (Figure 15A). For the following immunoprecipitations the number of A20 cells was increased to 2*10^7 cells and rabbit IκB$_{NS}$ antibodies were used. Only one unspecific band at 55 kDa was detected (heavy chain of antibody) in Western blot analysis (Figure 15B) and upon Coomassie Brilliant Blue staining (Figure 15C) using the rabbit IκB$_{NS}$ antibodies. The immunoprecipitation of IκB$_{NS}$ was successful with both rabbit antibodies. In comparison to the murine antibody, the rabbit antibody was the better choice for the immunoprecipitation of IκB$_{NS}$, since it gave a better purified elution fraction without any β-actin contamination (Figure 15B). Finally, the immunoprecipitation with rabbit IκB$_{NS}$ antibodies resulted in a protein band stainable with Coomassie Brilliant Blue (Figure 15C).

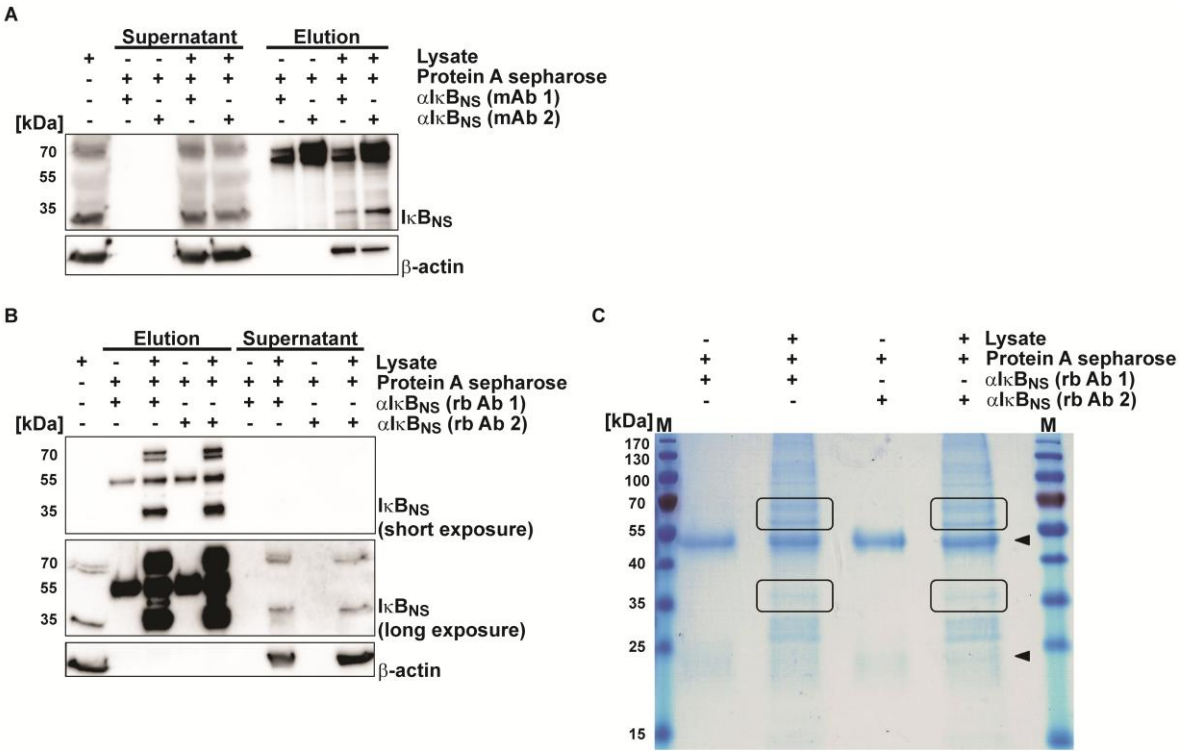

Figure 15: Immunoprecipitation of IκB$_{NS}$ via protein A sepharose beads. Monoclonal murine **(A)** or polyclonal rabbit **(B-C)** IκB$_{NS}$ antibodies (Ab) were bound to protein A sepharose beads and total cell lysates from A20 cells were added to the beads (in **(A)** 1*10^6 cells, in **(B-C)** 2*10^7 cells). After the incubation of the beads with the protein lysate a minor part of the supernatant was collected for analysis (supernatant). Three washing steps were performed followed by an elution step. The eluate was analysed by SDS-PAGE followed by Western blot analysis **(A-B)**, using antibodies directed to IκB$_{NS}$ and β-actin. Furthermore, the eluate was analysed via Coomassie Brilliant Blue staining, black boxes indicate the predicted protein bands of IκB$_{NS}$ and arrows show the heavy and light chain band of the rabbit IκB$_{NS}$ antibody **(C)**.

To obtain adequate protein amounts for mass spectrometry analysis the amount of cell lysate was increased and a affinity column was used for immunoprecipitation. Hence, the lysate of 1.5*10^8 A20 cells was added to columns coupled with rabbit IκB$_{NS}$ or rabbit IgG antibodies, respectively (Figure 16). After five washing steps (flow through), two elution steps were performed. No binding of IκB$_{NS}$ to the rabbit IgG coupled column, but specific binding of IκB$_{NS}$ to the IκB$_{NS}$ antibody coupled column could be detected by Western Blotting within the second elution (Figure 16A). Furthermore, no contamination with β-actin was discovered. In addition, the two elution fractions were analysed by Coomassie Brilliant Blue staining showing two protein bands at the predicted molecular weight of IκB$_{NS}$. Additionally, one band for the heavy as well as the light chain of the IκB$_{NS}$ antibody was detected (Figure 16B). Unexpectedly, the predicted protein bands were not only detectable in the elution of the IκB$_{NS}$ antibody-coupled column, but also within the elution of the rabbit IgG control column, indicating an unspecific contamination with random proteins either only in the control or in both columns. Consequently, prior to mass

spectrometry analysis further experiments are necessary to optimise the enrichment and purification of the IκB$_{NS}$ isoforms.

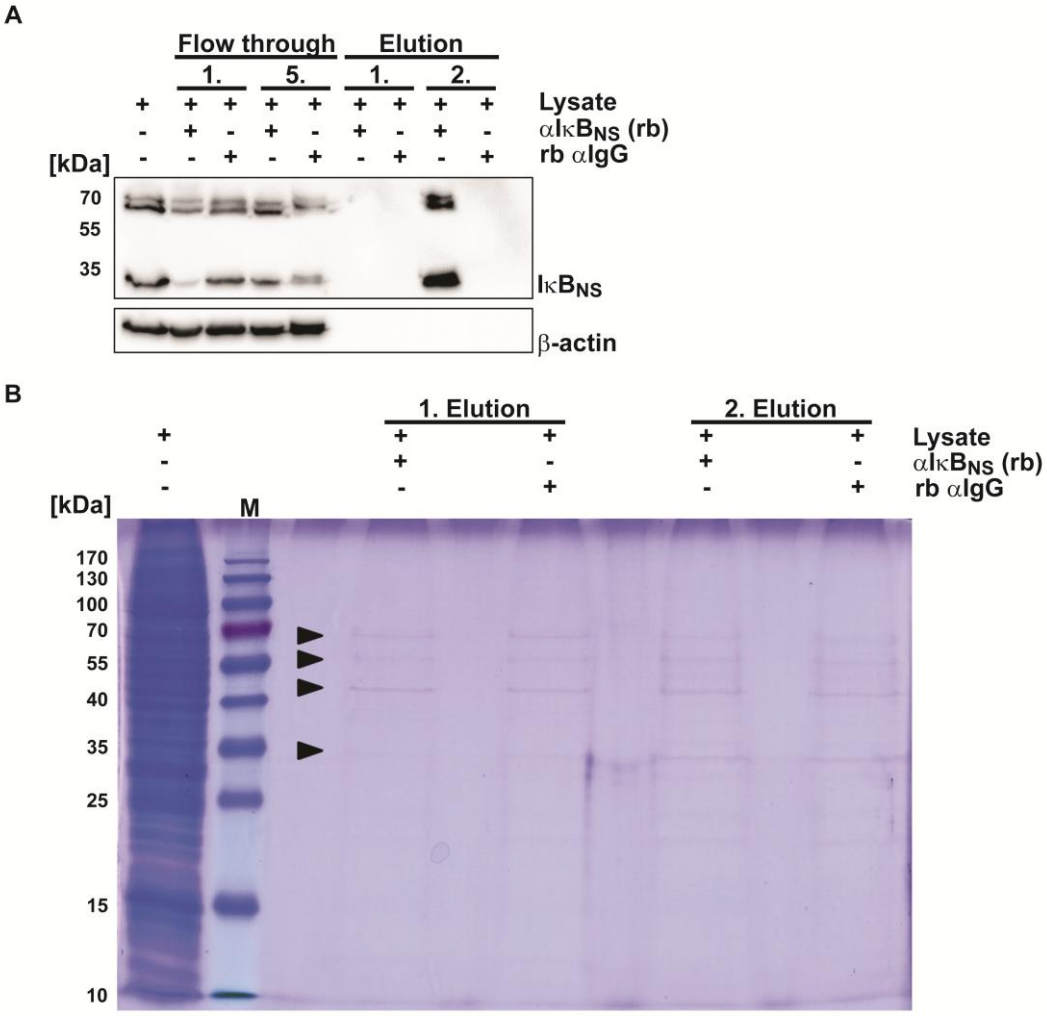

Figure 16: Affinity purification of IκB$_{NS}$ via a mini column. After the binding of antibodies directed to IκB$_{NS}$ or rabbit IgG to a MicroLink™ Protein Coupling column, the cell lysate of $1.5*10^8$ A20 cells was added to the column. Five washing steps and two elution steps were performed. The flow through of the first (1. flow through) and the last washing step (5. flow through) and the eluate (1. elution and 2. elution) of each column was analysed by SDS page followed by Western blot analysis **(A)** using antibodies directed against IκB$_{NS}$ and β-actin. Furthermore, the eluate was analysed via Coomassie Brilliant Blue staining, arrows shown from top to bottom: presumed 70 kDa IκB$_{NS}$, heavy chain band of the rabbit IκB$_{NS}$ antibody, presumed 35 kDa IκB$_{NS}$ and light chain band of the rabbit IκB$_{NS}$ antibody **(B)**.

3.2 The role of IκB$_{NS}$ in T$_H$17 cell development

3.2.1 Setup of an efficient *in vitro* polarisation of T$_H$17 cells

In the literature numerous protocols for the *in vitro* polarisation of T$_H$17 are reported [40,56,145,146]. The common ground of these reports is the necessity of IL6 and TGFβ [40,56,145,146]. In addition, several other cytokines like IL1β, IL21 and IL23 were described to play an important role in initiation, stabilisation and/ or maintenance of T$_H$17 cells [44,64,65,146,147].

Before starting with the *in vitro* polarisation of T$_H$17 cells, the genotype of mice was determined using biopsies of mouse tails (Figure 17). For the genotyping three primers were used, two IκB$_{NS}$ primer and one primer specific to the neomycin cassette, which was inserted while the generation of the IκB$_{NS}$ knockout. IκB$_{NS}$-deficient mice were distinguished from wildtype mice by the shorter DNA fragment size (Figure 17), induced via target gene disruption by deletion of 4.8kb from the IκB$_{NS}$ gene locus [128]. By this way, wildtype and IκB$_{NS}$-deficient mice were identified and used for further experiments.

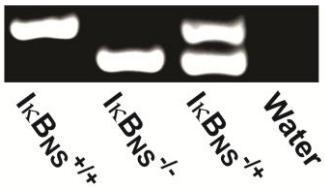

Figure 17: Genotyping of IκB$_{NS}$ offspring. Tail biopsies from IκB$_{NS}$ mice were lysed and DNA was used to genotype wildtype (IκB$_{NS}^{+/+}$), heterozygous (IκB$_{NS}^{-/+}$) and IκB$_{NS}$-deficient (IκB$_{NS}^{-/-}$) mice by polymerase chain reaction. The particular genotype was determined by DNA fragment size after agarose gel electrophoresis.

To identify the best working combination of cytokines and additives for the *in vitro* T$_H$17 cell polarisation, naïve T cells (CD4$^+$CD62L$^+$ CD25$^-$) were isolated from spleen, peripheral lymph nodes (pLN) and mesenteric lymph nodes (mLN) of IκB$_{NS}$-deficient and wildtype mice (Figure 18). As shown in the upper panel of Figure 18 the cell mixture of spleen, pLN and mLN cells contained only a minor fraction of the required cells. The reanalysis of the isolated cell population revealed a purity of 95 to 98% of CD4$^+$CD62L$^+$CD25$^-$ naïve T cells (Figure 18, lower panel).

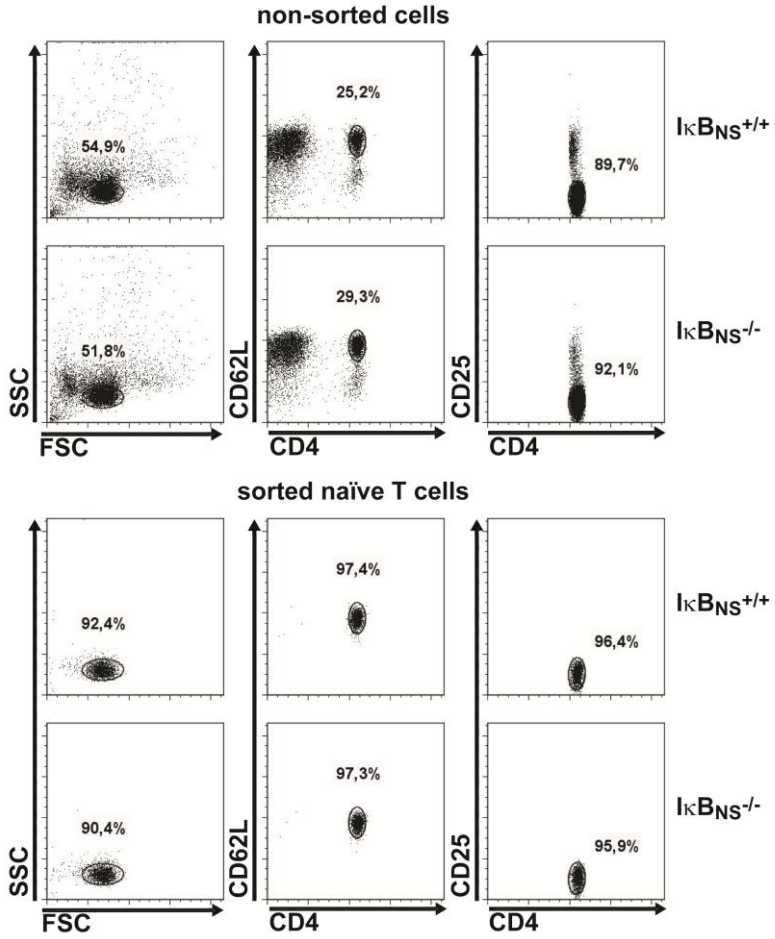

Figure 18: The isolation of naïve T cells by flow cytometry results in a highly pure population. Spleen, pLN and mLN were isolated from $I\kappa B_{NS}^{+/+}$ and $I\kappa B_{NS}^{-/-}$ mice. Cells were stained with antibodies directed to CD4, CD25 and CD62L. Flow cytometric cell sorting was used to isolate $CD4^{+}CD62L^{high}CD25^{-}$ naïve T cells. The upper panel shows dot blots of non-sorted primary cells and the lower panel a re-analysis of isolated naïve T cells from wildtype and $I\kappa B_{NS}$-deficient mice.

To determine the best working medium for T_H17 cells polarisation, the first experiment was performed using different media (Figure 19A). Furthermore, various concentrations of CD3 antibodies (αCD3, Figure 19B) as well as medium additives like TGFβ and IL6 (Figure 19D) were tested. In addition, different plate sizes (Figure 19B) and plate suppliers (Figure 19C) were used. All experiments were performed by using naïve wildtype T cells and the T_H17-basic condition (containing αCD3, αCD28, αIL4, αIFNγ, TGFβ, IL6). First, both media IMDM or RPMI as well as combinations of FCS (standard or tetracyclin-free), sodium pyruvate and non-essential amino acids (NEAA) were tested (Figure 19A). The cell number stayed stable in all five tested combinations. However, the medium containing RPMI plus FCS standard, sodium pyruvate and NEAA gave a mildly increased cell number after T_H17 polarisation, hence it was used for further experiments. The T_H17 polarisation using 2 µg/ml αCD3 in 24 well plates (Figure 19B)

resulted in the best proliferation. Furthermore, testing different 24 well plate suppliers showed the highest cell number using the plates from nunc, starlab, PAA, Millipore and CellStar. In following experiments the 24 well plates from nunc were used, because of the low variability of the cell number within the two experiments. The *in vitro* polarisation of T_H17 cells depended on the concentration of TGFβ and IL6 and the lowest concentration of both cytokines resulted in an increased cell proliferation (Figure 19D). Accordingly, the T_H17 polarisation of further experiments were performed in 24 well plates from nunc with plate-bound 2 µg/ml αCD3 using RPMI medium containing FCS standard, sodium pyruvate, NEAA, 0.5 ng/ml TGFβ and 20 ng/ml IL6.

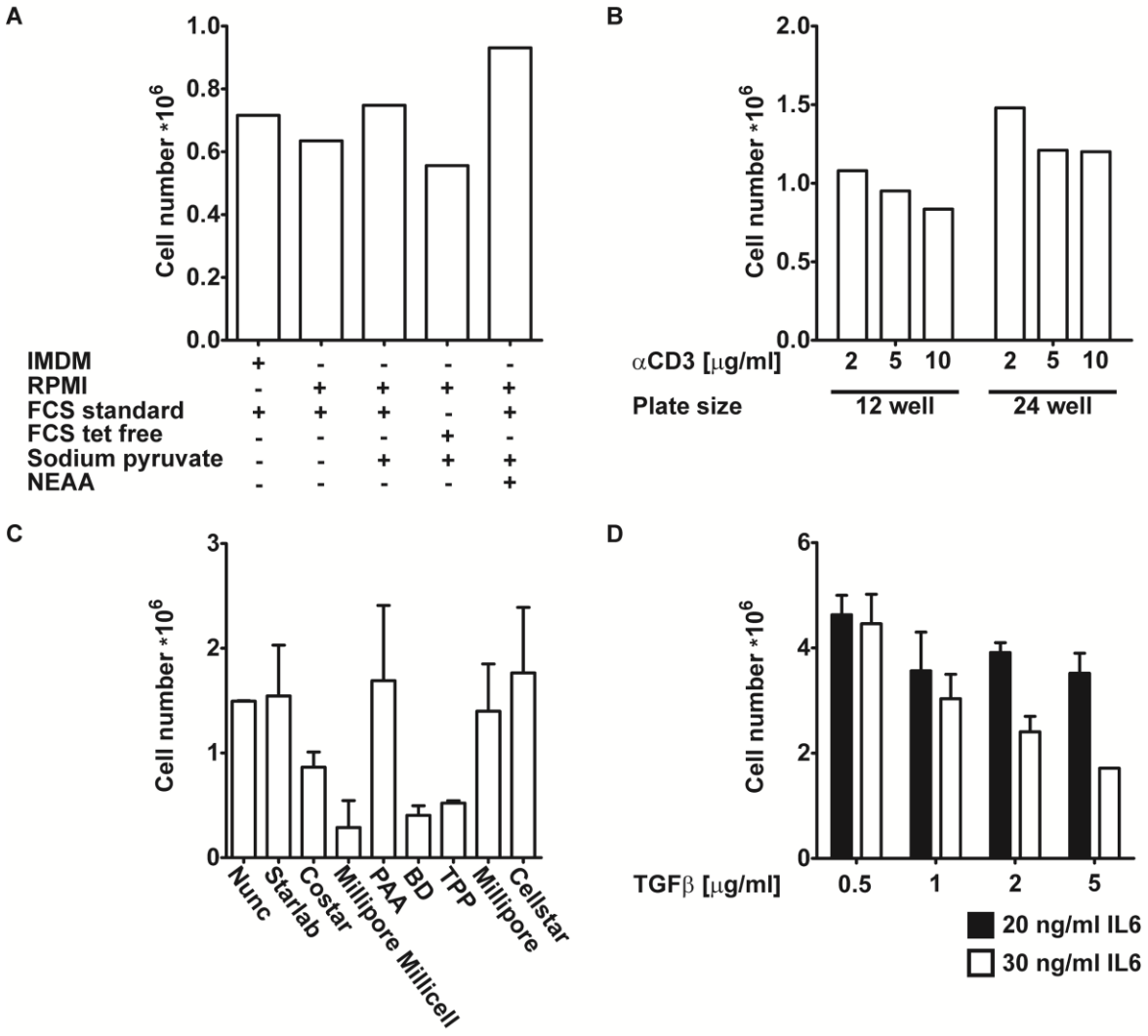

Figure 19: Determination of the most suitable condition for *in vitro* T_H17 polarisation. Naïve T cells were isolated by flow cytometry. $0.5*10^6$ **(A+C)** or $1*10^6$ **(B+D)** cells were cultured for 5 days under T_H17-polarising conditions. On day 5, the absolute cell number was determined. For the polarisation of T_H17 cells different medium additives **(A)**, concentrations of αCD3 and plate sizes **(B)**, plates of various suppliers **(C)** and concentrations of TGFβ and IL6 **(D)** were tested. Data represent one experiment **(A-B)** or are pooled from two independent experiments **(C-D)**.

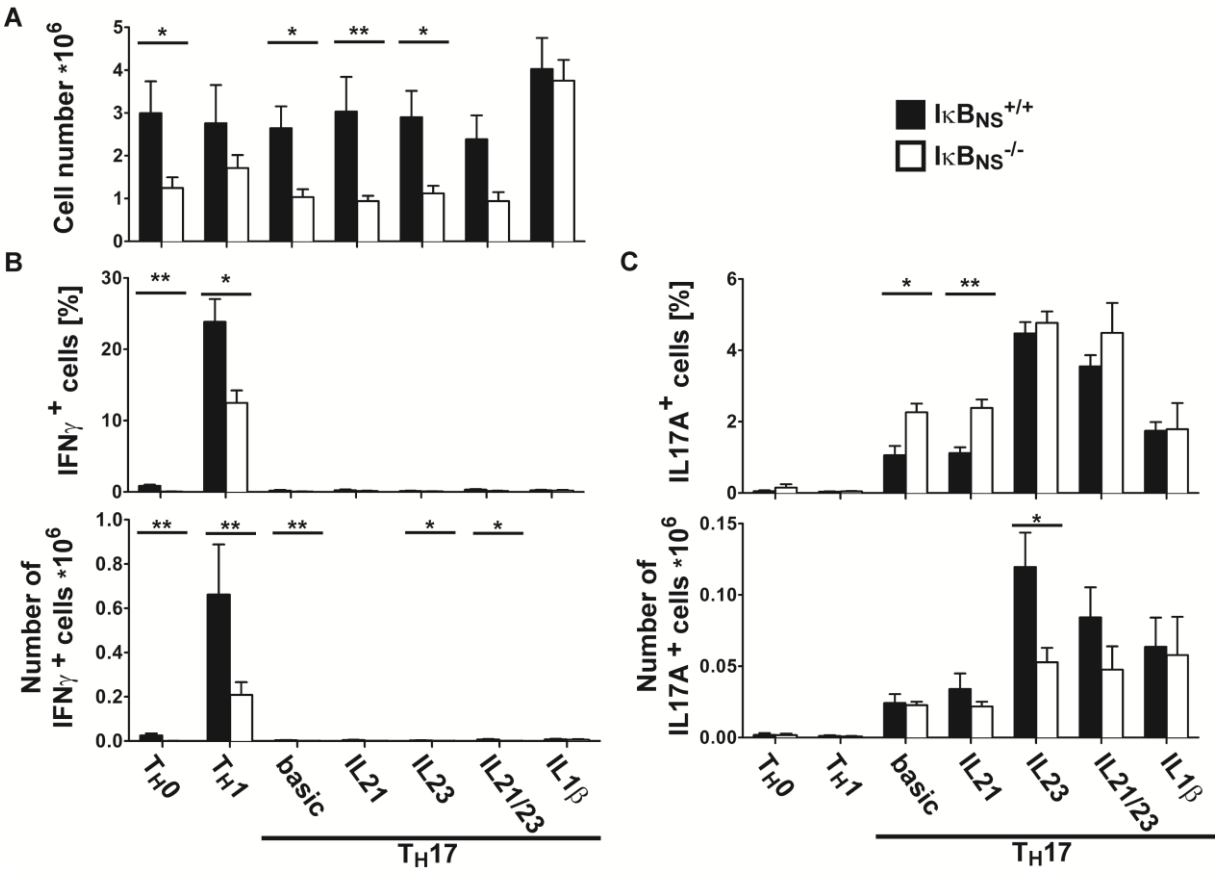

Figure 20: Test of different additive combinations for T_H17 cell polarisation. Naïve T cells were isolated and $1*10^6$ cells were cultured for 5 days under different T_H17-polarising conditions. At day 5, the cells were stimulated with PMA/ ionomycin (4 h) and BrefeldinA (2 h). The total cell number was determined (**A**) and the frequencies of $IFN\gamma^+$ (**B**) or $IL17A^+$ (**C**) cells were measured by flow cytometry (upper panel of **B** and **C**) and the number of $IFN\gamma^+$ or $IL17A^+$ cells was calculated (lower panel of **B** and **C**). Error bars display the s.e.m. and are representative for five independent experiments. Statistical analyses were performed by two-tailed Mann-Whitney U test; (*) $p<0.05$, (**) $p<0.01$.

To identify a promising cytokine combination for the *in vitro* T_H17 polarisation, naïve T cells were cultured under T_H17-basic condition (containing αCD3, αCD28, αIL4, αIFNγ, TGFβ, IL6) alone or in combination with IL1β (T_H17-IL1β), IL21 (T_H17-IL21), IL23 (T_H17-IL23) or IL21 plus IL23 (T_H17-IL21/23) (Figure 20). Additionally, cells were cultured under T_H1 and non-priming (T_H0) conditions (Figure 20). On day 5, a reduced number of $I\kappa B_{NS}$-deficient T cells compared to wildtype cells was determined in almost all conditions, except in the T_H17-IL1β condition (Figure 20A). The frequency of IL17A-producing cells showed an increased in $I\kappa B_{NS}$-deficient T_H17-basic and T_H17-IL21 polarised cells compared to wildtype cells (Figure 20C upper panel). Nevertheless, the number of $IL17A^+$ cells was comparable among T_H17-basic and T_H17-IL21 polarised $I\kappa B_{NS}$-deficient and wildtype T cells (Figure 20C lower panel). Additionally, while the frequency of T_H17-IL23 polarised $IL17A^+$ cells was similar in both genotypes, the number

of IL17A$^+$ cells was significantly reduced in IκB$_{NS}$-deficient cells (Figure 20C). The analysis of T$_H$17-IL21/23 and T$_H$17-IL1β polarised cells showed an equal frequency and cell number of IL17A$^+$ IκB$_{NS}$-deficient compared to wildtype T cells (Figure 20C). Furthermore, the determination of the frequency and the cell number of IFNγ^+ cells showed a reduced polarisation within the IFNγ^+ T$_H$0 and T$_H$1 IκB$_{NS}$-deficient T cells compared to wildtype T cells (Figure 20B). Thus, IκB$_{NS}$-deficient cells indicated a affected proliferation upon T$_H$17-polarisation.

The five T$_H$17 polarising conditions illustrated variable effects of IκB$_{NS}$ deficiency. Furthermore, the frequency of IL17A$^+$ cells was between 1.5 and 5 %, hence a majority of cells were non-polarised (Figure 20). To determine the best time point regarding number and frequency of IL17A$^+$ cells a differentiation kinetic was performed (Figure 21). The cell number mildly dropped within the first 24 h, then increased until day 5 (Figure 21A). The frequency of IL17A$^+$ cells was mildly increased at the first day followed by a peak at day 2 (Figure 21B). From day 2 to day 4 the frequency of IL17A$^+$ cells stayed stable. Furthermore, the frequency of IL17A$^+$ dropped by half at day 5 (Figure 21B). Hence, the following T$_H$17 polarisation experiments were performed over a period of 4 days.

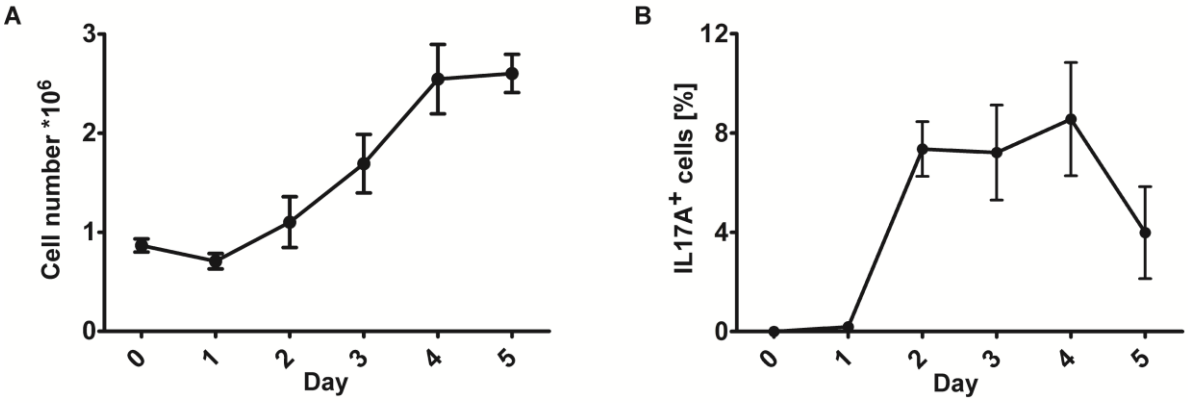

Figure 21: Differentiation kinetics of *in vitro* cultured T$_H$17 cell. 1*10^6 isolated naïve T cells were cultured for up to 5 days under T$_H$17-polarising conditions (T$_H$17-IL23 condition). The cells were stimulated for 4 h with PMA/ ionomycin together with Brefeldin A for the last 2 h and stained with antibodies directed to IL17A. The number of cells was counted **(A)** and the frequency of IL17A$^+$ cells was measured by flow cytometry **(B)**. Error bars display the s.e.m. and are representative for three independent experiments.

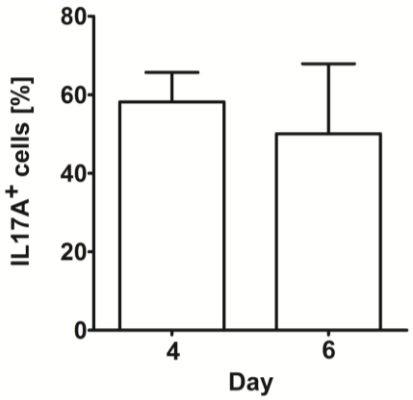

Figure 22: Modification of T_H17 polarisation conditions resulted in increased frequency of $IL17^+$ cells. Naïve T cells were isolated by flow cytometry and $1*10^6$ cells were cultured for 4 or 6 days under T_H17- polarising conditions. The cells were stimulated with PMA/ ionomycin (P/I, 4 h) together with Brefeldin A for the last 2 h. The frequency of $IL17A^+$ cells was measured by flow cytometry. Data are representative for two independent experiments. The s.e.m. is shown by error bars.

At that point, another T_H17 differentiation protocol, published by Carlson *et al.*, with an alternative cytokine combination was tested [148]. The new cytokine-antibody mixture, in the following called T_H17 condition, included αCD3 (3 µg/ml), αCD28 (5 µg/ml), αIL2 (10 µg/ml), αIFNγ (10 µg/ml), TGFβ (2 ng/ml), IL6 (30 ng/ml), IL1β (10 ng/ml) and TNFα (20 ng/ml). In contrast to previous T_H17 conditions, higher concentrations of αCD3 (3 µg/ml), αCD28 (5 µg/ml), TGFβ (2 ng/ml) and IL6 (30 ng/ml) were used. In the prior T_H17 polarisation experiments αIL4 was used to inhibit the polarisation into T_H2 cells. Instead, the new protocol included αIL2 to inhibit the IL2 induced suppression of T_H17 cell polarisation [41,43]. Furthermore, in contrast to previous T_H17 polarisation experiments TNFα was used as an additional cytokine. Prior T_H17 polarisation protocols resulted in an output of about 5% $IL17A^+$ cells. The new tested T_H17 polarisation protocol increased the frequency of $IL17A^+$ cells to roundabout 60% (Figure 22). For this reason, the following experiments were performed with the new T_H17 polarisation conditions.

3.2.2 $I\kappa B_{NS}$ drives the differentiation of both T_H17 and T_H1 cells.

The transcription factor NF-κB plays a key role in the immune system [12,93,149]. For instance, the proliferation and effector function of T cells depends on the T cell receptor (TCR)-triggered NF-κB-mediated activation of the cell [12,93,149]. The pathway leading from TCR and NF-κB activation to gene transcription is regulated by multiple components including the IκB protein family [123,128,131,150].

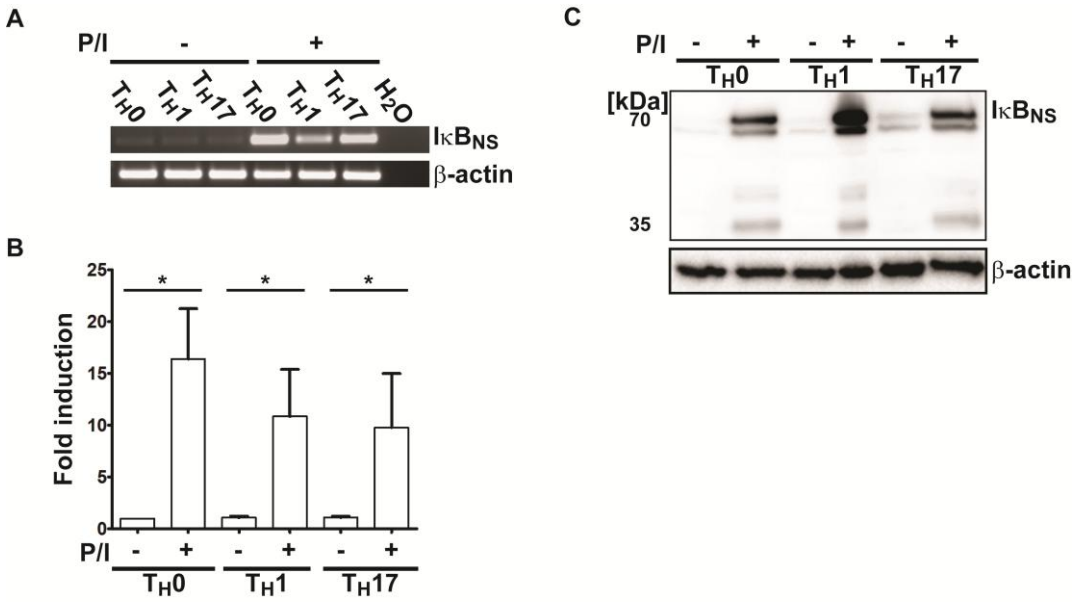

Figure 23: $I\kappa B_{NS}$ is expressed in *in vitro* differentiated activated T cells. Naïve T cells were isolated by flow cytometry and cultured for 4 days under T_H1-, T_H17- or non-polarising (T_H0) conditions **(A-C)**. The cells were left untreated or stimulated with PMA/ ionomycin (P/I, 4 h) and the induction of $I\kappa B_{NS}$ was measured by PCR (**A**), qPCR (**B**) or Western blotting (**C**). Data shown in **A** and **C** are representative for at least three independent experiments. Error bars display the s.e.m. of four experiments (**B**). Statistical analyses were performed by two-tailed Mann-Whitney U test; (*) $p<0.05$.

T_H1 and T_H17 cells are important in host protection to a variety of intracellular (T_H1) and extracellular (T_H17) pathogens. To identify whether the IκB protein family member $I\kappa B_{NS}$ is expressed in T_H1 and T_H17 cells, the expression of $I\kappa B_{NS}$ under T_H1-, T_H17- and non-polarising (T_H0) conditions was analysed. The expression of $I\kappa B_{NS}$ was determined on the mRNA level by conventional RT-PCR (Figure 23A) as well as qPCR (Figure 23B). Consistent with published data [127,134], the $I\kappa B_{NS}$ mRNA expression was induced upon T cell activation (Figure 23A and B). Additionally, the analysis by RT-PCR and qPCR displayed the highest expression level of $I\kappa B_{NS}$ mRNA in activated non-polarised (T_H0) cells (Figure 23A+B). RT-PCR analysis revealed an mildly reduced $I\kappa B_{NS}$ expression in T_H1 compared to T_H17 cells (Figure 23A), whereas T_H1 and T_H17 polarised cells showed an equal fold induction of $I\kappa B_{NS}$ mRNA analysed by qPCR (Figure 23B). In total, T_H0, T_H1 and T_H17 showed a similar $I\kappa B_{NS}$ mRNA expression. Furthermore, the expression of $I\kappa B_{NS}$ on the protein level (Figure 23C) was analysed. Again, $I\kappa B_{NS}$ expression could be detected after the activation of T cells with PMA/ ionomycin. The protein expression of $I\kappa B_{NS}$ was equal in T_H0 and T_H17 polarised cells. In contrast to the mRNA data, T_H1 polarised cells showed the highest $I\kappa B_{NS}$ protein level, which indicates diversified translational and/ or post-transcriptional modulation of the $I\kappa B_{NS}$ expression in the

different T cell subsets (Figure 23C). Taken together, the activation dependent expression of IκB$_{NS}$ directs the development of T$_H$1 and T$_H$17 cells, however its expression is not restricted to a single T helper subset.

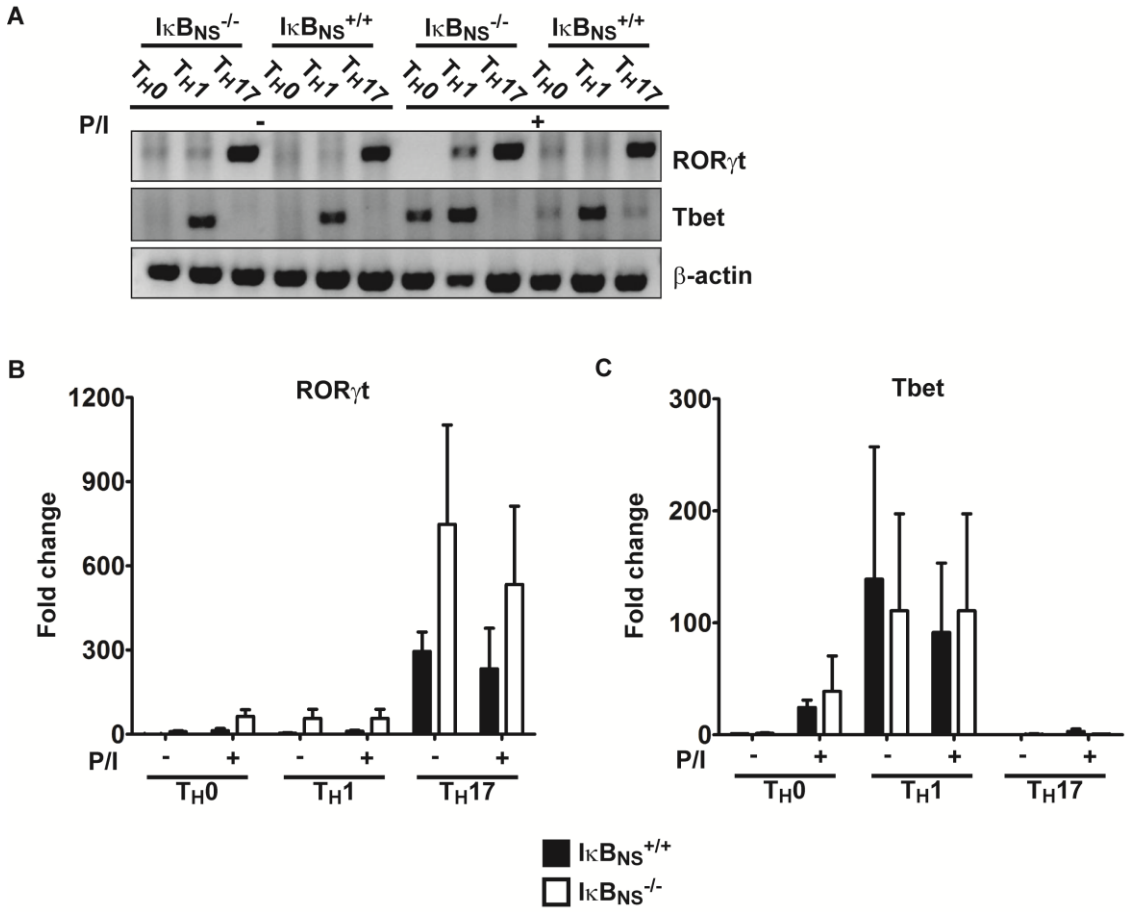

Figure 24: Tbet and RORγt are equally expressed in IκB$_{NS}^{+/+}$ and IκB$_{NS}^{-/-}$ T cells. Isolated naïve T cells were cultured for 4 days under T$_H$1-, T$_H$17- or non-polarising (T$_H$0) conditions. Subsequently, T cells were left untreated or stimulated with PMA/ ionomycin (P/I, 4h). The expression of RORγt **(A+B)** and Tbet **(A+C)** was analysed by RT-PCR **(A)** and qPCR **(B+C)**. The qPCR data were normalised to non stimulated T$_H$0 wildtype cells and the fold change was calculated. Error bars display the s.e.m. of three independent experiments.

Naïve T cells were cultured under T$_H$0-, T$_H$1- and T$_H$17-priming conditions, to analyse the effect of the IκB$_{NS}$ deficiency on the polarisation of T cell subsets. The mRNA expression of RORγt and Tbet was determined by RT-PCR (Figure 24A) as well as qPCR (Figure 24B-C). In RT-PCR analysis, the master transcription factor of T$_H$17 cells, RORγt was highly expressed in non-stimulated as well as stimulated T$_H$17 cells with a comparable expression level in both genotypes (Figure 24A). On the contrary, the qPCR analysis showed a mild increase of RORγt in IκB$_{NS}$-deficient T$_H$17 cells (Figure 24B). The master transcription factor of T$_H$1 cells, Tbet was equally expressed in IκB$_{NS}$-deficient and wildtype T$_H$1 cells (Figure 24A+C). In addition, T$_H$17 cells did not express Tbet (Figure

24A+C). Taken together, the master transcription factors of the T cell subsets T_H1 and T_H17, Tbet and RORγt, exhibited an equal expression pattern comparing wildtype and $I\kappa B_{NS}$-deficient cells.

Although the $I\kappa B_{NS}$ deficiency did not affect the mRNA expression of the master transcription factors of T_H1 and T_H17 cells, the defect can influence the differentiation of T cells as it was shown for IκBζ in T_H17 cell differentiation [121]. To identify if $I\kappa B_{NS}$ plays an essential role in driving the development of naïve T cells to T_H1 or T_H17 cells, wildtype and $I\kappa B_{NS}$-deficient T cells cultured under T_H1 or T_H17 polarising conditions were analysed by flow cytometry (Figure 25). A severely reduced frequency of $IFN\gamma^+$ T_H1 as well as $IL17A^+$ T_H17 cells was monitored in the absence of $I\kappa B_{NS}$, whereas the frequency of *in vitro* differentiated T_H1 and T_H17 cells showed a 2-fold reduction in $I\kappa B_{NS}$-deficient cells (Figure 25B and C, left panel). Additionally, the number of $IFN\gamma^+$ T_H1 as well as $IL17A^+$ T_H17 cells was reduced in $I\kappa B_{NS}$-deficient compared to wildtype cells (Figure 25B and C, right panel).

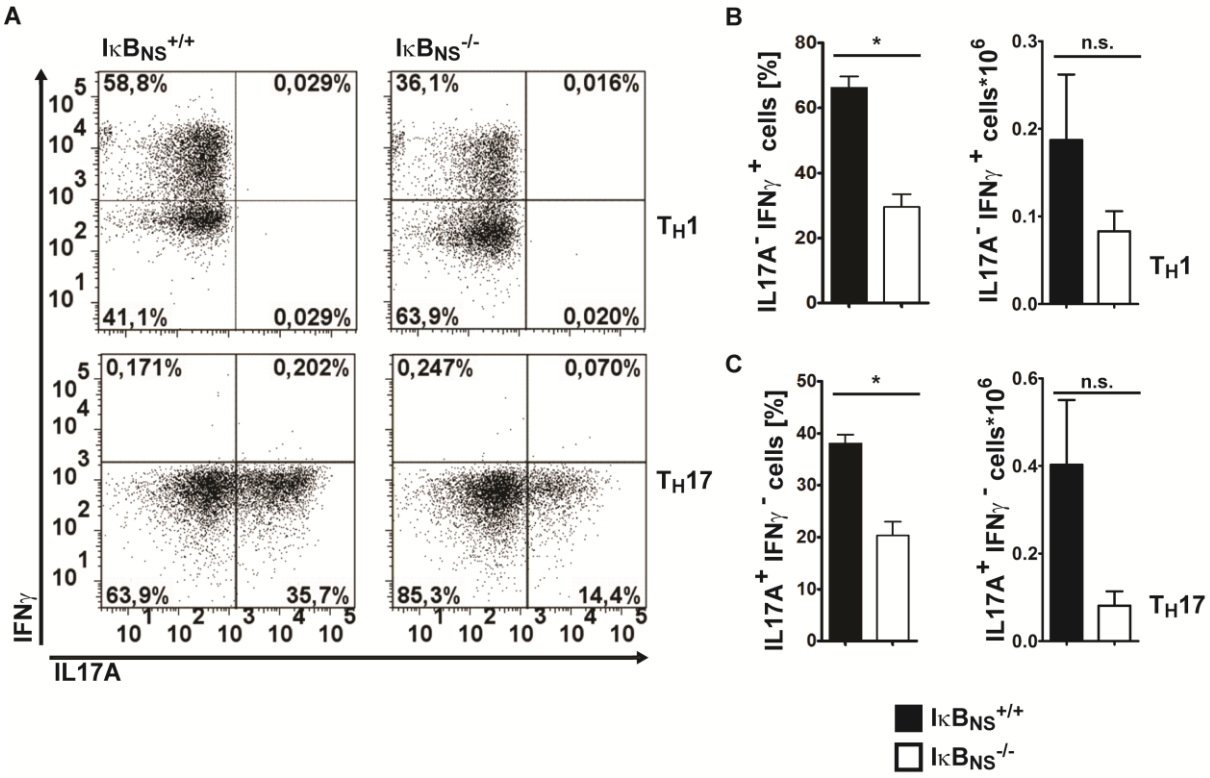

Figure 25: Impaired *in vitro* polarisation of T_H1 and T_H17 cells in the absence of $I\kappa B_{NS}$. Isolated naïve T cells were cultured under T_H1 or T_H17-polarising conditions. On day 4, the cells were stimulated with PMA/ ionomycin (4 h) and BrefeldinA (2 h). The frequencies of $IFN\gamma^+$ (left panel) and $IL17A^+$ (right panel) cells were measured by flow cytometry **(B)**. Representative dot plots are shown in **(A)**. The number of $IFN\gamma^+$ as well as $IL17A^+$ cells was calculated **(C)**. Error bars display the s.e.m. and are representative for four independent experiments. Statistical analyses were performed by two-tailed Mann-Whitney U test; n.s.= not significant, (*) $p<0.05$.

In addition, the effects induced by the IκB$_{NS}$ deficiency was further analysed by determination of cell numbers over time, to identify the reason for the reduced frequency of *in vitro* polarised T$_H$17 and T$_H$1 cells (Figure 26). The frequency (Figure 26A) as well as the cell number (Figure 26B) of IFNγ$^+$ T$_H$1-primed as well as IL17A$^+$ T$_H$17-primed cells was determined. Already at day 3, an impaired development of T$_H$1- and T$_H$17-polarised cells was detected upon the deficiency of IκB$_{NS}$ (Figure 26).

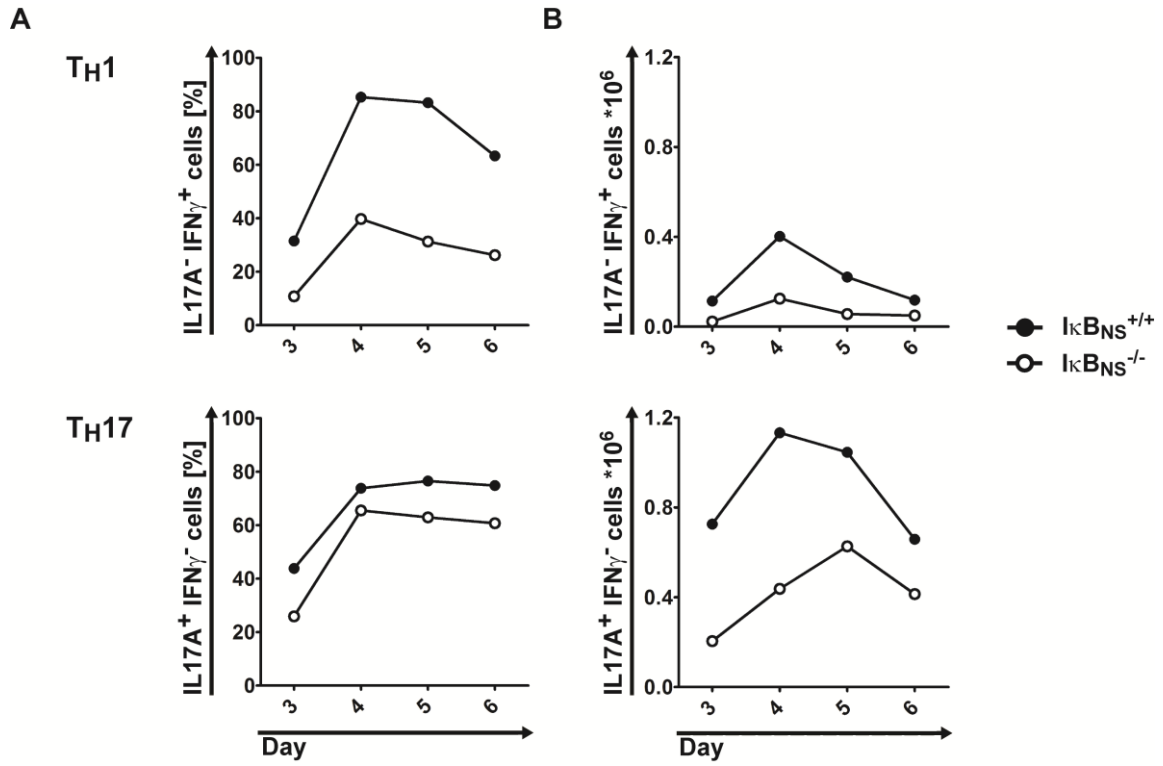

Figure 26: Division profile analysis of IκB$_{NS}$ wildtype and knockout T cells indicate a proliferation defect induced by IκB$_{NS}$-deficiency. After the isolation of naïve T cells, cells were cultured under T$_H$1- or T$_H$17-polarising conditions. From day 3 to 6, some cells were stimulated with PMA/ ionomycin (4 h) and BrefeldinA (2 h). The frequency of IFNγ$^+$ (upper panel) and IL17A$^+$ (lower panel) cells was measured by flow cytometry **(A)** During the differentiation, numbers of IFNγ$^+$ (upper panel) and IL17A$^+$ (lower panel) cells were determined at day 3 to day 6 **(B)**.

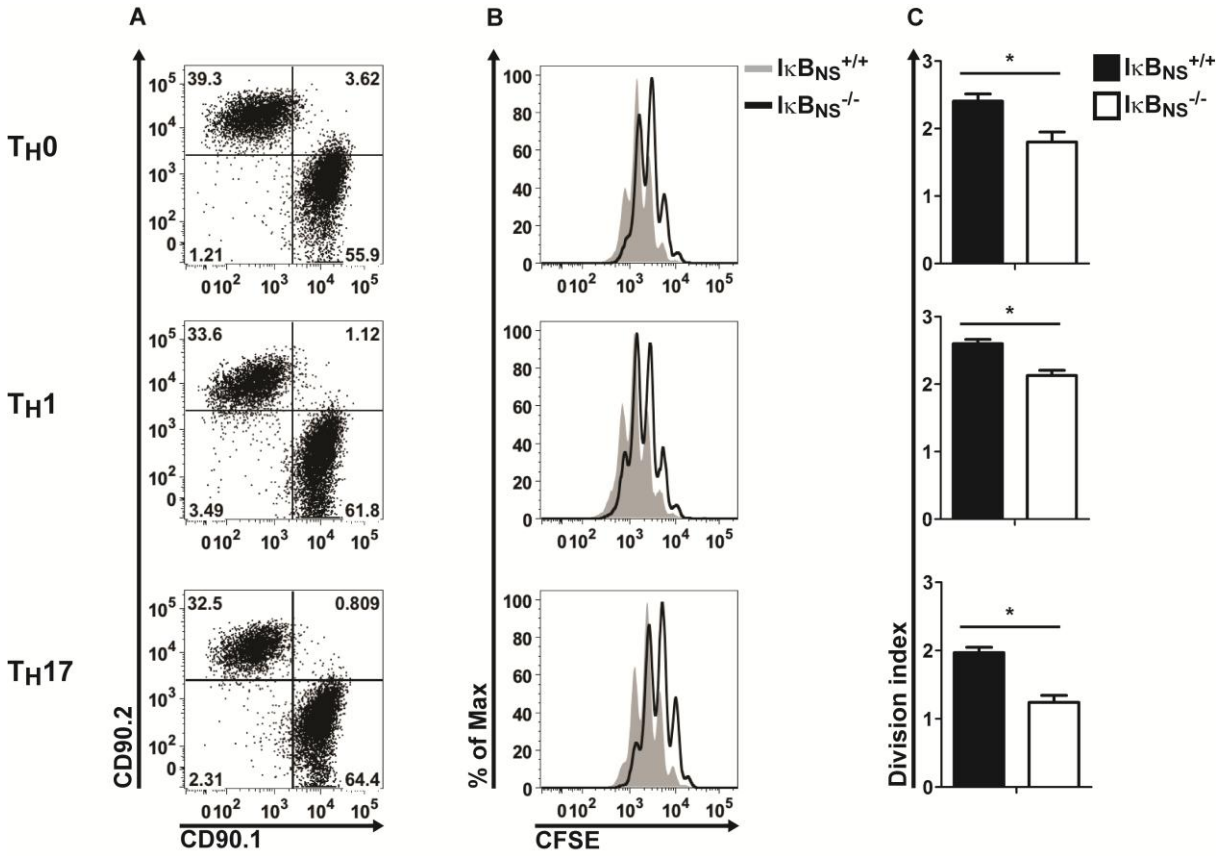

Figure 27: IκB$_{NS}$-deficient T cells display a cell intrinsic proliferation defect *in vitro*. Naïve T cells were isolated by flow cytometry from CD90.1$^+$ IκB$_{NS}^{+/+}$ and CD90.2$^+$ IκB$_{NS}^{-/-}$ mice. Cells were mixed in a ratio of 1:1. After CFSE-labelling T cells were cultured under T$_H$1- (middle panel), T$_H$17- (lower panel) or non-polarising (T$_H$0, upper panel) conditions **(A-C)**. At day 4, stimulated cells were analysed by flow cytometry regarding the CFSE intensity of IFNγ$^+$ or IL17A$^+$ cells within the two genotypes. Representative dot plots of IκB$_{NS}^{+/+}$ (CD90.1$^+$) and IκB$_{NS}^{-/-}$ (CD90.2$^+$) cells (pre-gated to viable cells) are shown in **(A)**. Representative histograms of the CFSE intensity of IFNγ$^+$ or IL17A$^+$ cells (pre-gated to CD90.1$^+$ or CD90.2$^+$ cells) are shown in **(B)**. Statistical analysis of the calculated division index of wildtype and knockout T cells are shown in **(C)**. Error bars displaying the s.e.m. are representative for four independent experiments and two-tailed Mann-Whitney U test was used; (*) $p<0.05$.

To determine whether this effect induced by IκB$_{NS}$ deficiency could be compensated by wildtype cells, CFSE stained naïve IκB$_{NS}$-deficient (CD90.2$^+$) T cells were cultured in the presence of CFSE stained naïve wildtype (CD90.1$^+$) T cells (Figure 27). Once again, the frequency of IκB$_{NS}$-deficient (CD90.2$^+$) T$_H$1 and T$_H$17 as well as T$_H$0 cells showed a reduction of 50% compared to wildtype (CD90.1$^+$) cells (Figure 27A). The CFSE proliferation profile revealed a T helper cell intrinsic effect due to the fact that wildtype cells undergo more proliferation steps in comparison to IκB$_{NS}$-deficient cells (Figure 27B). Furthermore, the mean number of divisions per cell (division index; including non-divided cells) was calculated from the CFSE profile shown in Figure 27B. Hence, the division index of the co-cultured T cells showed a significant decrease within the IκB$_{NS}$-deficient

T_H0, T_H1 and T_H17 cells confirming the hypothesis of a T helper cell intrinsic proliferation defect (Figure 27C).

3.2.3 The loss of $I\kappa B_{NS}$ alters the *in vitro* expression of cytokines by T_H17 cells.

Previous reports revealed that $I\kappa B_{NS}$ restricts IL6 and IL12p40 expression in macrophages and dendritic cells, whereas it enhances expression of IL2 and IFNγ in T cells [128,129,131]. Due to the effect of $I\kappa B_{NS}$ deficiency on T cell proliferation, it was analysed whether T_H17 cells display impaired cytokine expression upon the loss of $I\kappa B_{NS}$.

Naïve T cells were cultured under T_H1- and T_H17-priming conditions, to analyse the effect of the $I\kappa B_{NS}$ deficiency on the cytokine expression of T cell subsets. The mRNA expression of IL17A (Figure 28A-B) and IFNγ (Figure 28A+D) was determined by RT-PCR (Figure 28A) and qPCR (Figure 28B+D). In addition, the protein expression of IL17A (Figure 28C) and IFNγ (Figure 28E) was analysed by the measurement of the mean fluorescence intensity (MFI). In RT-PCR, IL17A expression was increased in non-stimulated $I\kappa B_{NS}$-defective T_H17 cells compared to wildtype cells (Figure 28A). Furthermore, the analysis by RT-PCR revealed a stimulation-induced expression of IL17A, which was comparable in $I\kappa B_{NS}$-deficient and wildtype T_H17 cells (Figure 28A). In contrast, qPCR analysis showed a stimulation-induced expression of IL17A in wildtype cells but not in $I\kappa B_{NS}$-deficient T_H17 cells (Figure 28B). Indeed, in qPCR analysis the IL17A expression was reduced in stimulated $I\kappa B_{NS}$-deficient cells compared to non-stimulated $I\kappa B_{NS}$-deficient as well as wildtype T_H17 cells (Figure 28B). Consistent with qPCR data, the loss of $I\kappa B_{NS}$ induced a mild, but not significant, reduction of the IL17A protein expression in T_H17 cells (Figure 28C). The RNA expression of the T_H1 effector cytokine, IFNγ was induced in T_H1 cells as well as T_H0 cells upon cell stimulation (Figure 28A+D). Furthermore, RT-PCR analysis revealed an increased expression of IFNγ in $I\kappa B_{NS}$-deficient non-stimulated T_H1 cells compared to wildtype, but a similar expression upon activation (Figure 28A). In qPCR analysis, IFNγ was equally expressed in non-stimulated as well as activated T_H1 cells of both genotypes (Figure 28D). In contrast, the analysis of the MFI of IFNγ uncovered a significant reduction of the protein expression in T_H1 $I\kappa B_{NS}$-defective cells (Figure 28E). Taken together, qPCR analysis indicated a reduced IL17A expression in $I\kappa B_{NS}$-deficient compared to wildtype T_H17 cells (Figure 28B). This reduction was confirmed by the analysis of IL17A protein expression (Figure 28C). Furthermore, the RNA of the T_H1 effector cytokine IFNγ is equally expressed in T_H1

cells comparing both genotypes (Figure 28A+D), but the IFNγ protein expression was reduced in IκB$_{NS}$-defective T$_H$1 cells (Figure 28E). Altogether, the protein expression on a per cell basis (MFI) was significantly reduced for IFNγ but not for IL17A.

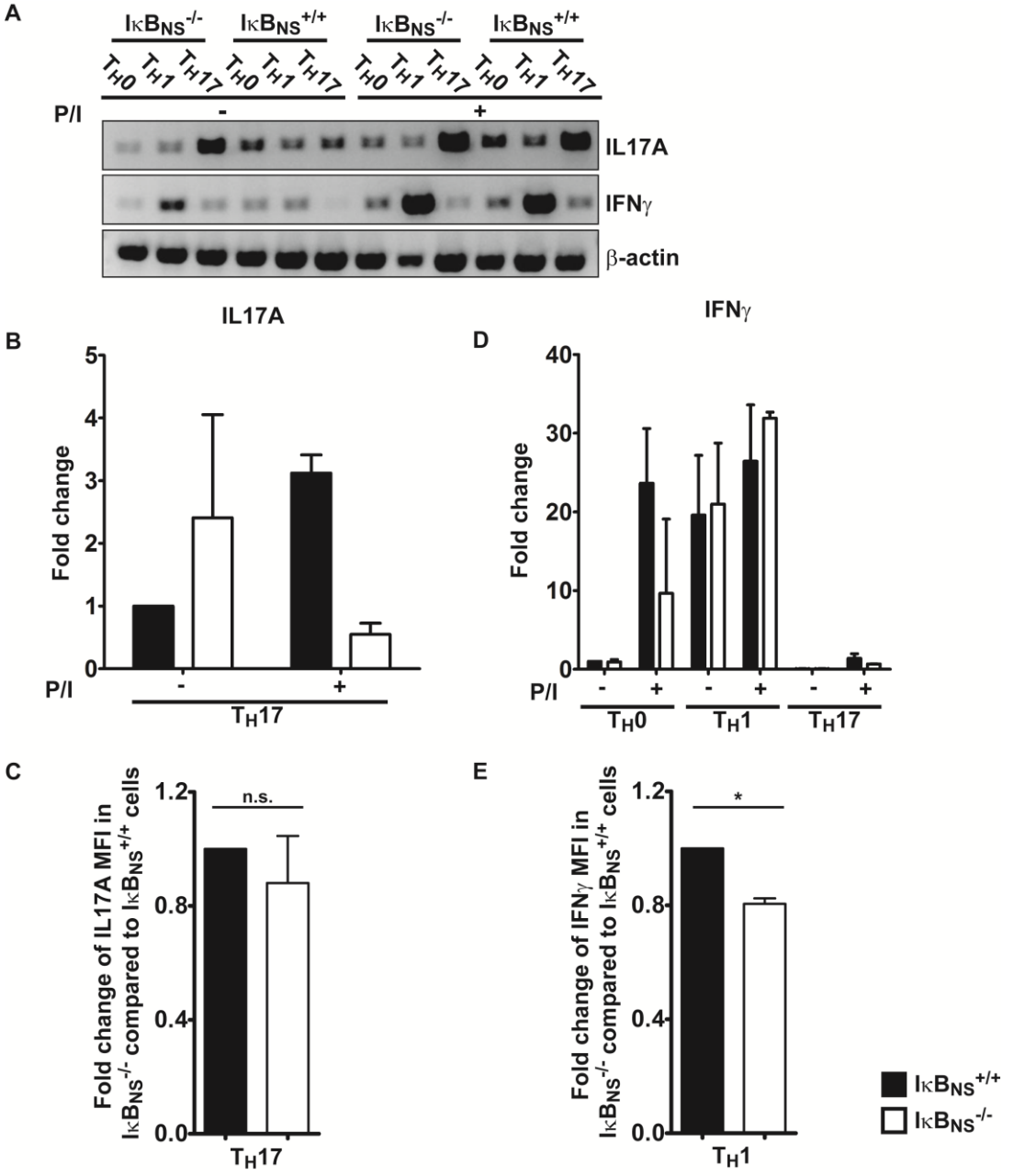

Figure 28: Similar RNA expression of IFNγ and IL17F in IκB$_{NS}^{+/+}$ and IκB$_{NS}^{-/-}$ T cells, but reduced protein expression of both cytokines. After the isolation of naïve T cells by flow cytometry the cells were cultured under T$_H$1-, T$_H$17- or non-polarising (T$_H$0) conditions. On day 4, the expression of IL17A **(A-C)** and IFNγ **(A,D-E)** was analysed by RT-PCR **(A)**, qPCR **(B+D)** or flow cytometry **(C+E)**. The RT-PCR data are representative for two independent experiments (A). The qPCR data were normalised to non-stimulated T$_H$17 wildtype cells **(B)** or non-stimulated T$_H$0 wildtype cells **(D)** and the fold change was calculated. Error bars display the s.e.m. of three **(B+D)** or four **(C+E)** independent experiments. Statistical analyses were performed by two-tailed Mann-Whitney U test; n.s.= not significant, (*) $p<0.05$.

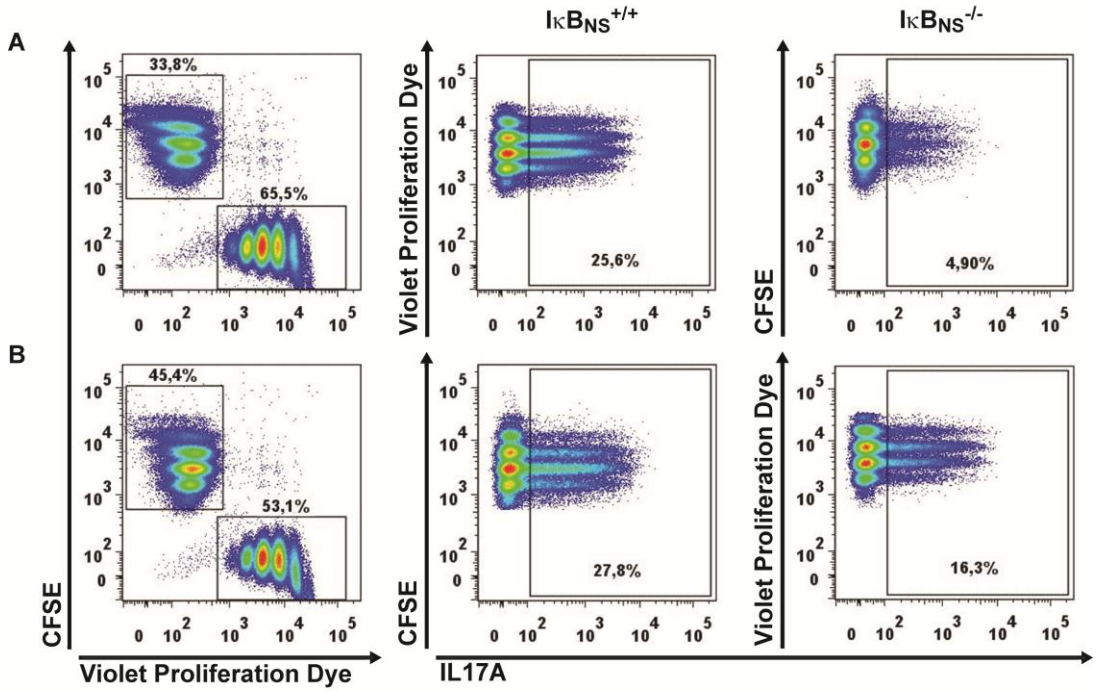

Figure 29: Reduced IL17A expression in IκB$_{NS}$-deficient T$_H$17-polarised cells. Naïve T cells were isolated by flow cytometry from IκB$_{NS}^{+/+}$ and IκB$_{NS}^{-/-}$ mice. Naïve wildtype and IκB$_{NS}$-deficient T cells were stained either with CFSE or CellTrace™ Violet Proliferation Dye, mixed in a ratio of 1:1 and cultured under T$_H$17-polarising conditions. On day 4, cells were stimulated with PMA/ ionomycin (4 h) and BrefeldinA (2 h). IL17A-producing cells were analysed by flow cytometric measurement. In **(A)** IκB$_{NS}^{+/+}$ cells were stained with Violet Proliferation dye and IκB$_{NS}^{-/-}$ cells with CFSE. In **(B)** IκB$_{NS}^{+/+}$ cells were stained with CFSE and IκB$_{NS}^{-/-}$ cells were stained with Violet Proliferation dye.

For further analysis of the reduced expression of IL17A, naïve T cells were stained using a proliferation dye, followed by cultivation of IκB$_{NS}$-deficient naïve T cells in the present of IκB$_{NS}$ wildtype naïve T cells (Figure 29). To exclude that the proliferation dye-induced effects, IκB$_{NS}$-deficient T cells were either stained with CFSE (Figure 29A) or CellTrace™ Violet Proliferation Dye (Figure 29B) and wildtype T cells were stained with the opposite dye. The T$_H$17 polarisation of naïve T cells indicated a diminished proliferation in IκB$_{NS}$-deficient cells (Figure 29). As already shown above, a bit more wildtype cells pass through five divisions compared to IκB$_{NS}$-defective cells. Furthermore, a reduced number of naïve IκB$_{NS}$-deficient T cells differentiated into IL17A expressing cells compared to wildtype cells. Moreover, apparently each proliferation step of IL17$^+$ IκB$_{NS}$-deficient T cells exhibited a reduced MFI of IL17A (Figure 29). Nevertheless, both proliferation dyes emit in a different colour, therefore a direct side-by-side comparison of IκB$_{NS}$-deficient and wildtype cells is impossible. For this reason, CFSE stained IκB$_{NS}$-deficient (CD90.2$^+$) naïve T cells were polarised together with CFSE stained congenic wildtype (CD90.1$^+$) cells (Figure 30). Single proliferation steps were gated in the dot blot (Figure 30, left

panel) and analysed for the MFI of IL17A (Figure 30, right panel). The deficiency of IκB$_{NS}$ in T$_H$17 cells induced a severely reduced expression of IL17A compared to wildtype T$_H$17 cells. This analysis indicated that IκB$_{NS}$ participates in cytokine expression of T$_H$17 cells.

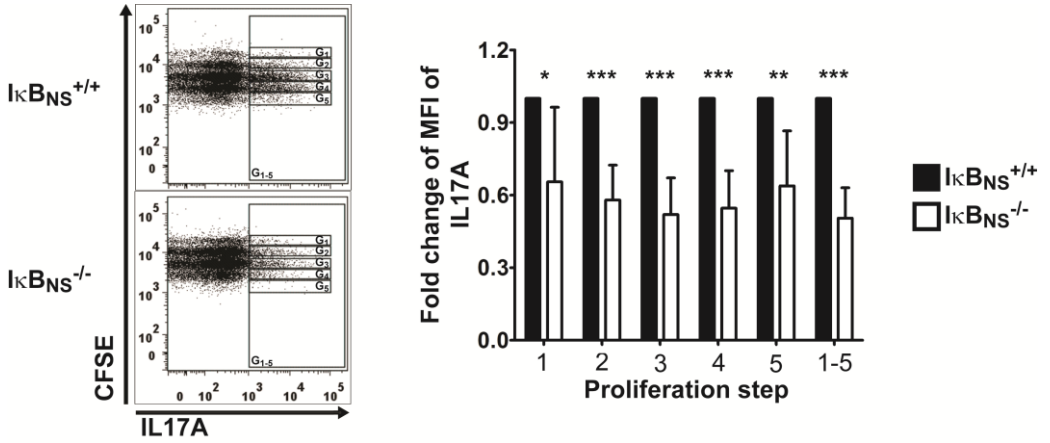

Figure 30: IκB$_{NS}$ deficiency impaires the expression of IL17A. Isolated naïve IκB$_{NS}^{+/+}$ (CD90.1$^+$) and IκB$_{NS}^{-/-}$ (CD90.2$^+$) T cells were mixed in a ratio of 1:1, stained with CFSE and cultured under T$_H$17- polarising conditions. On day 4, IL17A expression was analysed by flow cytometry. The mean fluorescence intensity (MFI) of IL17A$^+$ per each proliferation cycle was analysed. Representative dot plots indicating the MFI of IL17A within five proliferation steps (G1-G5, left panel). The fold change of MFI of IL17A in IκB$_{NS}^{-/-}$ compared to IκB$_{NS}^{+/+}$ cells was determined within the five proliferation steps (right panel). Error bars display the s.e.m. of four independent experiments. Statistical analyses were performed by two-tailed Mann-Whitney U test; (*) $p<0.05$, (**) $p<0.01$, (***) $p<0.001$.

To determine whether other cytokines were also impaired, *in vitro* generated wildtype and IκB$_{NS}$-deficient T$_H$17 cells were enriched to obtain similar frequencies of IL17$^+$ cells (Figure 31). Comparing the cell composition directly after the T$_H$17 cell polarisation (non-enriched, Figure 31A upper panel) to the enriched T$_H$17 cells (Figure 31A lower panel) most cells, which did not undergo efficient T$_H$17 polarisation, were removed. Additionally, the enrichment of IκB$_{NS}$-deficient and wildtype T$_H$17 cells resulted in similar frequencies of IL17A$^+$ cells (Figure 31).

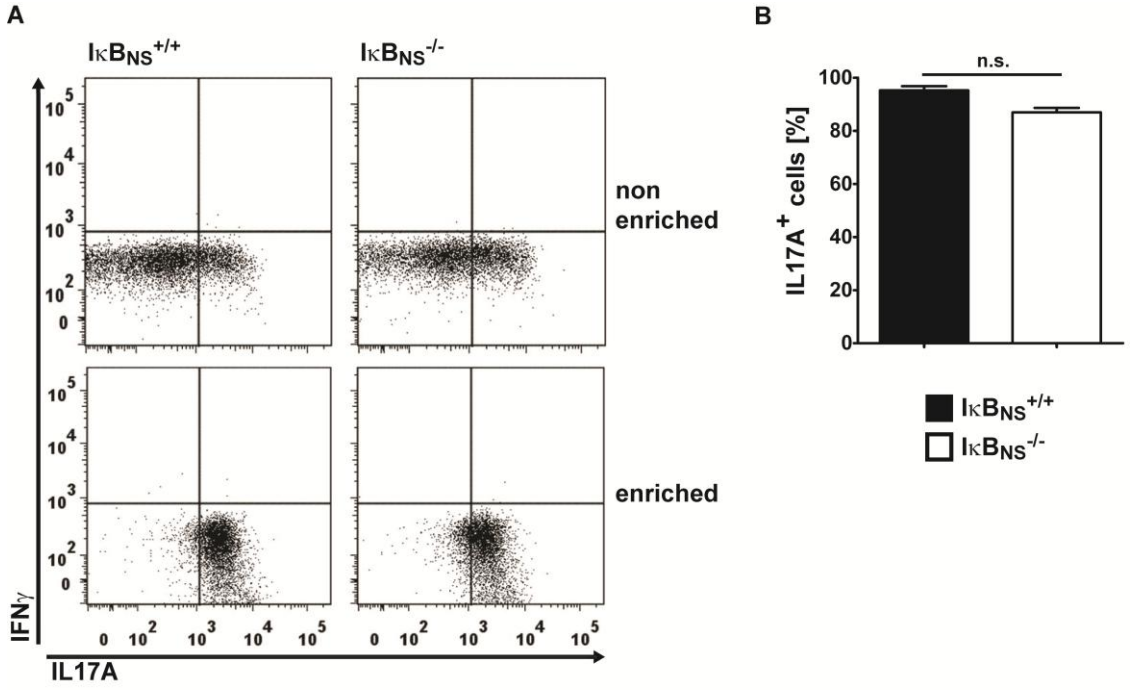

Figure 31: Enrichment efficiency of IL17A-secreting cells. Naïve T cells were isolated by flow cytometry and cultured for 4 days under T_H17-priming conditions. Prior to enrichment, the cells were stimulated with PMA/ ionomycin (3 h). The IL17A expressing cells were enriched using a mouse IL17 secretion assay. After the magnetic separation of IL17-secreting cells, IFNγ and IL17A-producing cells were identified by flow cytometry. Representative dot blots are illustrated in **(A)**, the upper panel shows the cells prior to enrichment and the lower panel the cells after enrichment. The frequency of $IL7A^+$ cells was analysed **(B)**. Error bars display the s.e.m. and are representative for three independent experiments. Statistical analyses were performed by two-tailed Mann-Whitney U test; n.s.= not significant.

First, enriched T_H17 cells were stimulated with PMA and ionomycin and the supernatant was used in a cytokine array membrane (Figure 32 and Figure 33A). This membrane revealed a reduced secretion of IL2, IL10, IL6 and MIP1α by $I\kappa B_{NS}$-deficient T_H17 cells. Secondly, flow cytometry-based cytokine measurement verified the reduced expression of these cytokines in $I\kappa B_{NS}$-deficient T_H17 cells (Figure 33B-C). Furthermore, the effect of the $I\kappa B_{NS}$ deficiency on the cytokine mRNA expression in stimulated T_H17 cells was analysed by qPCR (Figure 33D). While the expression of IL6 mRNA was hardly detectable (data not shown), the analysis of the mRNA expression exhibited an equal expression of IL2 and MIP1α in both genotypes. However, the anti-inflammatory cytokine IL10 showed a reduced expression in $I\kappa B_{NS}$-deficient compared to wildtype T_H17 cells, indicating a regulatory function of $I\kappa B_{NS}$ to IL10 expression.

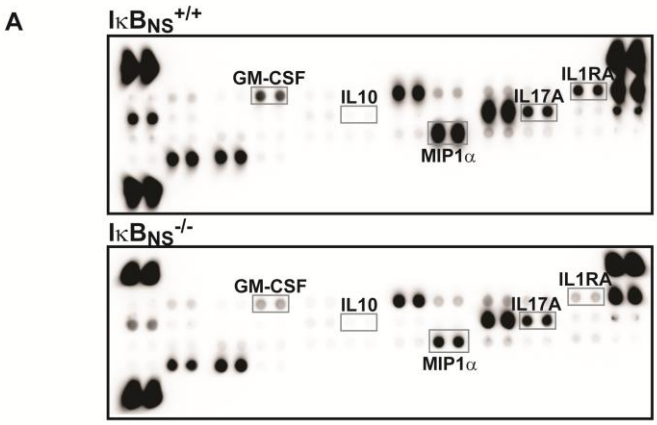

C

	1 2	3 4	5 6	7 8	9 10	11 12	13 14	15 16	17 18	19 20	21 22	23 24
A	pos.											pos.
B	CXCL 13	C5a	G-CSF	GM-CSF	CCL 1	CCL 11	ICAM1	IFNγ	IL1α	IL1β	IL1ra	IL2
C	IL3	IL4	IL5	IL6	IL7	IL10	IL13	IL12 p70	IL16	IL17A	IL23	IL27
D	CXCL 1	CXCL 11	KC	M-CSF	CCL 2	CCL 12	MIG	CCL3/ Mip1α	CCL 4	MIP2	CCL 5	CXCL 12
E	CCL 17	TIMP1	TNFα	TREM 1								
F	pos.											neg.

Figure 32: Diminished cytokine secretion of IκB$_{NS}$-deficient T$_H$17 cells was indicated by cytokine array membrane. Naïve T cells were isolated by flow cytometry and cultured for 4 days under T$_H$17-priming conditions. The IL17A expressing cells were enriched and stimulated with PMA/ ionomycin (4 h). The relative levels of several cytokines in the supernatant of IκB$_{NS}^{+/+}$ and IκB$_{NS}^{-/-}$ T$_H$17 cells were profiled with a cytokine array membrane from R&D. Membranes of two independent experiments are shown **(A** and **B)**. The location of positive (pos.) and negative (neg.) controls and cytokines on the array membrane are indicated in **(C)**.

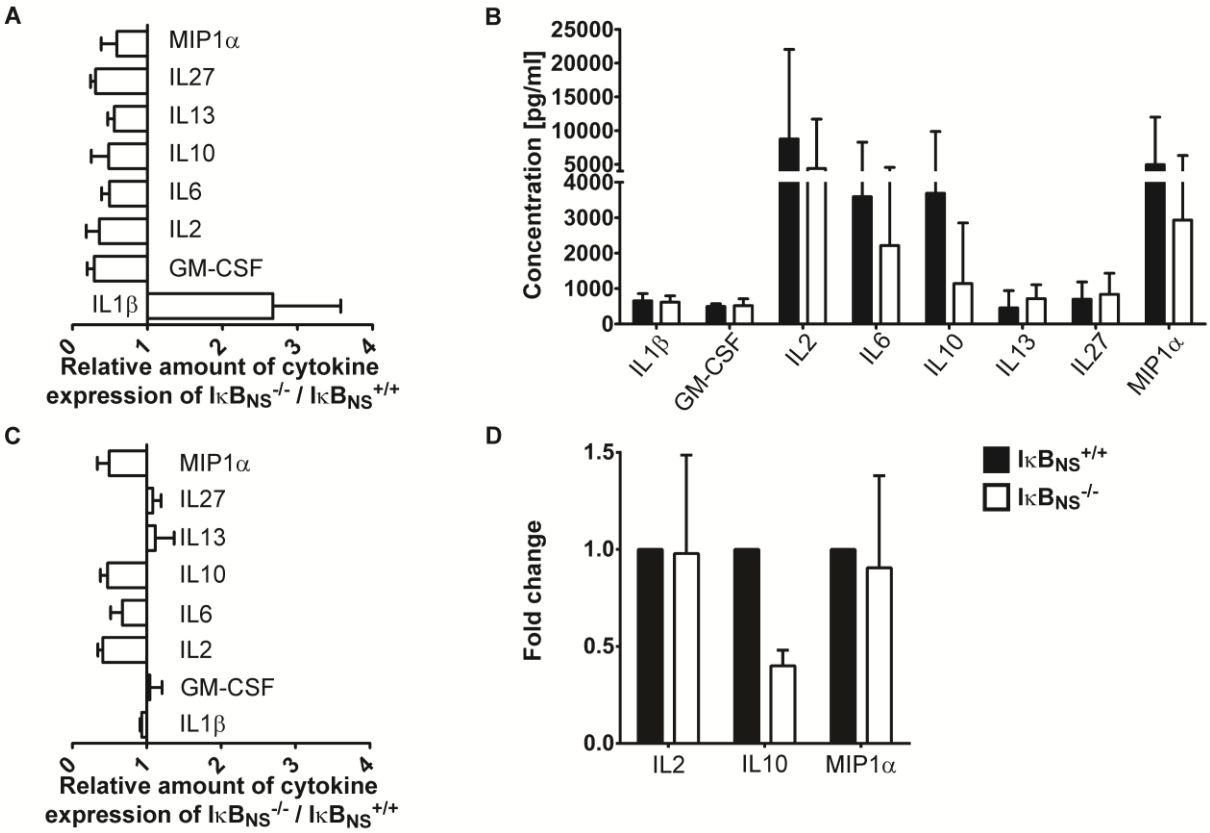

Figure 33: Verification of the diminished cytokine secretion of IκB$_{NS}$-deficient T$_H$17 cells. Naïve T cells were isolated by flow cytometry and cultured for 4 days under T$_H$17-priming conditions. The IL17A expressing cells were used directly **(D)** or were enriched **(A-C)**. After the stimulated with PMA/ ionomycin (4h), the relative levels of several cytokines in the supernatant of IκB$_{NS}^{+/+}$ and IκB$_{NS}^{-/-}$ T$_H$17 cells were profiled with a cytokine array membrane **(A)**, by flow cytometry **(B-C)** or by qPCR **(D)**. The summery of the cytokine array membrane is shown in **(A)**. The cytokine concentration in supernatant was measured by a bead-based flow cytometry array **(B)**. In **(C)** the relative amount of cytokines in IκB$_{NS}^{-/-}$ T$_H$17 cells was calculated from the cytokine concentrations shown in **(B)**. The fold change of MIP1α, IL10 and IL2 in T$_H$17 cells was measured by qPCR and normalised to stimulated T$_H$17 wildtype cells **(D)**. Error bars display the s.e.m. of two **(A)**, three **(D)** or four **(B-C)** independent experiments.

3.3 Function of IκB$_{NS}$ in autoimmunity and inflammation

3.3.1 IκB$_{NS}$ deficiency mildly delayed the onset of EAE

Studies on the autoimmune disorder multiples sclerosis and its animal model experimental autoimmune encephalomyelitis (EAE), suggested a T cell-mediated autoimmune demyelination [57,151–154]. Hilliard *et al.* reported about the importance of the NF-κB signalling in the onset of EAE [155,156]. Both, NF-κB1-deficient as well as cRel-deficient mice are largely protected to EAE induction [155,156].

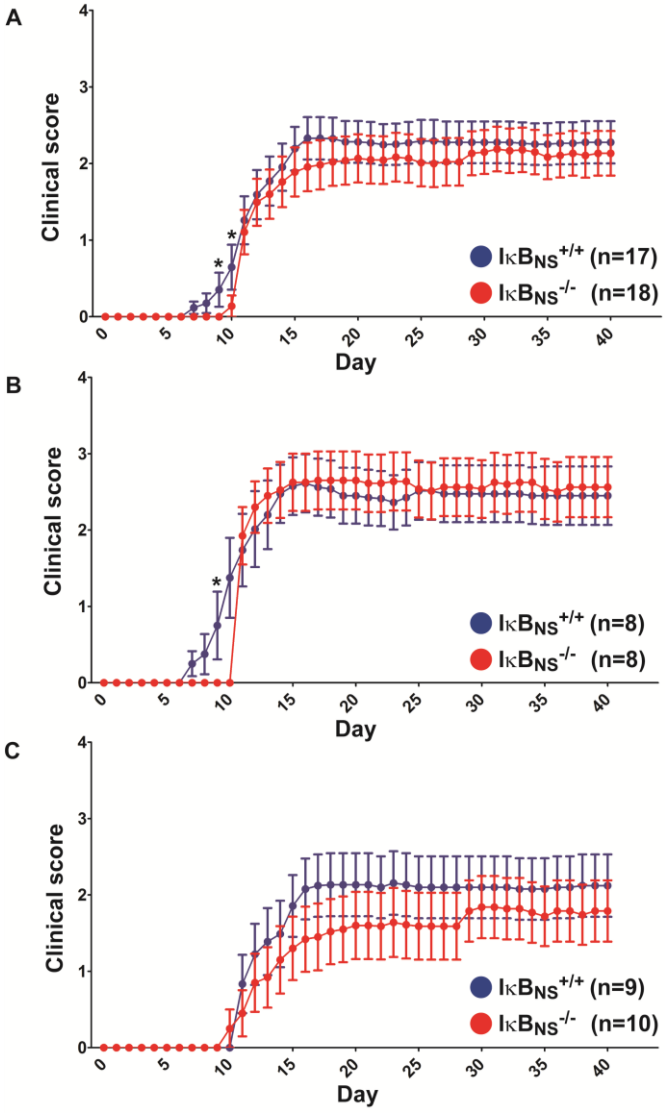

Figure 34: Mildly reduced progression of experimental autoimmune encephalomyelitis (EAE) in IκB$_{NS}$-deficient mice. EAE was induced in IκB$_{NS}^{+/+}$ (n=17) or IκB$_{NS}^{-/-}$ (n=18) mice by s.c. injection of MOG(35-55)-peptide and two subsequent i.p. injections of pertussis toxin. The clinical score for the mice was monitored over 40 days. The shown data are the mean of animals **(A)**, male mice **(B)** or female mice **(C)**. Error bars display the standard error of the mean of the mice of four independent experiments. Statistical analyses were performed by two-tailed Mann-Whitney U test; n.s.= not significant, (*) $p<0.05$.

To identify the role of $I\kappa B_{NS}$ in the formation of autoreactive myelin-specific T cells and the onset of EAE, the progression of this disease was monitored from the day of MOG(35-55)-peptide immunisation until day 40 (Figure 34). The first clinical symptoms could be monitored within the wildtype group 7 days after the immunisation.

$I\kappa B_{NS}$-deficient mice exhibited a delayed onset of EAE symptoms, first appearing at day 10. However, this difference was exclusively found between male mice with a significant change at day 9 (Figure 34, middle panel). Indeed, $I\kappa B_{NS}$-deficient female mice showed a reduced progression of EAE compared to wildtype mice. Hence, because of the narrow phenotypical differences comparing $I\kappa B_{NS}$-deficient and wildtype mice in EAE further *in vivo* analysis were performed (e.g. colitis induction, *Citrobacter rodentium* infection).

3.3.2 $I\kappa B_{NS}$ deficiency results in impaired T_H17 development and high susceptibility to chronic gut inflammation

High numbers of T_H17 cells are detectable in the uninfected gut compared to other tissues [44]. Intestinal inflammation, such as ulcerative colitis or Crohn´s disease induce even higher T_H17 numbers, which accumulate in the gut and the surrounding lymphoid tissues [157,158]. It was reported previously that innate immune cells are the important players in the acute form of DSS-induced colitis [159]. However, next to B cells, T_H1 and T_H17 cells promote the progression of chronic colitis, which can be induced by multiple cycles of DSS feeding [160].

To identify whether $I\kappa B_{NS}$ deficiency affects the formation of T_H17 cells and thereby contribute to the pathogenesis of colitis, in cooperation with Dr. Rainer Glauben and Dr. Anja A. Kühl from the Charité, Berlin (Germany), chronic colitis was induced in $I\kappa B_{NS}$-deficient and wildtype mice by multiple cycles of DSS feeding (Figure 35 and Figure 36). During the progression of colitis the $I\kappa B_{NS}$-deficient mice lost significantly more weight compared to wildtype (Figure 35A). However, the colon length was reduced similarly in both $I\kappa B_{NS}$-deficient and wildtype mice (Figure 35B). Even without DSS feeding, colon damage was increased in $I\kappa B_{NS}$-deficient compared to wildtype mice, whereas DSS fed $I\kappa B_{NS}$-deficient and wildtype mice showed no histological differences (Figure 35C-D). The frequency of $IL17A^+$ T cells was decreased in $I\kappa B_{NS}$-deficient non-treated as well as DSS-treated mice compared to wildtype mice (Figure 36).

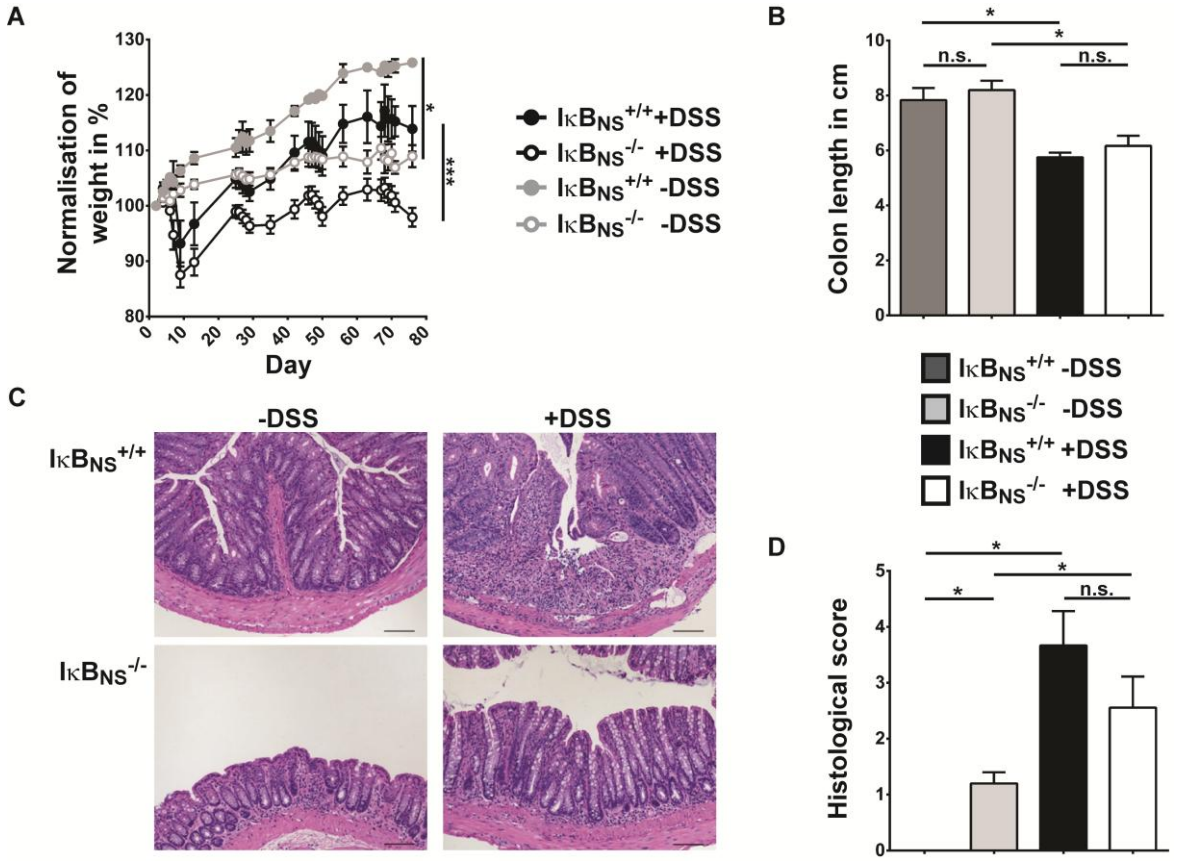

Figure 35: IκB$_{NS}$-deficiency results in a more efficient chronic inflammation of the gut during DSS-induced colitis. DSS colitis was induced in IκB$_{NS}^{+/+}$ (n=6) or IκB$_{NS}^{-/-}$ (n=9) mice by three rounds of DSS feeding and as control three wildtype and five IκB$_{NS}$-deficient mice received non-supplemented water. The normalised weight of mice during inflammation is shown in **(A)** and the length of colon in **(B)**. Representative hematoxylin and eosin staining of colon section are shown in **(C)** (scale bar represents 100 µm). The histological score is the sum of individual scores of inflammatory cell infiltration and tissue damage **(D)**. The frequency of IL17A^{+} within the CD4^{+} T cell subset was analysed by flow cytometry staining of the colon **(D)**. Horizontal lines in **(A-D)** represent the mean of animals and error bars display the standard error of the mean. Statistical analyses were performed by two-tailed Mann-Whitney U test; n.s.= not significant, (*) $p<0.05$.

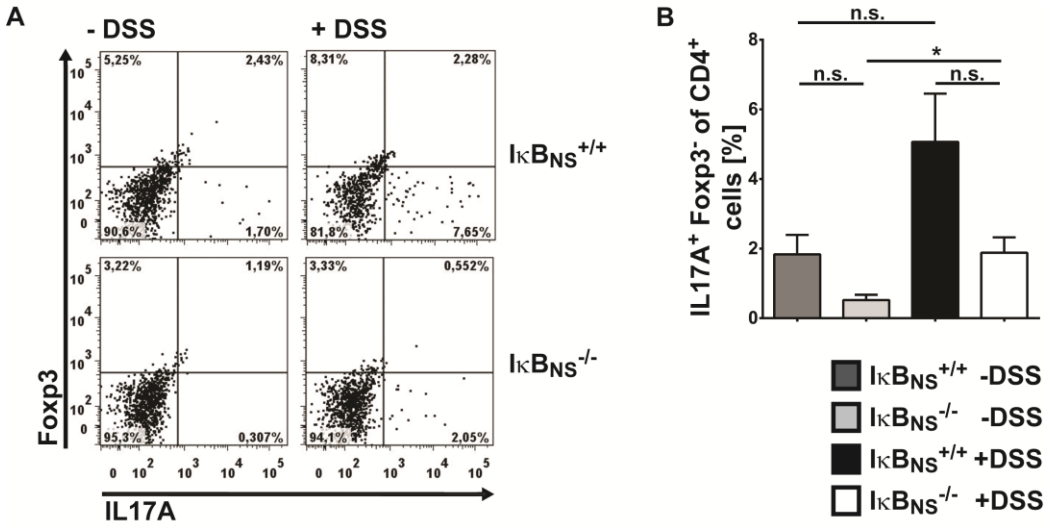

Figure 36: Reduced frequency of IL17A$^+$ cells in IκB$_{NS}$-deficient mice during DSS-induced colitis. In IκB$_{NS}^{+/+}$ (n=6) or IκB$_{NS}^{-/-}$ (n=9) mice DSS colitis was induced by three rounds of DSS feeding. As control three wildtype and five IκB$_{NS}$-deficient mice got normal water only. The frequency of IL17A$^+$ Foxp3$^-$ cells within the CD4$^+$ T cell subset was analysed by flow cytometry staining of the LPL **(A** and **B)**. Representative dot blots are shown **(A)**. Horizontal lines in **(B)** represent the mean of animals and error bars display the standard error of the mean. Statistical analyses were performed by two-tailed Mann-Whitney U test; n.s.= not significant, (*) $p<0.05$.

Due to the fact that the DSS colitis suggested an important role of IκB$_{NS}$ for T$_H$17 cell development during gut inflammation, it was determined in cooperation with Dr. Rainer Glauben and Dr. Anja A. Kühl from the Charité, Berlin (Germany) if T$_H$17 cell development is also impaired in T cell based transfer colitis (Figure 37 and Figure 38).

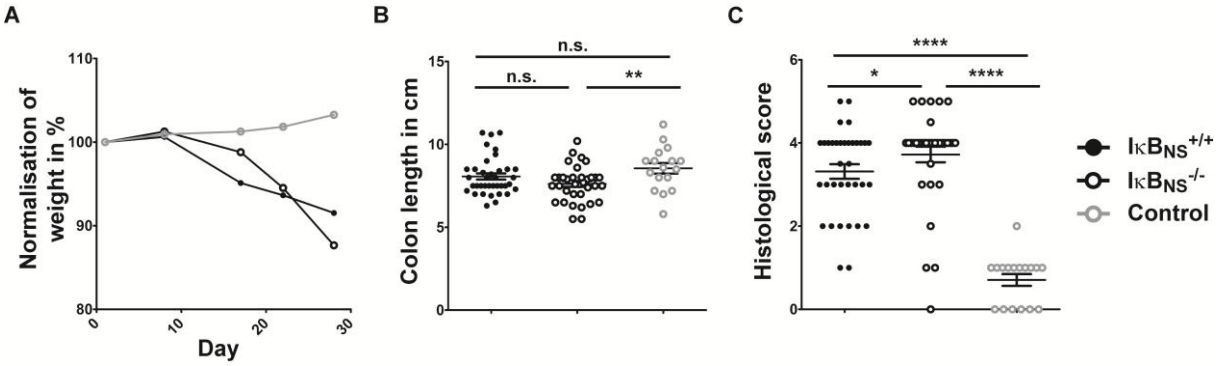

Figure 37: In transfer colitis IκB$_{NS}$-deficient T cells are more efficient to induce inflammation of the gut. Transfer colitis was triggered in RAG1$^{-/-}$ mice by adoptive transfer (i.p.) of freshly isolated CD4$^+$CD25$^-$ T cells from IκB$_{NS}^{+/+}$ (n=35) or IκB$_{NS}^{-/-}$ (n=36) mice. As control some mice were injected with PBS (n=17) only. The normalised weight of the mice during inflammation is shown in **(A)** and the length of the colon at the sampling day is represented in **(B)**. The histological score is the sum of individual scores of inflammatory cell infiltration and tissue damage **(C)**. Horizontal lines in **(A-C)** represent the mean of animals and error bars display the standard error of the mean. Statistical analyses were performed by two-tailed Mann-Whitney U test; n.s.= not significant, (*) $p<0.05$, (**) $p<0.01$, (***) $p<0.001$, (***) $p<0.0001$.

Hence, naïve $CD4^+CD25^-$ $I\kappa B_{NS}$-deficient or wildtype T cells were injected into $Rag1^{-/-}$ mice. During the progression of colitis the recipients of $I\kappa B_{NS}$-deficient T cells lost more weight compared to recipients of wildtype T cells (Figure 37A). Furthermore, recipients of $I\kappa B_{NS}$-deficient T cells showed a comparable colon length to wildtype group (Figure 37B), but the histological damage was significantly increased by the transfer of $I\kappa B_{NS}$-deficient T cells (Figure 37C). Above all, the T cell composition showed a drastic change after colitis induction by the transfer of $I\kappa B_{NS}$-deficient compared to wildtype T cells (Figure 38). On the one hand, a significantly reduced frequency of $IL17A^+$ (Figure 38A) as well as $IL17A^+IFN\gamma^+$ T cells (Figure 38C) in recipients of $I\kappa B_{NS}$-deficient T cells was observed. On the other hand, the frequency of $IL17A^-IFN\gamma^+$ T cells (Figure 38B) was significantly increased in recipients of $I\kappa B_{NS}$-deficient cells, demonstrating the relevance of $I\kappa B_{NS}$ for the formation of T_H17 cells in the inflamed gut. Taken together, both DSS as well as transfer colitis revealed the necessity of $I\kappa B_{NS}$ for the development of T_H17 cells in gut inflammation.

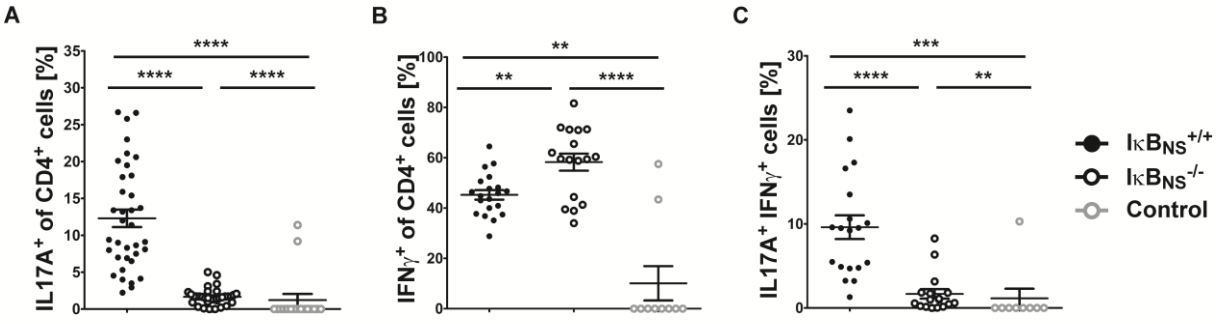

Figure 38: Less $IL17A^+$ and $IL17A^+/IFN\gamma^+$ cells are induced during transfer colitis in $I\kappa B_{NS}$-deficient mice. Freshly isolated $CD4^+CD25^-$ T cells from $I\kappa B_{NS}{}^{+/+}$ (n=35) or $I\kappa B_{NS}{}^{-/-}$ (n=36) mice were injected (i.p.) to $RAG1^{-/-}$ mice and thereby transfer colitis was triggered. Mice injected with PBS (n=17) only served as control. The frequency of $IL17A^+$ **(A)**, $IFN\gamma^+$ **(B)** and double positive cells **(C)** within the $CD4^+$ T cell subset was analysed by flow cytometry staining of the colon. Horizontal lines in **(A-C)** represent the mean of animals. Error bars display the s.e.m. Statistical analyses were performed by two-tailed Mann-Whitney U test; (*) $p<0.05$, (**) $p<0.01$, (***) $p<0.001$, (***) $p<0.0001$.

3.4 Mice defective in IκB$_{NS}$ display a high susceptibility to *Citrobacter rodentium* gut infection associated with an impaired T$_H$17 development.

Citrobacter rodentium is a non-invasive pathogen, which establishes acute infections of the murine large intestinal mucosa [161]. To clear the infection, antibodies produced by B cells are required and the help of CD4$^+$ T cells, especially T$_H$17 cells, is needed to produce resolving antibody titres [78,162].

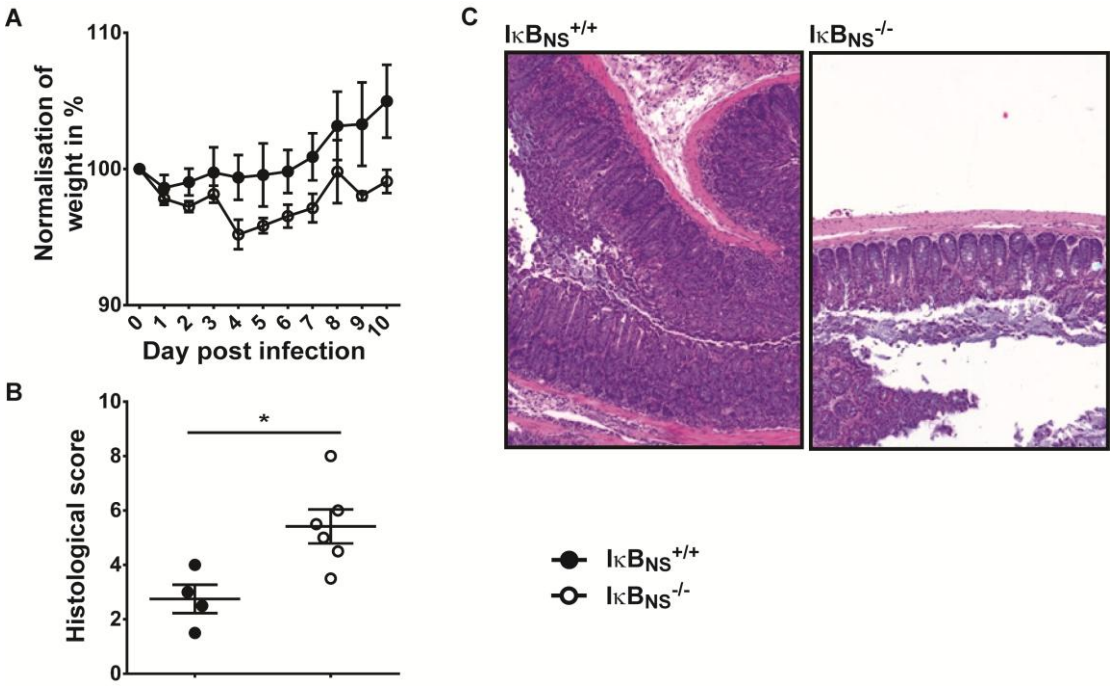

Figure 39: IκB$_{NS}$-deficient mice are more susceptible to *Citrobacter rodentium* infection. IκB$_{NS}^{+/+}$ or IκB$_{NS}^{-/-}$ mice were infected orally with 1*10^{10} *C. rodentium* expressing the *lux*-operon and analysed at day 10 post infection. The normalised weight of mice during the course of infection **(A)**, the histological score after infection **(B)** and representative hematoxylin and eosin staining of colon section **(C)** are shown. Horizontal lines in **(A-B)** represent the mean of animals and error bars display the s.e.m. Data are representative for one experiment of at least three individual experiments **(A)** or were pooled from two individual **(B)** experiments with at least three mice per group. Statistical analyses were performed by two-tailed Mann-Whitney U test; (*) $p<0.05$.

In cooperation with Zuobai Wang (Institute for infection immunology, TWINCORE, Hannover, Germany) *Citrobacter rodentium* was administered orally to IκB$_{NS}$-deficient and wildtype mice to clarify the function of IκB$_{NS}$ in T$_H$17 cells during gut infection (Figure 39, Figure 40 and Figure 41). An impaired growth rate in IκB$_{NS}$-deficient mice was observed after the inoculation of bacteria, since these mice gained less body weight than age-matched wildtype mice (Figure 39A). On day 10, IκB$_{NS}$-deficient mice exhibited a significantly increased damage of the large intestine, demonstrated by strongly thickened colon and more hyperplasia compared to wildtype mice (Figure 39B-C).

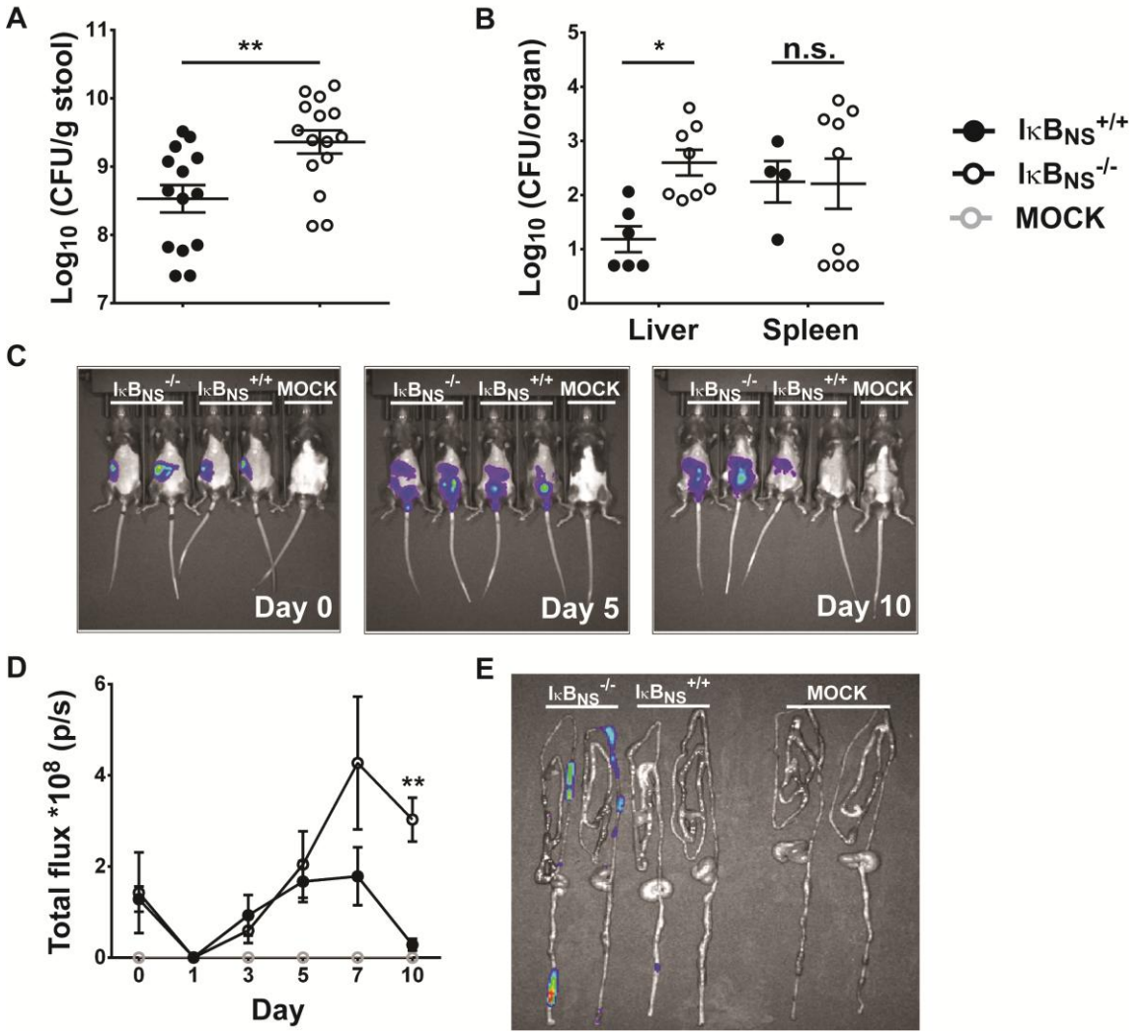

Figure 40: Extended bacterial load in IκB$_{NS}$-deficient mice during *Citrobacter rodentium* infection. 1*10^{10} *C. rodentium* expressing the *lux*-operon were used for oral infection of IκB$_{NS}^{+/+}$ or IκB$_{NS}^{-/-}$ mice. At day 10 post infection, the mice were analysed for the spread of bacteria. The analysis of the *C. rodentium* burden in stool **(A)** and the bacterial load in liver and spleen **(B)** are shown. After the infection of mice with *lux*-operon expressing *C. rodentium* the bacterial load in intestinal tract **(E)** or the whole mice **(C+D)** was measured *in vivo* by bioluminescence imaging (IVIS-CT) at the day of infection (day 0), day 5 as well as day 10 **(C)** or at day 10 only **(E)**. Horizontal lines in **(A-B)** represent the mean of animals and error bars display the standard error of the mean. Data were pooled from at least three individual **(A-B)** experiments with at least three mice per group or data are representative for one experiment with two **(E)** three **(C-D)** mice per group. Statistical analyses were performed by two-tailed Mann-Whitney U test; n.s.= not significant, (*) $p<0.05$, (**) $p<0.01$.

The bacterial burden was slightly increased in the spleen (Figure 40B) and significantly increased in stool (Figure 40A) as well as liver (Figure 40B) of IκB$_{NS}$-deficient mice. Furthermore, whole body imaging of both genotypes displayed an equal accumulation of luminescent bacteria in the gut at the day of infection, which similarly spread into the intestinal tract at day 5 (Figure 40C-D). On day 10, wildtype and IκB$_{NS}$-deficient mice had a significantly different luminescence signal, which showed that IκB$_{NS}$-deficient mice did not clear the *Citrobacter rodentium* infection in contrast to wildtype mice (Figure 40C-E).

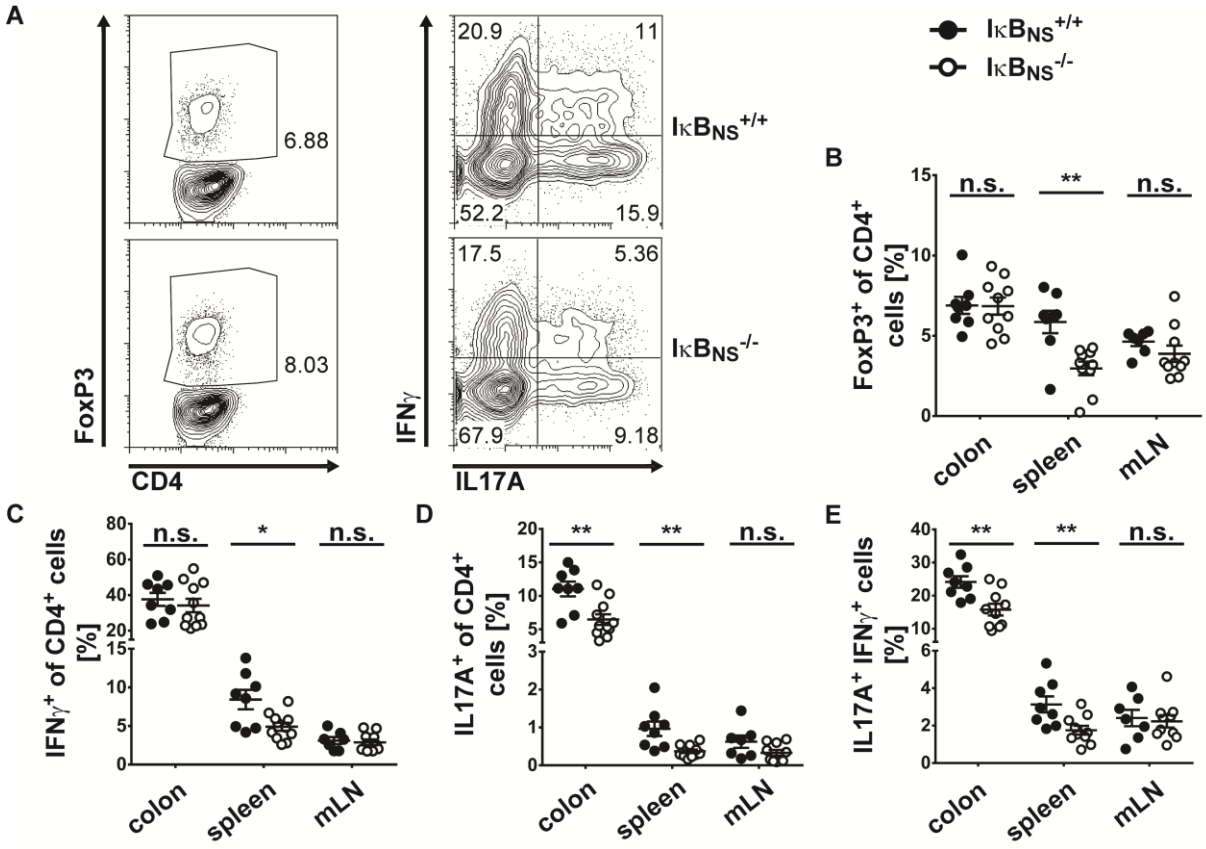

Figure 41: Altered cellularity in IκB$_{NS}$-deficient mice upon *Citrobacter rodentium* infection. At day 10 post infection, IκB$_{NS}^{+/+}$ (n=8) or IκB$_{NS}^{-/-}$ (n=10) mice administered orally with 1*10^{10} *C. rodentium* (expressing the *lux*-operon) were analysed. Cells from colon, spleen and mLN were isolated and measured by flow cytometry. Representative dot blots (pre-gated to CD4$^+$CD3$^+$ cells) of the colon are shown in **(A)**. The frequency of Foxp3$^+$ **(B)**, IFNγ$^+$ **(C)**, IL17A$^+$ **(D)** and IL17A/ IFNγ double positive cells **(E)** within the CD4$^+$CD3$^+$ T cell subset was analysed. Horizontal lines in **(B-E)** represent the mean of animals and error bars display the standard error of the mean. Data were pooled from three individual experiments with two to four mice per group **(B-E)**. Statistical analyses were performed by two-tailed Mann-Whitney U test; n.s.= not significant, (*) $p<0.05$, (**) $p<0.01$.

Moreover, at day 10 systemic and mucosal tissues of both genotypes showed reduced frequencies of IL17A$^+$ T$_H$17 and IFNγ$^+$ IL17A$^+$ double positive cells, where both frequencies were slightly reduced in the mLN and significantly reduced in colon and spleen of IκB$_{NS}$-deficient compared to wildtype mice (Figure 41D-E). Additionally, the frequencies of IFNγ$^+$ T$_H$1 cells were equal in mLN and colon, but significantly reduced in spleens from IκB$_{NS}$-deficient compared to wildtype mice (Figure 41A-C). Furthermore, while the Treg cell frequencies of colon and mLN were equal in both genotypes, the Treg frequencies were significantly decreased in spleens from IκB$_{NS}$-deficient compared to wildtype animals (Figure 41A-B). Altogether, IκB$_{NS}$ promotes the development of T$_H$17 cells to fight intestinal pathogens, whereas its loss causes an exacerbated course of disease.

4 Discussion

4.1 The loss of IκB$_{NS}$ alters the development of B cells

Signalling via the transcription factor NF-κB is one of the key mechanism activated by pre-B cell receptor (BCR) and BCR signals in mature cells. The BCR signalling causes a rapid IKKβ-dependent translocation of NF-κB dimers from the cytoplasm into the nucleus. The major NF-κB dimer found in pre-B cells is p50/p65, which is largely replaced by p50/cRel heterodimers in mature B cells [163]. Hence, it is not surprising, that the disruption of NF-κB family members or NF-κB regulators impairs the BCR-mediated proliferation, survival and Ig class switching of B cells [140,141,164–169]. Feng *et al.* suggested that NF-κB activity is required for the overall survival of B cells in all developmental stages [169]. Furthermore, inhibition of NF-κB blocks B cell development at two checkpoints. First, NF-κB inhibition affects B cell differentiation at the pro-B to pre-B cell transition, secondly the survival as well as the maturation of transitional/ immature B cells into follicular B cells is affected in the periphery [169].

Arnold *et al.* reported a fast induction of IκB$_{NS}$ after cross-linking of the BCR [133]. Due to this fact and because B cell proliferation and effector function depends on NF-κB activity, the function of IκB$_{NS}$ in B cells was analysed in this thesis. The number of B220^{+} B cells was impaired in the bone marrow and the blood of IκB$_{NS}$-deficient mice. In line with this finding, the group of Touma *et al.* described a mild reduction within the B cell (B220^{+}) compartment in spleen and lymph nodes of 6 to10 weeks old IκB$_{NS}^{-/-}$ mice [128]. Four years later, a more detailed analysis of IκB$_{NS}$-deficient B cells was performed in 9 month old mice [132]. Compared to young mice, the development of IκB$_{NS}^{-/-}$ B220^{+} cells in spleen and lymph nodes was more delayed and this reduction was most pronounced in the blood [132]. In contrast, Arnold *et al.* used IκB$_{NS}$-deficient *N*-ethyl-*N*-nitrosourea (ENU)-mutagenised mice and observe an equal frequency of immature and mature B cells compared to wildtype mice [133]. However the mice used in this thesis and in the publication of Arnold *et al.* were younger than the one used by Touma *et al.*. Hence, one may suggest that the older the mice, the stronger the effect of IκB$_{NS}$ to the formation of B220^{+} B cells. Furthermore, both groups described a severe reduction or the entire loss of B1 B cells in IκB$_{NS}$-deficient mice [132,133], as it was shown for the deficiency of NF-κB1 and cRel/ NF-κB1 [167]. Additionally, the generation of MZ B cells is highly sensitive to the disruption of NF-κB.

Hence, even the deficiency of only one of the NF-κB subunits reduces the numbers of MZ B cells. [164–166,168] In mice deficient for $I\kappa B_{NS}$ Touma *et al.* identified a delayed development of MZ B cells [132] and Arnold *et al.* a lack of the MZ B cell population [133] compared to wildtype mice. In contrast, in this thesis no changes of the MZ B cell subsets were observed. The mice used in the analysis of Touma *et al.* as well as in this thesis are from the lab of Linda K. Clayton. Hence, the differences in the MZ B cell formation may arise from the different age of the mice, another gating strategy or different housing conditions (e.g. microbiota).

It is possible, that the reduction of $I\kappa B_{NS}$-defective $B220^+$ cells is the result of an increased cell death rate. This hypothesis is substantiated by a previous study revealing that NF-κB1-deficient cells exhibit an enhanced mitogen-induced apoptosis [141]. Senftleben and colleagues observed an increased turnover of $IKK\alpha^{-/-}$ B cells, which correlated with a higher rate of spontaneous apoptosis [170]. However, the knockdown of $I\kappa B_{NS}$ within the B cell line A20 did not influence the sensitivity to apoptosis compared to wildtype A20 cells in this thesis. Nevertheless, Touma *et al.* and Arnold *et al.* identified a diminished B cell proliferation in response to LPS in spleens of $I\kappa B_{NS}$-deficient mice [132,133]. In addition, a dramatically reduced level of serum IgM was detected by Touma *et al.* as well as Arnold *et al.* in $I\kappa B_{NS}$-deficient mice. Hence, cytoplasmic IgM was not detectable by any of these groups, but surface IgM levels were increased in $I\kappa B_{NS}$-deficient compared with wildtype mice, suggesting a defect in IgM secretion. Furthermore, beside the reduction of IgM, levels of IgG3 was dramatically reduced in serum of $I\kappa B_{NS}$-deficient mice [132,133]. The class switching to the IgG3 heavy chain gene was dramatically impaired in $I\kappa B_{NS}$-deficient mice, which was underlined by the lack of IgG3 in serum [132]. In contrast to wildtype mice, no germinal centre (GC) formation could be detected upon the immunisation of $I\kappa B_{NS}$-deficient mice with sheep red blood cells [132]. This is in line with the impaired formation of GC B cells in $IKK\alpha^{-/-}$ reconstituted as well as p52- RelB- and Bcl3-deficient mice [164,165,168,170,171]. In contrast, Arnold *et al.* observed normal GC formation in immunised $I\kappa B_{NS}$-deficient mice. Hence, Arnold *et al.* concluded that $I\kappa B_{NS}$ is to a lesser extent required for the formation of GC or memory B-cell responses rather than for differentiation of extra follicular antibody-secreting cells [133]. Altogether, this thesis shows that $I\kappa B_{NS}$ is a significant regulator of the formation of $B220^+$ B cells, but apparently has no impact in apoptosis sensitivity. Additionally, Touma *et al.* as well as Arnold *et al.* uncovered the crucial function of $I\kappa B_{NS}$ in proliferation and immunoglobulin (Ig)

production of B cells as well as plasma cell differentiation [132,133]. Besides, the regulatory mechanism needs to be examined in detail and possible target genes of IκB$_{NS}$ in B cells remains to be elucidated.

4.2 Novel isoform of IκB$_{NS}$ may arise from posttranslational modifications

Western blot analysis of the murine B cell line A20 or stimulated primary T cells revealed two 70 kDa IκB$_{NS}$ isoforms in addition to the known 35 kDa form. Upon stimulation of wildtype expanded CD4^{+} T cells both IκB$_{NS}$ isoforms appeared with a similar increase over time as well as a comparable signal intensity. This is consistent with the previous report of Schuster *et al.* showing a 35 kDa IκB$_{NS}$ in the cytoplasm and the nucleus as well as a nuclear 70 kDa IκB$_{NS}$, with a mildly stronger expression [134]. Cross-reactivity of the IκB$_{NS}$ antibody does not explain the appearance of the 70 kDa isoform because of the absence of both IκB$_{NS}$ isoforms in IκB$_{NS}$-deficient cells. In addition, two monoclonal murine as well as two polyclonal rabbit IκB$_{NS}$ antibodies detected the expression of the IκB$_{NS}$ isoforms. Consequently, cross-reactivity of the antibodies could be ruled out. Furthermore, both the 35 kDa IκB$_{NS}$ form as well as the 70 kDa IκB$_{NS}$ form were stable to denaturation by urea. Therefore, posttranslational modifications were suggested to be responsible for the shift in the molecular mass. Reports about Bcl3, which has a high sequence similarity to IκB$_{NS}$, revealed that Bcl3 can switch between a cytoplasmic as well as a nuclear isoform [111,112,172]. Furthermore, the effect of Bcl3 on p50 or p52 homodimers depends on the phosphorylation of Bcl3 [110,111]. Bundy *et al.* demonstrated that the regulation of p52 homodimers by Bcl3 depends, additionally to phosphorylation status of Bcl3, on the concentration of Bcl3 to p52 dimers [110]. Accordingly, phosphorylated Bcl3 was not able to inhibit the binding of p52 to κB-sites, not even at high Bcl3 concentrations [110]. In addition, even low concentrations of phosphorylated Bcl3 enhanced the binding of p52. On the other hand, the de-phosphorylation of Bcl3 efficiently inhibited the binding of p52 to κB-sits [110]. In contrast, Caamaño *et al.* showed that Bcl-3 needs to be phosphorylated to increase the binding of p50 homodimers to κB-sites [111]. Additionally, ubiquitination as well as the SUMOylation are two further potential mechanism for IκB$_{NS}$ modification. The ubiquitination can affect the cellular localisation as well as the interaction of proteins or signal for proteasomal degradation [173]. Massoumi *et al.* analysed mice lacking the deubiquitinating enzyme CYLD (cylindromatosis) and suggested a role in

inhibition of tumour formation as well as keratinocyte proliferation [172]. Hence, CYLD translocates to the perinuclear region and removes K63-linked polyubiquitin from Bcl3, which results in cytoplasmic remigration. Thereby CYLD inhibits the nuclear accumulation of Bcl3 and inactivates Bcl3 [172]. The other strongly suggested modification of $I\kappa B_{NS}$, the SUMOylation is a mechanism at which a small ubiquitin-like modifier (SUMO) is covalently added to a protein. The SUMO modification of proteins is important in transcriptional regulation and can lead to the adjustment of protein expression via protein degradation in the nucleus as well as the cytoplasm [174]. The degradation of the cytoplasmic IκB protein, IκBα, depends on the ubiquitination of lysine 21 (K21). This ubiquitination targets the IκBα protein for proteasomal degradation. In contrast, the SUMOylation of K21 by attachment of SUMO-1 acts antagonistically and inhibits signal-induced NF-κB activation [175]. Instead, the integration of SUMO-2/3 mediates the formation of ubiquitin chains to IκBα. These SUMO-2/3-ubiquitin chains promote the proteasomal degradation of IκBα and the activation of NF-κB [176]. Hence, one may hypothesis that the predominantly nuclear location of the 70 kDa $I\kappa B_{NS}$ isoform based on posttranslational modifications, which are also essential for the activity as well as the nuclear translocation of $I\kappa B_{NS}$.

In brief, posttranslational modifications of REL-subunits as well as atypical IκB proteins such as Bcl3 are essential steps, which regulate the NF-κB pathway. It remains to be clarified whether the 70 kDa $I\kappa B_{NS}$ is the functional active isoform or if both regulate the NF-κB pathway antagonistically or synergistically. Therefore, the modification of the 70 kDa $I\kappa B_{NS}$ isoform has to be identified by mass spectrometry to draw conclusions to the function of both $I\kappa B_{NS}$ isoforms.

4.3 $I\kappa B_{NS}$ is essential for T_H17 development and enhances the expression of IL10

The recent report of Schuster *et al.* revealed that $I\kappa B_{NS}$ controls the development of thymic and induced Treg cells by regulating the induction of Foxp3. Hence, mice defective in $I\kappa B_{NS}$ exhibit an accumulation of Treg precursor cells in the thymus, but a reduction of mature Treg cells. Although, the $I\kappa B_{NS}$ deficiency did not affect the suppressor function of Treg cells, their number was significantly reduced. [134] For this reason, an increased formation of auto-reactive T cells in $I\kappa B_{NS}$-deficient mice was expected. Since it was

possible that, because of the reduction of mature Treg cells, not all developing autoreactive T cells were suppressed. This may led to an expansion of self-reactive cells and, thus, autoimmunity. Surprisingly, it becomes apparent that IκB$_{NS}$-defective mice do not suffer from autoimmune symptoms [128,131]. Consequently, one aim of this thesis was to determine, whether IκB$_{NS}$ affects the activation, development or function of other T helper subsets as well.

In this thesis, it was observed that IκB$_{NS}$ does neither influence the activation of cytoplasmic signalling pathways nor cytoplasmic intermediates downstream of the TCR in CD4$^+$ T cells. Accordingly, the phosphorylation of tyrosine as well as the phosphorylation and expression of Erk, Akt, and p38 was equal in IκB$_{NS}$-deficient and wildtype cells. Furthermore, IκBα was identically phosphorylated and degraded in both genotypes upon T cell activation. Thus, IκB$_{NS}$ does not affect proximal TCR signalling in *ex vivo* CD4$^+$ T cells. This is in line with the literature, showing normal activation of conventional T cells and thymocytes in IκB$_{NS}$-deficient mice [128,134]. Furthermore, it is known that IκB$_{NS}$ itself has no DNA-binding motif. Instead atypical IκB proteins indirectly bind to the DNA via NF-κB transcription factors. For instance, IκBζ associates with the NF-κB proteins p50 and p65 [117,119]. IκB$_{NS}$ itself interacts with p50 and mildly with cRel [127,129,134]. Additionally, Kuwata *et al.* identified the function of IκB$_{NS}$ in macrophages. The loss IκB$_{NS}$ induces a prolonged NF-κB activation, indicating a function of IκB$_{NS}$ for termination of NF-κB activity [131]. In this study, the loss of IκB$_{NS}$ did not impair the expression of the NF-κB subunits cRel, RelB, p65, NF-κB1 and NF-κB2 in stimulated CD4$^+$ T cells. This suggests that IκB$_{NS}$ regulates the NF-κB binding activity to κB sites via direct binding to different NF-κB subunits, preferentially to p50 or cRel as reported in Treg cells [134] or other promoter bound proteins. Thus, IκB$_{NS}$ might regulate the activity of promoters, which could be important for T helper cells. Consequently, the identification of IκB$_{NS}$-binding partners and T cell-specific target genes are subject for further investigations.

A number of studies indicated, that the disruption of IκB$_{NS}$ does not affect the numbers of double-negative (DN), double-positive (DP), CD4 and CD8 single-positive cells *in vivo* [128,133,134]. Nevertheless, it was published by Touma *et al.* that *ex vivo* IκB$_{NS}$-deficient CD4$^+$ and CD8$^+$ lymph node cells as well as thymocytes displayed a reduced proliferation upon the cultivation with anti-CD3ε and anti-CD3ε together with anti-CD28, however, specific CD4 subsets were not individually examined [128]. For this reason, the function of IκB$_{NS}$ in the pro-inflammatory T helper subsets, T$_H$17 and T$_H$1, was

investigated in this study. First of all, the expression of IκB$_{NS}$ in T$_H$17 as well as in T$_H$1 cells was identified. As previously reported [127,134], the IκB$_{NS}$ expression by T$_H$17 as well as T$_H$1 cells was induced upon cell stimulation. In addition, it was investigated, that the atypical IκB protein IκB$_{NS}$ is an important factor during the development of naïve T cells to T$_H$1 and T$_H$17 cells *in vitro*, since fewer IκB$_{NS}$-defective naïve T cells primed into T$_H$17 cells undergo less proliferation cycles. This theory is supported by the observation that even the presence of naïve wildtype T cells could overcome the proliferation defect *in vitro*, suggesting that IκB$_{NS}$ function is T cell intrinsic. Interestingly, Okamoto *et al.* showed that IκBζ regulates T$_H$17 proliferation in a cell intrinsic way [121]. Thus it could be demonstrated in this thesis that next to IκBζ, IκB$_{NS}$ is intrinsically involved into the development of T$_H$17 cells *in vitro*. Notably, the expression of IκB$_{NS}$ was detected in stimulated T$_H$1 and T$_H$0 cells, as well. As a result of IκB$_{NS}$ deficiency impaired T$_H$1 proliferation was identified and less T$_H$1 cells were generated in *in vitro* polarisation. This finding further underlined the initial hypothesis that Treg reduction does not cause an autoimmune phenotype in IκB$_{NS}$-deficient mice, since T$_H$1 and T$_H$17 proliferation was impaired. Of note, proliferation of IκB$_{NS}$-deficient Treg cells is not altered [134]. Thus, IκB$_{NS}$ is as a key regulator of T$_H$1 and T$_H$17 cell proliferation.

In Treg cells IκB$_{NS}$ associates via p50 and mildly with cRel to the Foxp3 promoter and the conserved non-coding sequence 3 (CNS3) of the Foxp3 locus [134]. In contrast, an IκB$_{NS}$-independent RNA expression of the master transcription factors Tbet and RORγt were revealed in T$_H$1 and T$_H$17 cells. The recent report of Okamoto *et al.*, identifying a IκBζ-independent expression of RORγt in T$_H$17 cells, too [121]. In addition, Okamoto *et al.* identified the binding of IκBζ together with RORγt to the IL17A promoter, inducing an enhanced expression of IL17A [121]. In this thesis the RNA as well as the protein expression of IL17A showed a divergent output. On the one hand, RT-PCR data indicate a equal expression of IL17A in stimulated cells. On the other hand, the IL17A protein expression was mildly reduced on per cell basis (MFI) in stimulated IκB$_{NS}$ -deficient compared to wildtype cells and, furthermore, qPCR analysis revealed a stronger, but not significant reduction. These differences may arise from varying effectiveness of cell activation or variable sensitivity of the used methods. Thus further analysis like the use of the same cells for all three analysis are necessary. Nevertheless, the loss of IκB$_{NS}$ mildly reduced the IL17A expression (qPCR and MFI analyses). This suggests that IκB$_{NS}$ may stabilise the expression of IL17A in T$_H$17 cells, but is not an essential factor for this. Furthermore, the

RNA expression of IFNγ was comparable in T_H1 cells of both genotypes upon PMA/ ionomycin stimulation. Additionally, the defect in $I\kappa B_{NS}$ significantly reduced the MFI of IFNγ. This suggests that a robust IFNγ protein expression by T_H1 cells is mediated by $I\kappa B_{NS}$. Furthermore, post-translational modifications may induce an affected stability of IFNγ in $I\kappa B_{NS}$-deficient T_H1 cells. Further studies demonstrated regulatory function of nuclear IκB proteins on cytokine expression. For instance, both $I\kappa B_{NS}$ and IκBζ regulates the expression of the cytokines IL6 and IL12p40 in macrophages, at which $I\kappa B_{NS}$ inhibits and IκBζ enhances the expression [119,131]. In this thesis, measurements of cytokine secretion revealed that $I\kappa B_{NS}$ regulates of MIP1α, IL6 and IL2 in *in vitro* polarised T_H17 cells. However, the mRNA level of MIP1α, IL6 and IL2 was comparable in both genotypes. Previous studies demonstrated that IL6 and IL2 are direct target genes of $I\kappa B_{NS}$ [128,129,131]. Hence, it is possible that $I\kappa B_{NS}$ indirectly regulates the secretion or stability of IL6 and IL2, but is dispensable for the gene expression of these two cytokines in T_H17 cells. Kuwata *et al.* identified impaired mRNA expression of IL10 in $I\kappa B_{NS}$-deficient macrophages upon LPS stimulation [131]. Consistent with this report, a decreased mRNA level as well as secretion of IL10 was detected in $I\kappa B_{NS}$-deficient T_H17 cells in comparison to wildtype cells. This finding indicates that $I\kappa B_{NS}$ positively regulates the expression of IL10 in T_H17 cells. Furthermore, Hirotami *et al.* reported that IL10-deficient mice do not express the two nuclear IκB proteins Bcl-3 and $I\kappa B_{NS}$ [129]. Additionally, IL10 treatment strongly induced the expression of $I\kappa B_{NS}$ [129]. This suggests that $I\kappa B_{NS}$ and IL10 potentially regulate each other by a feedforward loop. Touma *et al.* reported that $I\kappa B_{NS}$ binds together with some unknown DNA-binding proteins to the IL2 promoter and thereby regulates the IL2 expression [128]. Hence, further investigations are necessary to elucidate if IL10 expression is regulated by $I\kappa B_{NS}$ binding to the IL10 promoter, as well.

Altogether, $I\kappa B_{NS}$ is dispensable for NF-κB activity in T cells but drives the differentiation of T_H17 as well as T_H1 cells and is essential for IL10 expression by T_H17 cells. In the future, the identification of $I\kappa B_{NS}$-binding partners in developing T_H17 cells and the identification of T_H17-specific target genes are subject for further investigations.

4.4 T_H17 formation is supported by $I\kappa B_{NS}$ in the inflamed gut

The progression of experimental autoimmune encephalomyelitis (EAE) is mediated by T_H1 and T_H17 cells and signalling via NF-κB [57,151–156]. Due to the impaired proliferation of $I\kappa B_{NS}$-deficient T_H1 and T_H17 cells, it was suggested, that $I\kappa B_{NS}$-deficient mice are protected to EAE or at least develop a less severe course of disease. Hence, the sensitivity of $I\kappa B_{NS}$-deficient mice to the induction of clinical EAE symptoms was analysed. The loss of $I\kappa B_{NS}$ delayed the onset of the disease in male mice. Similarly, at the beginning $I\kappa B_{NS}$-defective female mice were as sensitive as wildtype mice, but a reduced clinical score was observed during the course of disease. On the contrary, Okamoto *et al.* demonstrated that the disruption of IκBζ induce a T_H17 intrinsic differentiation defect and a complete resistance to EAE induction [121]. It is conceivable, that the myelin-specificity of T cells upon EAE induction overcomes the proliferation defect of T_H1 or/ and T_H17 cells. Thus, further investigations are necessary to clarify if both T cell subsets proliferate similar in $I\kappa B_{NS}$-deficient and wildtype mice upon induction of EAE. Furthermore, it remains to be elucidated if the loss of $I\kappa B_{NS}$ alters the T_H1 and/ or T_H17 cell infiltration into the central nervous system as well as the myelin-specificity.

It was previously reported that $I\kappa B_{NS}$-deficient mice are sensitive to acute DSS-induced colitis as well as transfer colitis, showing severe inflammation of the colon [131,134]. In this study, the DSS colitis led to a reduced number of $IL17A^+$ T_H17 cells in $I\kappa B_{NS}$-defective compared to wildtype mice. In addition to the DSS colitis, the transfer colitis was performed. In this colitis model, the loss of $I\kappa B_{NS}$ caused an increased susceptibility to inflammation. During the transfer colitis less $IL17A^+$ $IFN\gamma^-$ T_H17 cells as well as $IL17A^+$ $IFN\gamma^+$ T cells developed from transferred $I\kappa B_{NS}$-deficient T cells, accompanied by an higher frequency of $IFN\gamma^+$ T cells. Furthermore, the histological score was increased in recipients of $I\kappa B_{NS}$-deficient T cells. Hence, $I\kappa B_{NS}$ is not only an important regulator of T_H17 cell priming *in vitro* but is also prominent during the development of T_H17 and $IL17A^+$ $IFN\gamma^+$ T cells in mouse models of gut inflammation. Although both $I\kappa B_{NS}$-deficient T_H1 and T_H17 cells showed a proliferation defect *in vitro*, T_H1 cell development was not affected during colon inflammation *in vivo*. This might be due to the severely reduced induction of Treg cells [134], or indicates the presence of additional signals, which promote T_H1 development *in vivo*.

Taken together, while $I\kappa B_{NS}$ seems to be almost dispensable for the course of EAE, it is an important modulator in colitis. Nevertheless, $I\kappa B_{NS}$ is circumstantial for the development

of T_H1 cells in gut inflammation. Hence, one might assume that the formation of myelin-specific T_H1 cells is unaffected by the loss of $I\kappa B_{NS}$ and this may hide the effect of a proliferation defect of myelin-specific T_H17 cells. Consequently, further experiments like an adoptive transfer of either T_H1 or T_H17 cells or a conditional T_H17-specific knockout of $I\kappa B_{NS}$ are necessary to elucidate the function of $I\kappa B_{NS}$ in EAE. Still, the NF-κB pathway and especially the IκB-protein family members might be important targets for anti-inflammatory drugs.

4.5 $I\kappa B_{NS}$ promote the development of T_H17 cells in *Citrobacter rodentium* gut infection

To corroborate the previously described findings, mice were challenged with *Citrobacter rodentium*, which colonise the large intestine with a peak of infection at day 10. An elevated sensitivity of $I\kappa B_{NS}$-deficient mice to *Citrobacter rodentium* infection was observed, associated with an increased bacterial burden and histological score. As demonstrated in the in vitro and the colitis experiments, $I\kappa B_{NS}$-deficient T cells showed a reduced development in colon and spleen of infected mice. While the regulatory effect of $I\kappa B_{NS}$ in T_H1 cells was only mild, $I\kappa B_{NS}$ was an important factor for T_H17 as well as $IL17A^+$ $IFN\gamma^+$ cell generation in gut infection. Symonds *et al.* recommend a role of Treg cells in *Citrobacter rodentium* infection, because of an increased induction of Foxp3 [78]. The recent report on the function of $I\kappa B_{NS}$ in Treg cells indicated the importance of $I\kappa B_{NS}$ for the transition of Treg precursors ($GITR^+CD25^+Foxp3^-$) to mature Treg cells in the thymus. In this report, Schuster *et al.* demonstrated a reduction of mature Treg cells in $I\kappa B_{NS}$-deficient mice [134]. After the infection of $I\kappa B_{NS}$-deficient mice with *Citrobacter rodentium* Treg frequencies were reduced in systemic tissues (spleen) compared to wildtype mice, as well. However, the deficiency of $I\kappa B_{NS}$ did not affect the frequency of Treg cells in the infected colon or mesenteric lymph nodes. Hence, it is conceivable that *Citrobacter rodentium* infection induces extrinsic or intrinsic factors, which overcome the $I\kappa B_{NS}$-deficiency, but are irrelevant for thymic Treg development. Alternatively, *Citrobacter rodentium* infection might enhance the Treg migration into the gut. A further explanation could be the increased formation of inducible Treg (iTreg) cells in the gut of infected $I\kappa B_{NS}$-deficient mice. This raised iTreg-formation is maybe mediated by ghrelin. Ghrelin was found in IBD patients [177], TNBS-induced mice colitis [178] and

Citrobacter rodentium infections [78], where it was suggested to induce the expression of Foxp3. In line with the responses in IκB$_{NS}$ wildtype mice, it was previously reported that infection with *Citrobacter rodentium* predominantly induces T$_H$1 and T$_H$17 cells [78,179,180]. The idea of a T$_H$1-dependent defence to *Citrobacter rodentium* is supported by the induction of IL12, IFNγ as well as TNFα expression during infection [179]. On the other hand, Symonds *et al*. suggested a T$_H$17 response, supported by the finding of only minimal changes in the T$_H$1 pathway together with an increased expression of IL6, IL17 and TNFα, which is suggested to amplify the T$_H$17 response. Furthermore, it was shown by McGeachy *et al.*, that IL10 is expressed by T$_H$17 cells generated with TGFβ and IL6. This IL10 co-expression by T$_H$17 cells is supposed to be a self-regulating mechanism to minimise the inflammatory damage of T$_H$17 cells [85]. The reduced expression of IL10 by IκB$_{NS}$-deficient T cells may lead to a reduced self-regulation of T$_H$17 cells. This implies an increased bystander inflammatory damage induced by T$_H$17 cells. Nevertheless, it remains to be clarified if the loss of IκB$_{NS}$ also induces T$_H$17 cells expressing less IL10 during infection.

4.6 Concluding remarks

The transcription factor NF-κB is an important regulator in T cell activation, proliferation and survival and, thus, basic requirement for effective immune responses. Therefore, it is crucial to understand the regulation of NF-κB in immune cells, inflammatory as well as infectious diseases to design effective treatments. In this thesis, it was investigated that beside the nuclear IκB protein IκBζ, IκB$_{NS}$ is an essential regulator in adaptive immunity, demonstrated by its supportive function in T$_H$17 cell differentiation.

IκB$_{NS}$ does not affect the proximal TCR signalling and the expression of NF-κB subunits in *ex vivo* CD4$^+$ T cells. In addition, an IκB$_{NS}$-independent expression of the master transcription factors RORγt in T$_H$17 cells as well as Tbet in T$_H$1 was revealed. Interestingly, IκB$_{NS}$ is an important modulator during the polarisation of naïve T cells to T$_H$1 and T$_H$17 cells *in vitro* and *in vivo*. Additionally, IκB$_{NS}$ is intrinsically involved in the development of T$_H$1 and T$_H$17 cells, as it was shown for IκBζ [121], although the molecular mechanism needs to be decoded more detailed. Furthermore, IκB$_{NS}$ is an essential regulator of IL10 expression by T$_H$17 cells. *In vivo*, IκB$_{NS}$ seems to be dispensable for the course of EAE, while it is crucial for the formation of T$_H$1 and T$_H$7 cells in gut

inflammation as well as infection. Furthermore, IκB$_{NS}$ modulates the T$_H$17 cell induction, while it is less important for T$_H$1 cell development during inflammation and infection of the gut.

In the future, the following open questions should be addressed by additional investigations. Firstly, it remains to be clarified if IκB$_{NS}$ binds to the IL10 promoter and thereby regulate IL10 expression, as it was shown for IL2 [128]. Secondly, further analyses are necessary to elucidate if IκB$_{NS}$ is also an important modulator of IL10 expression by T$_H$17 cells in infections. Finally, the identification of IκB$_{NS}$-binding partners in developing T$_H$17 cells as well as T$_H$17-specific target genes are of major importance on the molecular level.

In conclusion, IκB$_{NS}$ not only enhances thymic Foxp3 induction and thereby the development of immuno-suppressive Treg cells, but is also necessary for the generation of pro-inflammatory T$_H$17 cells *in vitro* and *in vivo*. Thus, IκB$_{NS}$ exhibits diverse regulatory functions for T cell proliferation and cytokine secretion. Consequently, IκB$_{NS}$ may represent a T cell specific pharmacological target in the future.

5 Abbreviations

APC	antigen-presenting cell
ARD	ankyrin repeat domain
BCR	B cell receptor
CD	Cluster of differentiation
CFSE	Carboxyfluorescein succinimidyl ester
CMJ	Corticomedullary junction
CNS3	Conserved non-coding sequence 3
cTECs	cortical thymic epithelial cells
DC	Dendritic cell
DN	Double negative ($CD4^-CD8^-$)
DNA	deoxyribonucleic acid
DP	Double positive ($CD4^+CD8^+$)
EAE	Experimental autoimmune encephalomyelitis
FCS	Fetal calf serum
Foxp3	Forkhead box protein 3
GITR	Glycocorticoid-induced TNF receptor
GRR	Glycine rich region
HSC	hematopoietic stem cell
IBD	Inflammatory bowel disease
IFNγ	Interferon γ
Ig	Immunoglobulin
IKK	IκB kinase
IL	Interleukin
IL23R	Interleukin 23 receptor
IRF4	Interferon regulatory factor 4
IκBs	Inhibitor of NFκB protein
LPS	Lipopolysaccharide
m	mouse
MHC	Major histocompatibility complex
mLN	mesenteric lymph nodes
mTEC	Medullary thymic epithelial cell
NF-κB	Nuclear factor κ B

NIK	NF-κB inducing kinase
NLS	Nuclear localisation signal
PAMP	Pathogen-associated molecular pattern
PCR	Polymerase chain reaction
pLN	peripheral lymph nodes
PMA	phorbol-12-myristate-13-acetate
PRR	Pattern recognition receptors
qPCR	Quantitative real-time detection PCR
RAG1	Recombination activating gene 1
rb	rabbit
RHD	REL-homology domain
RNA	ribonucleic acid
RORγt	Retinoic-acid-receptor-related orphan receptor-γt
Runx1	Runt-related transcription factor 1
SCZ	subcapsular zone
SFB	Segmented filamentous bacteria
shRNA	short hairpin RNA
SP	Single-positive
STAT	Signal transducer of activated T cells
SUMO	Small ubiquitin-like modifier
TAD	Transcription activation domain
TCR	T cell receptor
TGFβ	Transforming growth factor β
T_H cell	T helper cell
TNFα	Tumor necrosis factor α
Treg	Regulatory T cell
TSPs	thymus-settling progenitors

6 References

1. Brestoff, J. R. & Artis, D. Commensal bacteria at the interface of host metabolism and the immune system. *Nat. Immunol.* **14,** 676–84 (2013).

2. Brown, E. M., Sadarangani, M. & Finlay, B. B. The role of the immune system in governing host-microbe interactions in the intestine. *Nat. Immunol.* **14,** 660–7 (2013).

3. Maynard, C. L., Elson, C. O., Hatton, R. D. & Weaver, C. T. Reciprocal interactions of the intestinal microbiota and immune system. *Nature* **489,** 231–41 (2012).

4. Purchiaroni, F. *et al.* The role of intestinal microbiota and the immune system. *Eur. Rev. Med. Pharmacol. Sci.* **17,** 323–333 (2013).

5. Lee, Y. K., Menezes, J. S., Umesaki, Y. & Mazmanian, S. K. Proinflammatory T-cell responses to gut microbiota promote experimental autoimmune encephalomyelitis. *Proc. Natl. Acad. Sci. U. S. A.* **108 Suppl ,** 4615–22 (2011).

6. Berer, K. *et al.* Commensal microbiota and myelin autoantigen cooperate to trigger autoimmune demyelination. *Nature* **01,** 1–5 (2011).

7. Wu, H., Ivanov, I., Darce, J. & Hattori, K. Gut-residing segmented filamentous bacteria drive autoimmune arthritis via T helper 17 cells. *Immunity* **32,** 815–827 (2010).

8. Kriegel, M. *et al.* Naturally transmitted segmented filamentous bacteria segregate with diabetes protection in nonobese diabetic mice. *Proc. Natl. Acad. Sci.* 2–7 (2011). doi:10.1073/pnas.1108924108/-/DCSupplemental.www.pnas.org/cgi/doi/10.1073/pnas.1108924108

9. Mathis, D. & Benoist, C. Microbiota and Autoimmune Disease: The Hosted Self. *Cell Host Microbe* **10,** 297–301 (2011).

10. Mitrović, M., Arapović, J. & Traven, L. Innate immunity regulates adaptive immune response: lessons learned from studying the interplay between NK and CD8+ T cells during MCMV infection. *Med. Microbiol. ...* **201,** 487–495 (2012).

11. Michalek, R. D. & Rathmell, J. C. The metabolic life and times of a T-cell. *Immunol. Rev.* **236,** 190–202 (2010).

12. Schmitz, M. L. & Krappmann, D. Controlling NF-kappaB activation in T cells by costimulatory receptors. *Cell Death Differ.* **13,** 834–42 (2006).

13. Bhandoola, A., von Boehmer, H., Petrie, H. T. & Zúñiga-Pflücker, J. C. Commitment and developmental potential of extrathymic and intrathymic T cell precursors: plenty to choose from. *Immunity* **26,** 678–89 (2007).

14. Koch, U. & Radtke, F. Mechanisms of T cell development and transformation. *Annu. Rev. Cell Dev. Biol.* **27,** 539–62 (2011).

15. Serwold, T., Ehrlich, L. I. R. & Weissman, I. L. Reductive isolation from bone marrow and blood implicates common lymphoid progenitors as the major source of thymopoiesis. *Blood* **113,** 807–15 (2009).

16. Lind, E. F., Prockop, S. E., Porritt, H. E. & Petrie, H. T. Mapping precursor movement through the postnatal thymus reveals specific microenvironments supporting defined stages of early lymphoid development. *J. Exp. Med.* **194,** 127–34 (2001).

17. Porritt, H. E., Gordon, K. & Petrie, H. T. Kinetics of steady-state differentiation and mapping of intrathymic-signaling environments by stem cell transplantation in nonirradiated mice. *J. Exp. Med.* **198,** 957–62 (2003).

18. Prockop, S. E. *et al.* Stromal cells provide the matrix for migration of early lymphoid progenitors through the thymic cortex. *J. Immunol.* **169,** 4354–61 (2002).

19. Zúñiga-Pflücker, J. C. T-cell development made simple. *Nat. Rev. Immunol.* **4,** 67–72 (2004).

20. Kyewski, B. & Klein, L. A central role for central tolerance. *Annu. Rev. Immunol.* **24,** 571–606 (2006).

21. Norment, a M. & Bevan, M. J. Role of chemokines in thymocyte development. *Semin. Immunol.* **12,** 445–55 (2000).

22. Xu, X. *et al.* Maturation and Emigration of Single-Positive Thymocytes. *Clin. Dev. Immunol.* **2013,** 282870 (2013).

23. Goldrath, a W. & Bevan, M. J. Selecting and maintaining a diverse T-cell repertoire. *Nature* **402,** 255–62 (1999).

24. Griesemer, A., Sorenson, E. & Hardy, M. The role of the thymus in tolerance. *Transplantation* **90,** 465–474 (2010).

25. Klein, L., Hinterberger, M., Wirnsberger, G. & Kyewski, B. Antigen presentation in the thymus for positive selection and central tolerance induction. *Nat. Rev. Immunol.* **9,** 833–44 (2009).

26. Mosmann, T. R., Cherwinski, H., Bond, M. W., Giedlin, M. A. & Coffman, R. L. Two types of murine helper T cell clone. I. Definition according to profiles of lymphokine activities and secreted proteins. *J Immunol* **136,** 2348–2357 (1986).

27. Aggarwal, S., Ghilardi, N., Xie, M.-H., de Sauvage, F. J. & Gurney, A. L. Interleukin-23 promotes a distinct CD4 T cell activation state characterized by the production of interleukin-17. *J. Biol. Chem.* **278,** 1910–4 (2003).

28. Wan, Y. Y. Multi-tasking of helper T cells. *Immunology* **130,** 166–71 (2010).

29. Wilson, C. B., Rowell, E. & Sekimata, M. Epigenetic control of T-helper-cell differentiation. *Nat. Rev. Immunol.* **9,** 91–105 (2009).

30. Zhu, J. & Paul, W. E. Peripheral CD4+ T-cell differentiation regulated by networks of cytokines and transcription factors. *Immunol. Rev.* **238,** 247–62 (2010).

31. Zhu, J., Yamane, H. & Paul, W. E. Differentiation of effector CD4 T cell populations (*). *Annu. Rev. Immunol.* **28,** 445–89 (2010).

32. Harrington, L. E. *et al.* Interleukin 17-producing CD4+ effector T cells develop via a lineage distinct from the T helper type 1 and 2 lineages. *Nat. Immunol.* **6,** 1123–32 (2005).

33. Park, H. *et al.* A distinct lineage of CD4 T cells regulates tissue inflammation by producing interleukin 17. *Nat Immunol* **6,** 1133–1141 (2005).

34. Zhu, J. & Paul, W. E. Heterogeneity and plasticity of T helper cells. *Cell Res.* **20,** 4–12 (2010).

35. Zhu, J. & Paul, W. E. CD4 T cells: fates, functions, and faults. *Blood* **112,** 1557–69 (2008).

36. Murphy, C. a *et al.* Divergent pro- and antiinflammatory roles for IL-23 and IL-12 in joint autoimmune inflammation. *J. Exp. Med.* **198,** 1951–7 (2003).

37. Sakaguchi, S., Wing, K. & Miyara, M. Regulatory T cells - a brief history and perspective. *Eur. J. Immunol.* **37 Suppl 1,** S116–23 (2007).

38. Ohkura, N., Kitagawa, Y. & Sakaguchi, S. Development and Maintenance of Regulatory T cells. *Immunity* **38,** 414–423 (2013).

39. Von Boehmer, H. Mechanisms of suppression by suppressor T cells. *Nat. Immunol.* **6,** 338–44 (2005).

40. Mangan, P. R. *et al.* Transforming growth factor-beta induces development of the T(H)17 lineage. *Nature* **441,** 231–4 (2006).

41. Quintana, F. J. *et al.* Aiolos promotes T(H)17 differentiation by directly silencing Il2 expression. *Nat. Immunol.* **13,** (2012).

42. Harrington, L. E. *et al.* Interleukin 17-producing CD4+ effector T cells develop via a lineage distinct from the T helper type 1 and 2 lineages. *Nat Immunol* **6,** 1123–1132 (2005).

43. Laurence, A. *et al.* Interleukin-2 signaling via STAT5 constrains T helper 17 cell generation. *Immunity* **26,** 371–81 (2007).

44. Kryczek, I., Wei, S., Vatan, L., Escara-wilke, J. & Szeliga, W. Cutting Edge: Opposite Effects of IL-1 and IL-2 on the Regulation of IL-17 T Cell Pool IL-1 Subverts. *J. Immunol.* 1423–1426 (2007).

45. Yang, X. O. *et al.* STAT3 regulates cytokine-mediated generation of inflammatory helper T cells. *J. Biol. Chem.* **282,** 9358–63 (2007).

46. Zhou, L. *et al.* IL-6 programs T(H)-17 cell differentiation by promoting sequential engagement of the IL-21 and IL-23 pathways. *Nat Immunol* **8,** 967–974 (2007).

47. Mathur, A. N. *et al.* Stat3 and Stat4 direct development of IL-17-secreting Th cells. *J. Immunol.* **178,** 4901–7 (2007).

48. Zhang, F., Meng, G. & Strober, W. Interactions among the transcription factors Runx1, RORgammat and Foxp3 regulate the differentiation of interleukin 17-producing T cells. *Nat. Immunol.* **9,** 1297–306 (2008).

49. Ivanov, I. I. *et al.* The orphan nuclear receptor RORgammat directs the differentiation program of proinflammatory IL-17+ T helper cells. *Cell* **126,** 1121–33 (2006).

50. Ruan, Q. *et al.* The Th17 immune response is controlled by the Rel-RORγ-RORγ T transcriptional axis. *J. Exp. Med.* **208,** 2321–33 (2011).

51. Yang, X. O. *et al.* T helper 17 lineage differentiation is programmed by orphan nuclear receptors ROR alpha and ROR gamma. *Immunity* **28,** 29–39 (2008).

52. Nurieva, R. *et al.* Essential autocrine regulation by IL-21 in the generation of inflammatory T cells. *Nature* **448,** 480–483 (2007).

53. Harris, T., Grosso, J. & Yen, H. An In Vivo Requirement for STAT3 Signaling in TH17 Development and TH17-Dependent Autoimmunity. *J.* ... (2007). at <http://www.jimmunol.org/content/179/7/4313.short>

54. Kimura, A. & Kishimoto, T. IL-6: Regulator of Treg/Th17 balance. *Eur. J. Immunol.* **40,** 1830–1835 (2010).

55. Bettelli, E. *et al.* Reciprocal developmental pathways for the generation of pathogenic effector TH17 and regulatory T cells. *Nature* **441,** 235–238 (2006).

56. Veldhoen, M., Hocking, R. J., Atkins, C. J., Locksley, R. M. & Stockinger, B. TGFbeta in the context of an inflammatory cytokine milieu supports de novo differentiation of IL-17-producing T cells. *Immunity* **24,** 179–89 (2006).

57. Ivanov, I. I. *et al.* The orphan nuclear receptor RORgammat directs the differentiation program of proinflammatory IL-17+ T helper cells. *Cell* **126,** 1121–33 (2006).

58. Park, H. *et al.* A distinct lineage of CD4 T cells regulates tissue inflammation by producing interleukin 17. **6,** 1133–1141 (2006).

59. Zhou, L. *et al.* TGF-beta-induced Foxp3 inhibits T(H)17 cell differentiation by antagonizing RORgammat function. *Nature* **453,** 236–40 (2008).

60. Korn, T. *et al.* IL-21 initiates an alternative pathway to induce proinflammatory T(H)17 cells. *Nature* **448,** 484–7 (2007).

61. Yang, X. O. *et al.* STAT3 regulates cytokine-mediated generation of inflammatory helper T cells. *J. Biol. Chem.* **282,** 9358–63 (2007).

62. Dunay, I. R., Fuchs, A. & Sibley, L. D. Inflammatory monocytes but not neutrophils are necessary to control infection with Toxoplasma gondii in mice. *Infect. Immun.* **78,** 1564–70 (2010).

63. Huber, M. *et al.* IRF4 is essential for IL-21-mediated induction, amplification, and stabilization of the Th17 phenotype. *Proc. Natl. Acad. Sci. U. S. A.* **105,** 20846–51 (2008).

64. Hebel, K. *et al.* IL-1β and TGF-β Act Antagonistically in Induction and Differentially in Propagation of Human Proinflammatory Precursor CD4+ T Cells. *J. Immunol.* (2011). doi:10.4049/jimmunol.1003998

65. Shaw, M. H., Kamada, N., Kim, Y.-G. & Nunez, G. Microbiota-induced IL-1 , but not IL-6, is critical for the development of steady-state TH17 cells in the intestine. *J. Exp. Med.* (2012). doi:10.1084/jem.20111703

66. Zielinski, C. E. *et al.* Pathogen-induced human T(H)17 cells produce IFN-γ or IL-10 and are regulated by IL-1β. *Nature* 1–6 (2012). doi:10.1038/nature10957

67. Chung, Y., Chang, S., Martinez, G. & Yang, X. Critical regulation of early Th17 cell differentiation by interleukin-1 signaling. *Immunity* **30,** 576–587 (2009).

68. Sutton, C., Brereton, C., Keogh, B., Mills, K. H. G. & Lavelle, E. C. A crucial role for interleukin (IL)-1 in the induction of IL-17-producing T cells that mediate autoimmune encephalomyelitis. *J. Exp. Med.* **203,** 1685–91 (2006).

69. Brüstle, A. *et al.* The development of inflammatory T(H)-17 cells requires interferon-regulatory factor 4. *Nat. Immunol.* **8,** 958–66 (2007).

70. Ivanov, I. I. *et al.* Specific microbiota direct the differentiation of IL-17-producing T-helper cells in the mucosa of the small intestine. *Cell Host Microbe* **4,** 337–49 (2008).

71. Salzman, N., Hung, K. & Haribhai, D. Enteric defensins are essential regulators of intestinal microbial ecology. *Nat. I* **11,** 76–83 (2010).

72. Ivanov, I., Atarashi, K., Manel, N. & Brodie, E. Induction of intestinal Th17 cells by segmented filamentous bacteria. *Cell* **139,** 485–498 (2009).

73. McGeachy, M. & McSorley, S. Microbial-Induced Th17: Superhero or Supervillain? *J. Immunol.* **189,** 3285–3291 (2012).

74. Alber, G. & Kamradt, T. Regulation of Protective and Pathogenic Th17 Responses. *Curr. Immunol. Rev.* **3,** 3–16 (2007).

75. Ouyang, W., Kolls, J. K. & Zheng, Y. The biological functions of T helper 17 cell effector cytokines in inflammation. *Immunity* **28,** 454–67 (2008).

76. Raffatellu, M. *et al.* Simian immunodeficiency virus-induced mucosal interleukin-17 deficiency promotes Salmonella dissemination from the gut. *Nat. Med.* **14,** 421–8 (2008).

77. Frank, K. M. *et al.* Host response signature to Staphylococcus aureus alpha-hemolysin implicates pulmonary Th17 response. *Infect. Immun.* **80,** 3161–9 (2012).

78. Symonds, E. L. *et al.* Involvement of T helper type 17 and regulatory T cell activity in Citrobacter rodentium invasion and inflammatory damage. *Clin. Exp. Immunol.* **157,** 148–54 (2009).

79. Leppkes, M. *et al.* RORgamma-expressing Th17 cells induce murine chronic intestinal inflammation via redundant effects of IL-17A and IL-17F. *Gastroenterology* **136,** 257–67 (2009).

80. Littman, D. R. & Rudensky, A. Y. Th17 and regulatory T cells in mediating and restraining inflammation. *Cell* **140,** 845–58 (2010).

81. Afzali, B., Lombardi, G., Lechler, R. I. & Lord, G. M. The role of T helper 17 (Th17) and regulatory T cells (Treg) in human organ transplantation and autoimmune disease. *Clin. Exp. Immunol.* **148,** 32–46 (2007).

82. Segal, B. M. Th17 cells in autoimmune demyelinating disease. *Semin. Immunopathol.* **32,** 71–7 (2010).

83. Lovett-Racke, A. E., Yang, Y. & Racke, M. K. Th1 versus Th17: are T cell cytokines relevant in multiple sclerosis? *Biochim. Biophys. Acta* **1812,** 246–51 (2011).

84. Huang, G. *et al.* Signaling via the kinase p38α programs dendritic cells to drive T(H)17 differentiation and autoimmune inflammation. *Nat. Immunol.* **13,** 152–161 (2012).

85. McGeachy, M. J. *et al.* TGF- b and IL-6 drive the production of IL-17 and IL-10 by T cells and restrain T H -17 cell – mediated pathology. *Nat. Immunol.* **8,** 1390–1397 (2007).

86. Cua, D. J. *et al.* Interleukin-23 rather than interleukin-12 is the critical cytokine for autoimmune inflammation of the brain. *Nature* **421,** 744–8 (2003).

87. Codarri, L. *et al.* RORγt drives production of the cytokine GM-CSF in helper T cells, which is essential for the effector phase of autoimmune neuroinflammation. *Nat. Immunol.* **12,** 560–567 (2011).

88. El-Behi, M. *et al.* The encephalitogenicity of T(H)17 cells is dependent on IL-1- and IL-23-induced production of the cytokine GM-CSF. *Nat. Immunol.* **12,** 568–75 (2011).

89. Sen, R. & Baltimore, D. Multiple nuclear factors interact with the immunoglobulin enhancer sequences. *Cell* **46,** 705–16 (1986).

90. Gilmore, T. D. & Wolenski, F. S. NF-κB: where did it come from and why? *Immunol. Rev.* **246,** 14–35 (2012).

91. Hayden, M. S. & Ghosh, S. NF- B, the first quarter-century: remarkable progress and outstanding questions. *Genes Dev.* **26,** 203–234 (2012).

92. Espinosa, L., Bigas, A. & Mulero, M. C. Alternative nuclear functions for NF-κB family members. *Am. J. Cancer Res.* **1,** 446–59 (2011).

93. Hayden, M. S. & Ghosh, S. NF-κB in immunobiology. *Cell Res.* 223–244 (2011). doi:10.1038/cr.2011.13

94. Rahman, M. M. & McFadden, G. Modulation of NF-κB signalling by microbial pathogens. *Nat. Rev. Microbiol.* **9,** 291–306 (2011).

95. Siebenlist, U., Brown, K. & Claudio, E. Control of lymphocyte development by nuclear factor-kappaB. *Nat. Rev. Immunol.* **5,** 435–45 (2005).

96. Gosh, S. & Hayden, M. S. Celebrating 25 years of NF-kappaB. *Immunol. Rev.* **246,** 5–13 (2012).

97. Gerondakis, S. & Siebenlist, U. Roles of the NF-kappaB pathway in lymphocyte development and function. *Cold Spring Harb. Perspect. Biol.* **2,** a000182 (2010).

98. Ghosh, S., May, M. J. & Kopp, E. B. NF-kappa B and Rel proteins: evolutionarily conserved mediators of immune responses. *Annu. Rev. Immunol.* **16,** 225–60 (1998).

99. Ghosh, S. & Hayden, M. S. New regulators of NF-kappaB in inflammation. *Nat. Rev. Immunol.* **8,** 837–48 (2008).

100. Hinz, M., Arslan, S. Ç. & Scheidereit, C. It takes two to tango: IκBs, the multifunctional partners of NF-κB. *Immunol. Rev.* **246,** 59–76 (2012).

101. Oeckinghaus, A. & Ghosh, S. The NF-kappaB family of transcription factors and its regulation. *Cold Spring Harb. Perspect. Biol.* **1,** a000034 (2009).

102. Schuster, M., Annemann, M., Plaza-Sirvent, C. & Schmitz, I. Atypical IκB proteins - nuclear modulators of NF-κB signaling. *Cell Commun. Signal.* **11,** 23 (2013).

103. Chen, L.-F. & Greene, W. C. Shaping the nuclear action of NF-kappaB. *Nat. Rev. Mol. Cell Biol.* **5,** 392–401 (2004).

104. Hayden, M. S. & Ghosh, S. Shared principles in NF-kappaB signaling. *Cell* **132,** 344–62 (2008).

105. Ohno, H., Takimoto, G. & McKeithan, T. W. The candidate proto-oncogene bcl-3 is related to genes implicated in cell lineage determination and cell cycle control. *Cell* **60,** 991–7 (1990).

106. Hövelmeyer, N. *et al.* Overexpression of Bcl-3 inhibits the development of marginal zone B cells. *Eur. J. Immunol.* 1–8 (2013). doi:10.1002/eji.201343655

107. Schwarz, E. M., Krimpenfort, P., Berns, a & Verma, I. M. Immunological defects in mice with a targeted disruption in Bcl-3. *Genes Dev.* **11,** 187–197 (1997).

108. Kuwata, H. *et al.* IL-10-inducible Bcl-3 negatively regulates LPS-induced TNF-alpha production in macrophages. *Blood* **102,** 4123–9 (2003).

109. Liou, H. & Scott, M. L. The bcl-3 Proto-Oncogene Encodes a Nuclear IidB-Like Molecule That Preferentially Interacts with NF-KB p50 and p52 in a Phosphorylation-Dependent Manner. **13,** 3557–3566 (1993).

110. Bundy, D. L. Diverse Effects of BCL3 Phosphorylation on Its Modulation of NF-kappa B p52 Homodimer Binding to DNA. *J. Biol. Chem.* **272,** 33132–33139 (1997).

111. Caamaño, J. H., Perez, P., Lira, S. a & Bravo, R. Constitutive expression of Bc1-3 in thymocytes increases the DNA binding of NF-kappaB1 (p50) homodimers in vivo. *Mol. Cell. Biol.* **16,** 1342–8 (1996).

112. Brasier, A. R., Lu, M., Hai, T., Lu, Y. & Boldogh, I. NF-kappa B-inducible BCL-3 expression is an autoregulatory loop controlling nuclear p50/NF-kappa B1 residence. *J. Biol. Chem.* **276,** 32080–93 (2001).

113. Bours, V. *et al.* The oncoprotein Bcl-3 directly transactivates through kappa B motifs via association with DNA-binding p50B homodimers. *Cell* **72,** 729–39 (1993).

114. Dechend, R. *et al.* The Bcl-3 oncoprotein acts as a bridging factor between NF-kappaB/Rel and nuclear co-regulators. *Oncogene* **18,** 3316–23 (1999).

115. Motoyama, M., Yamazaki, S., Eto-Kimura, A., Takeshige, K. & Muta, T. Positive and negative regulation of nuclear factor-kappaB-mediated transcription by IkappaB-zeta, an inducible nuclear protein. *J. Biol. Chem.* **280,** 7444–51 (2005).

116. Yamazaki, S. *et al.* Gene-specific requirement of a nuclear protein, IkappaB-zeta, for promoter association of inflammatory transcription regulators. *J. Biol. Chem.* **283,** 32404–11 (2008).

117. Totzke, G. *et al.* A novel member of the IkappaB family, human IkappaB-zeta, inhibits transactivation of p65 and its DNA binding. *J. Biol. Chem.* **281,** 12645–54 (2006).

118. Yamazaki, S., Muta, T. & Takeshige, K. A novel IkappaB protein, IkappaB-zeta, induced by proinflammatory stimuli, negatively regulates nuclear factor-kappaB in the nuclei. *J. Biol. Chem.* **276,** 27657–62 (2001).

119. Yamamoto, M. *et al.* Regulation of Toll/IL-1-receptor-mediated gene expression by the inducible nuclear protein IkappaBzeta. *Nature* **430,** 218–22 (2004).

120. Okuma, A. *et al.* Enhanced Apoptosis by Disruption of the STAT3-IκB-ζ Signaling Pathway in Epithelial Cells Induces Sjögren's Syndrome-like Autoimmune Disease. *Immunity* **38,** 450–460 (2013).

121. Okamoto, K. *et al.* IkappaBzeta regulates T(H)17 development by cooperating with ROR nuclear receptors. *Nature* (2010). doi:10.1038/nature08922

122. Yamauchi, S., Ito, H. & Miyajima, A. IκBη, a nuclear IκB protein, positively regulates the NF-κB–mediated expression of proinflammatory cytokines. *PNAS* **107,** 11924–11929 (2010).

123. Chiba, T. *et al.* IkappaBL , a novel member of the nuclear IkappaB family , inhibits inflammatory cytokine expression. *FEBS Lett.* (2011). doi:10.1016/j.febslet.2011.10.024

124. Chiba, T. *et al.* NFKBIL1 confers resistance to experimental autoimmune arthritis through the regulation of dendritic cell functions. *Scand. J. Immunol.* **73,** 478–85 (2011).

125. Baeuerle, P. A. & Baltimore, D. Activation of DNA-Binding Activity in an Apparently Cytoplasmic Precursor Factor of the NF-KB Transcription. **53,** 211–217 (1988).

126. Kanarek, N. & Ben-Neriah, Y. Regulation of NF-κB by ubiquitination and degradation of the IκBs. *Immunol. Rev.* **246,** 77–94 (2012).

127. Fiorini, E. *et al.* Peptide-induced negative selection of thymocytes activates transcription of an NF-kappa B inhibitor. *Mol. Cell* **9,** 637–48 (2002).

128. Touma, M. *et al.* Functional Role for IkappaBNS in T Cell Cytokine Regulation As Revealed by Targeted Gene Disruption. *J. Immunol.* **179,** 1681–1692 (2007).

129. Hirotami, T. *et al.* The nuclear IkappaB Protein IkappaBNS selektively inhibits lipopolysaccharide-induced IL6 production in macrophages of the colonic lamina propria. *J. Immunol.* **174,** 3650–3657 (2005).

130. Fujita, S. *et al.* Regulatory dendritic cells act as regulators of acute lethal systemic inflammatory response. *Blood* **107,** 3656–64 (2006).

131. Kuwata, H. *et al.* IkappaBNS inhibits induction of a subset of Toll-like receptor-dependent genes and limits inflammation. *Immunity* **24,** 41–51 (2006).

132. Touma, M. *et al.* Impaired B Cell Development and Function in the Absence of I{kappa}BNS. *J. Immunol.* **187,** 3942–52 (2011).

133. Arnold, C. N. *et al.* A forward genetic screen reveals roles for Nfkbid , Zeb1 , and Ruvbl2 in humoral immunity. **109,** (2012).

134. Schuster, M. *et al.* IκB(NS) protein mediates regulatory T cell development via induction of the Foxp3 transcription factor. *Immunity* **37,** 998–1008 (2012).

135. Courtois, G. & Gilmore, T. D. Mutations in the NF-kappaB signaling pathway: implications for human disease. *Oncogene* **25,** 6831–43 (2006).

136. Yamamoto, M. & Takeda, K. Role of nuclear IkappaB proteins in the regulation of host immune responses. *J. Infect. Chemother.* **14,** 265–9 (2008).

137. Snell , G.D.; Cherry, M. Loci determining cell surface antigens. *RNA Viruses Host Genome Oncog.* (1972).

138. Mombaerts, P. *et al.* RAG-1-deficient mice have no mature B and T lymphocytes. *Cell* **68,** 869–77 (1992).

139. Sen, R. & Baltimore, D. Multiple nuclear factors interact with the immunoglobulin enhancer sequences. *Cell* **46,** 705–16 (1986).

140. Kontgen, F. *et al.* Mice lacking the c-rel proto-oncogene exhibit defects in lymphocyte proliferation, humoral immunity, and interleukin-2 expression. *Genes Dev.* **9,** 1965–1977 (1995).

141. Grumont, R. J. *et al.* B Lymphocytes Differentially Use the Rel and Nuclear Cycle Progression and Apoptosis in Quiescent and Mitogen-activated Cells. *J. Exp. Med.* **187,** (1998).

142. Cabannes, E., Khan, G., Aillet, F., Jarrett, R. F. & Hay, R. T. Mutations in the IkappaBalpha gene in Hodgkin ' s disease suggest a tumour suppressor role for IkappaBalpha. (1999).

143. Davis, R. E., Brown, K. D., Siebenlist, U. & Staudt, L. M. Constitutive nuclear factor kappaB activity is required for survival of activated B cell-like diffuse large B cell lymphoma cells. *J. Exp. Med.* **194,** 1861–74 (2001).

144. Visekruna, A. *et al.* c-Rel is crucial for the induction of Foxp3(+) regulatory CD4(+) T cells but not T(H)17 cells. *Eur. J. Immunol.* **40,** 671–6 (2010).

145. Bettelli, E. *et al.* Reciprocal developmental pathways for the generation of pathogenic effector TH17 and regulatory T cells. *Nature* **441,** 235–8 (2006).

146. Wilson, N. J. *et al.* Development, cytokine profile and function of human interleukin 17-producing helper T cells. *Nat. Immunol.* **8,** 950–7 (2007).

147. Ghoreschi, K. *et al.* Generation of pathogenic TH17 cells in the absence of TGF-β signalling. *Nature* **467,** 967–971 (2010).

148. Carlson, M. J. *et al.* In vitro-differentiated TH17 cells mediate lethal acute graft-versus-host disease with severe cutaneous and pulmonary pathologic manifestations. *Blood* **113,** 1365–74 (2009).

149. Blonska, M. & Lin, X. Dampening NF-κB Signaling by "Self-Eating."*Immunity* **36,** 895–896 (2012).

150. Yamauchi, S., Ito, H. & Miyajima, A. IkappaBeta, a nuclear IkappaB protein, positively regulates the NF-kappaB-mediated expression of proinflammatory cytokines. *PNAS* **107,** 11924–9 (2010).

151. Pettinelli, C. B. & McFarlin, D. E. Adoptive transfer of experimental allergic encephalomyelitis in SJL/J mice after in vitro activation of lymph node cells by myelin basic protein: requirement for Lyt 1+ 2- T lymphocytes. *J. Immunol.* **127,** 1420–3 (1981).

152. Bettelli, E. *et al.* Loss of T-bet, but not STAT1, prevents the development of experimental autoimmune encephalomyelitis. *J. Exp. Med.* **200,** 79–87 (2004).

153. Kroenke, M. a, Carlson, T. J., Andjelkovic, A. V & Segal, B. M. IL-12- and IL-23-modulated T cells induce distinct types of EAE based on histology, CNS chemokine profile, and response to cytokine inhibition. *J. Exp. Med.* **205,** 1535–41 (2008).

154. Stromnes, I. M., Cerretti, L. M., Liggitt, D., Harris, R. a & Goverman, J. M. Differential regulation of central nervous system autoimmunity by T(H)1 and T(H)17 cells. *Nat. Med.* **14,** 337–42 (2008).

155. Hilliard, B. A. *et al.* Critical roles of c-Rel in autoimmune inflammation and helper T cell differentiation. **110,** (2002).

156. Hilliard, B., Samoilova, E. B., Liu, T. S., Rostami, a & Chen, Y. Experimental autoimmune encephalomyelitis in NF-kappa B-deficient mice:roles of NF-kappa B in the activation and differentiation of autoreactive T cells. *J. Immunol.* **163,** 2937–43 (1999).

157. Fujino, S. Increased expression of interleukin 17 in inflammatory bowel disease. *Gut* **52,** 65–70 (2003).

158. Annunziato, F. *et al.* Phenotypic and functional features of human Th17 cells. *J. Exp. Med.* **204,** 1849–61 (2007).

159. Dieleman, L. A. *et al.* Dextran sulfate sodium-induced colitis occurs in severe combined immunodeficient mice. *Gastroenterology* **107,** 1643–1652 (1994).

160. Takedatsu, H. *et al.* TL1A (TNFSF15) Regulates the Development of Chronic Colitis By Modulating both T helper (TH) 1 and TH17 Activation. *Development* **135,** 552–567 (2009).

161. Barthold, S., Coleman, G., Bhatt, P., Osbaldiston, G. & Jonas, A. The etiology of transmissible murine colonic hyperplasia. *Lab. Anim. …* **26,** 889–894 (1976).

162. Simmons, C. P. *et al.* Central Role for B Lymphocytes and CD4+ T Cells in Immunity to Infection by the Attaching and Effacing Pathogen Citrobacter rodentium. *Infect. Immun.* **71,** 5077–5086 (2003).

163. Grumont, R. J. & Gerondakis, S. The Subunit Composition of NF-kappaB complex changes during B-Cell Development. *Cell Growth Differ.* **5,** 1321–1331 (1994).

164. Franzoso, G. *et al.* Mice deficient in nuclear factor (NF)-kappa B/p52 present with defects in humoral responses, germinal center reactions, and splenic microarchitecture. *J. Exp. Med.* **187,** 147–59 (1998).

165. Weih, D. S., Yilmaz, Z. B. & Weih, F. Essential role of RelB in germinal center and marginal zone formation and proper expression of homing chemokines. *J. Immunol.* **167,** 1909–19 (2001).

166. Cariappa, a, Liou, H. C., Horwitz, B. H. & Pillai, S. Nuclear factor kappa B is required for the development of marginal zone B lymphocytes. *J. Exp. Med.* **192,** 1175–82 (2000).

167. Pohl, T. *et al.* The combined absence of NF-kappa B1 and c-Rel reveals that overlapping roles for these transcription factors in the B cell lineage are restricted to the activation and function of mature cells. *Proc. Natl. Acad. Sci. U. S. A.* **99,** 4514–9 (2002).

168. Caamaño, B. J. H. *et al.* Nuclear Factor (NF)-kappaB2 (p100/p52) is required for normal splenic microarchitecture and B cell-mediated immune responses. *J. Exp. Med.* 147–159 (1998).

169. Feng, B., Cheng, S., Pear, W. S. & Liou, H.-C. NF-kB inhibitor blocks B cell development at two checkpoints. *Med. Immunol.* **3,** 1 (2004).

170. Senftleben, U. *et al.* Activation by IKKalpha of a second, evolutionary conserved, NF-kappa B signaling pathway. *Science* **293,** 1495–9 (2001).

171. Schwarz, E. M., Krimpenfort, P., Berns, a & Verma, I. M. Immunological defects in mice with a targeted disruption in Bcl-3. *Genes Dev.* **11,** 187–197 (1997).

172. Massoumi, R., Chmielarska, K., Hennecke, K., Pfeifer, A. & Fässler, R. Cyld inhibits tumor cell proliferation by blocking Bcl-3-dependent NF-kappaB signaling. *Cell* **125,** 665–77 (2006).

173. Chen, J. & Chen, Z. J. Regulation of NF-κB by ubiquitination. *Curr. Opin. Immunol.* **25,** 4–12 (2013).

174. Ahner, A., Gong, X. & Frizzell, R. a. Cystic fibrosis transmembrane conductance regulator degradation: cross-talk between the ubiquitylation and SUMOylation pathways. *FEBS J.* **280,** 4430–8 (2013).

175. Desterro, J. M. P., Rodriguez, M. S. & Hay, R. T. SUMO-1 Modification of IkappaBalpha Inhibits NF-kappaB Activation. **2,** 233–239 (1998).

176. Aillet, F. *et al.* Heterologous SUMO-2/3-ubiquitin chains optimize IκBα degradation and NF-κB activity. *PLoS One* **7,** e51672 (2012).

177. Peracchi, M. *et al.* Circulating ghrelin levels in patients with inflammatory bowel disease. *Gut* **55,** 432–3 (2006).

178. Zhao, D. *et al.* Ghrelin stimulates interleukin-8 gene expression through protein kinase C-mediated NF-kappaB pathway in human colonic epithelial cells. *J. Cell. Biochem.* **97,** 1317–27 (2006).

179. Higgins, L. M., Frankel, G., Douce, G., Dougan, G. & MacDonald, T. T. Citrobacter rodentium infection in mice elicits a mucosal Th1 cytokine response and lesions similar to those in murine inflammatory bowel disease. *Infect. Immun.* **67,** 3031–9 (1999).

180. Simmons, C. P. *et al.* Impaired Resistance and Enhanced Pathology During Infection with a Noninvasive, Attaching-Effacing Enteric Bacterial Pathogen, Citrobacter rodentium, in Mice Lacking IL-12 or IFN- γ. *J. Immunol.* **168,** 1804–1812 (2002).

7 Acknowledgments

First of all I want to thank my supervisor Prof. Dr. Ingo Schmitz for giving me the opportunity to work on this interesting and challenging project. Particularly, I want to thank him for the willingness to share his scientific expertise, for helpful discussions and support as well as the kind atmosphere.

I also want to thank colleagues Frida, Yvonne, Sabrina, Svenja, Alisha, Neda, Daniela, Tanja, Stephanie, Marc, Carlos, Tobias and Ralf for the pleasant and helpful atmosphere in the lab.

I am deeply grateful to my family and friends, especially my mother Christine, my father Ralf, my sister Nicole and my friend Kerstin for all the support they provided me through my entire life and for the interest in my work.

Finally, I want to thank Thomas for his affectionately support, helpful suggestions, tolerance and love.

8 Declaration of originality

Michaela Annemann
Robert-Koch-Straße 6
38106 Braunschweig

Hiermit erkläre ich, dass ich die von mir eingereichte Dissertation zu dem Thema

"Functional studies on the role of IκB$_{NS}$ in T helper cell differentiation"

selbständig verfasst, nicht schon als Dissertation verwendet habe und die benutzen Hilfsmittel und Quellen vollständig angegeben wurden.

Weiterhin erkläre ich, dass ich weder diese noch eine andere Arbeit zur Erlangung des akademischen Grades doctor rerum naturalium (Dr. rer. nat.) an anderen Einrichtungen eingereicht habe.

Magdeburg, den 18.12.2013

Michaela Annemann

9 Curriculum vitae

Persönliche Daten

Name:	Michaela Annemann
Geburt:	14.08.1983
Geburtsort:	Neindorf-Beckendorf
Familienstand:	ledig
Nationalität:	deutsch

Bildungsweg

1990-1991	Oberschule Eilsleben
1991-1994	Grundschule Ummendorf
1994-2003	Allertal- Gymnasium Eilsleben/ Völpke
2003-2009	Diplomstudium der Biologie, Technische Universität Braunschweig
10/08-09/09	Diplomarbeit am Helmholtz- Zentrum für Infektionsforschung, Braunschweig mit dem Thema "Characterisation of the novel adjuvants PQS and PQSMPEG"

Wissenschaftliche Tätigkeit

01/10	Beginn der Dissertation am Helmholtz- Zentrum für Infektionsforschung, Braunschweig in der AG von Prof. Dr. Ingo Schmitz

Sonstiges

11/09	Erwerb des Fachkundenachweises gem. §9 des Tierschutzgesetzes

Veröffentlichungen

1 Schuster, M., Annemann, M., Plaza-Sirvent, C., & Schmitz, I. (2013). Atypical IκB proteins - nuclear modulators of NF-κB signaling. *Cell communication and signaling : CCS*, *11*(1), 23. doi:10.1186/1478-811X-11-23

2 Schuster, M., Glauben, R., Plaza-Sirvent, C., Schreiber, L., Annemann, M., Floess, S., … Schmitz, I. (2012). IκB(NS) protein mediates regulatory T cell development via induction of the Foxp3 transcription factor. *Immunity*, *37*(6), 998–1008. doi:10.1016/j.immuni.2012.08.023

3 Telieps, T., Ewald, F., Gereke, M., Annemann, M., Rauter, Y., Schuster, M., … Schmitz, I. (2013). Cellular-FLIP, Raji isoform (c-FLIP R) modulates cell death induction upon T-cell activation and infection. *European journal of immunology*, *43*(6), 1499–510. doi:10.1002/eji.201242819